UNIVERSITY OF CALGARY

Characterization of EphrinB in Cellular Signaling and Chick Neural Tube Development

by

Laura Rachelle Gauthier

A THESIS

SUBMITTED TO THE FACULTY OF GRADUATE STUDIES

IN PARTIAL FULFILMENT OF THE REQUIREMENTS FOR THE

DEGREE OF DOCTOR OF PHILOSOPHY

DEPARTMENT OF BIOCHEMISTRY & MOLECULAR BIOLOGY

CALGARY, ALBERTA

MARCH, 2008

UNIVERSITY OF CALGARY

FACULTY OF GRADUATE STUDIES

The undersigned certify that they have read, and recommend to the Faculty of Graduate Studies for acceptance, a thesis entitled "Characterization of EphrinB in Cellular Signaling and Chick Neural Tube Development" submitted by Laura Rachelle Gauthier in partial fulfilment of the requirements of the degree of Doctor of Philosophy.

Supervisor, Dr. Stephen Robbins, Department of Biochemistry & Molecular Biology

---

Dr. Christopher Brown, Department of Biochemistry & Molecular Biology

---

Dr. Julie Deans, Department of Biochemistry & Molecular Biology

---

Dr. Cairine Logan, Department of Neuroscience

Dr. Patrick Whelan, Department of Neuroscience

External Examiner, Dr. Nathalie Lamarche-Vane, Department of Anatomy & Cell Biology, McGill University

---

Date

Abstract

Eph receptor tyrosine kinases and their membrane-bound ligands the ephrins are required for regulation of numerous processes including angiogenesis, neuronal differentiation, and axon guidance, through modulation of cytoskeletal reorganization and cell adhesion signalling pathways. Transmembrane B-class ephrin signaling is largely uncharacterized and is the focus of this thesis.

EphrinB1 signaling is dependent on its cytoplasmic tail and may be spatially regulated in membrane microdomains commonly referred to as lipid rafts. The lipid raft association of ephrinB1 following stimulation with soluble EphB receptor ectodomains was characterized as occuring independently of phosphorylation at four conserved tyrosine residues and was likely mediated by a conserved 21 amino acid cytosolic stretch. EphrinB1 tyrosine phosphorylation, induced by soluble EphB receptor ectodomains or Platelet-derived growth factor (PDGF), was found to require the carboxy PDZ-motif of ephrinB1, thus suggesting PDZ-based interactions mediated these responses.

Phospho-carboxy-terminal fragments (pCTF) of ephrinB1 that may possess signaling abilities were identified in ephrinB1-expressing cells as well as in chick tissue, and their production coincided with agonist-induced tyrosine phosphorylation of ephrinB1. pCTF were characterized as membrane-associated fragments resulting from ephrinB1 ectodomain shedding. Regulation of pCTF was found to involve the proteasome, the intramembrane protease gamma-secretase, and the carboxy PDZ-motif of ephrinB1.

B-class ephrins are expressed dorsally in the early developing neural tube and their developmental function in this tissue was investigated by a gain-of-function *in ovo* electroporation approach. Overexpression of full-length ephrinB1 resulted in dramatic defects in neural tube morphogenesis, including involution of the dorsal neural tube and disordered neurogenesis. This phenotype was linked to the presence of the conserved C-terminal domain of ephrinB1 suggesting signalling from ephrinB1 was required. In contrast, a striking decrease in neural tube size was observed when a construct mimicking membrane-tethered, ectodomain-shed ephrinB1 was overexpressed. These studies suggested B-class ephrins function early during neural tube formation to maintain correct neural tube morphology and that signaling from ephrinB1 is involved in this process.

Preface

The work presented in this thesis from Chapter 4 and Chapter 5 has been submitted for publication to the Journal of Comparative Neurology.

Title: EphrinB Reverse Signaling Modulates Morphogenesis in the Developing Neural Tube

Authors: Laura R. Gauthier, Katerina Tumova, C. Cairine Logan and Stephen M. Robbins

Acknowledgements

Thank you to my supervisory committee, Dr. Chris Brown, Dr. Julie Deans, and Dr. Cairine Logan, who have provided valuable insight, kind support and encouragement throughout my thesis work. I am also grateful for the privilege of having participated in research in each of their labs which were very enriching experiences.

I am very grateful to my supervisor Dr. Steve Robbins for his constant encouragement throughout my studies. Dr. Robbins has been a mentor for my research, an excellent teacher and always seems to have my best interest in mind. His inspiring creativity and enthusiasm for science are remarkable and I am very thankful for his mentorship and commitment to me throughout my degree.

I am very grateful to Dr. Cairine Logan who welcomed me into her lab as one of her own. Her interest and generosity, not to mention enthusiasm, with both her resources and time towards my project were inexhaustible. Quite simply, the chick work in this thesis could not have been done without her invaluable expertise and assistance for which it is not possible to thank her enough.

Thank you to Katerina Tumova and Lulu Liu from the Logan lab for training me in chick manipulations and dissections, as well as processing of embryos. Both these ladies were encouraging and enthusiastic teachers, greatly facilitating the learning of and

development of my technical skills. Furthermore, their technical assistance, particularly when I first started with the chick studies, was invaluable and sincerely appreciated.

Thank you also to Kate Mak of the Logan lab and Mary Resek of the Robbins lab for technical assistance with egg opening and sectioning, as well as their friendship.

Through my initiation in developmental biology in Dr. Logan's lab I also became fascinated by the chick embryo and its development – it is simply amazing to watch it unfold. I also thank the dozens upon dozens of chick embryos who made the ultimate sacrifice for scientific research on my behalf.

Thank you to Dr. Karen Kopciuk for her help and advice with statistical calculations.

I am deeply grateful to Dr. Jennifer Rahn, Dr. Trina Johnson, Anthony Berndt, and Dr. Tessa Campbell whom provided invaluable thesis critiquing and editing.

Thank you to my family and friends for their support and encouragement throughout my degree. Thanks to my parents, Georges and Cécile, and my brother Luc for their love and support. Thank you to Dr. Trina Johnson and Dr. Maria Polyak, whose enriching discussions and friendships have greatly contributed to my life. Dr. Jennifer Rahn has acted as a mentor over the past few years and I deeply value her friendship as knowing her has considerably added to joy in my life. Thank you to Iris for her help and wise

counsel. As well, thank you to my new extended family, Lois, Garry, Arlene, Kevin & Karen, for their interest and support in my studies.

Thank you in particular to my husband Ken who has been by my side from the beginning of my studies and has provided support, love and encouragement for which I am deeply grateful for each and everyday.

Finally, thank you to the Canadian Institutes of Health Research and the Alberta Heritage Foundation for Medical Research for funding this project without which this work could not have been completed.

Dedication

Pour mes parents,

Georges et Cécile,

mon frère,

Luc,

et mon époux,

Ken

Table of Contents

List of Tables

List of Figures and Illustrations

List of Symbols, Abbreviations and Nomenclature

Symbol	Definition
aa	Amino acid
ADAM	A disintegrin and metalloproteinases
A/L	Aprotonin/leupeptin
Amp	Ampicillin
AP	Alkaline phosphatase
APP	Amyloid precursor protein
BCIP	5-bromo-4-chloro-3-indolyl-phosphate, toluidine salt
BMP	Bone-Morphogenetic-Protein
bp	Base pair
BSA	Bovine Serum Albumin
CASK	Calcium/calmodulin-dependent serine protein kinase
CCS	Cosmic calf serum
cDNA	Complementary deoxyribose nucleic acid
CFNS	Craniofrontonasal syndrome
CIAP	Calf Intestinal Alkaline Phosphatase
CSL	CBF1, Suppressor of Hairless, and Lag-1
CTF	Carboxy-terminal fragment
CTF′	Carboxy-terminal fragment′
CXCR	Cytokine Receptor containing a specific motif: cysteine-any amino acid- cysteine
DAB	Diaminobenzidine tetrahydrochloride
DAPT	N-[N-(3,5-Difluorophenacetyl-L-alanyl)]-S-phenylglycine t-Butyl
DEPC	Diethyl pyrocarbonated
dI	dorsal interneuron
DIG	Digoxygenin
DMEM	Dulbecco’s modified Eagle minimal media
DMSO	Dimethyl sulfoxide
DNA	Deoxyribose nucleic acid
dNTP	Deoxyribose nucleotide triphosphate
DTT	Dithiothreotol
DV	Dorso-ventral
ECD	extracellular domain
ECL	enhanced chemiluminescent
EDTA	Ethylenediaminetetraacetic acid
EGFR	Epidermal Growth Factor Receptor
EGTA	Ethylene glycol-bis-(2-aminoethyl)-N,N,N', N'-tetraacetic acid
Eph	Erythropoeitin producing hepatocellular carcinoma
Ephrin	Eph-receptor-interacting protein
ERK	extracellular-signal-regulated kinase
FACS	Fluorescence-activated cell sorter
FBS	Fetal bovine serum

Fc	Fragment, crystallizable
FGF	Fibroblast growth factor
GAP	GTPase activating protein
GEF	Guanine nucleotide exchange factor
GFP	Green Fluorescent Protein
GIT	G protein-coupled receptor kinase-interacting protein
GlcNAc	N-acetyl glucosamine
GPI	Glycosylphosphatidylinositol
Grb4	Growth factor receptor binding protein 4
GRIP	Glutamate receptor interacting protein
GST	Glutathione-S-transferase
GTP	Guanidine triphosphate
HA	Hemagluttanin
HCl	Hydrochloride
HEPES	4-(2-Hydroxylethyl)-1-piperazineethanesulfonic acid
HH	Hamilton-Hamburger stage
HPLC	High performance liquid chromatography
HRP	Horseradish peroxidase
ICD	Intracellular domain
Ig	Immunoglobulin
IRES	Internal ribosome entry site
IV	Intervening sequence
Jak	Janus kinase
kDa	Kilodalton
KLR	Namesake of ephrinB1 polybasic domain mutant
LB	Luria Broth
LIM	Lin-1, Isl-1, and Mec-3
LMW-PTP	Low molecular weight protein tyrosine phosphatase
MALDI	Matrix-assisted laser desorption ionization
MAPK	Mitogen-activated protein kinase
MARCKS	Myristoylated alanine-rich C-kinase substrate
mda	Melanoma differentiation associated
MDCK	Madine darby canine kidney
MEF	mouse embryonic fibroblast
MES	4-Morpholineethanesulfonic acid
MMP	Matrix metalloproteinases
MS	Mass spectrometer
Myc	Myelocytic leukemia
NBT	Nitroblue tetrazolium chloride
NTS	nuclear translocation sequence
PBS	Phosphate-buffered saline
PCR	Polymerase chain reaction
pCTF	Phospho-carboxy-terminal fragment
pCTF′	Phospho-carboxy-terminal fragment′
PDGF	Platelet-derived growth factor
PDGFR	Platelet-derived growth factor receptor

PDZ	PSD-95, Dlg, and ZO-1 homology
PECAM	Platelet/endothelial cell adhesion molecule
PFA	Paraformaldehyde
Phos	Phosphate
$PI(4,5)P_2$	Phosphatidylinositol 4,5-bisphosphate
PIP2	Phosphatidylinositol 4,5-bisphosphate
PMSF	Phenylmethylsulfonyl fluoride
PNGaseF	Peptide N-Glycosidase F
PP2	4-Amino-5-(4-chlorophenyl)-7-(*t*-butyl)pyrazolo[3,4-d]pyrimidine
PS	Presenilin
PTP	Protein tyrosine phosphatase
PTP-BL	Protein tyrosine phosphatase-basophil like
Ptpro	Protein-tyrosine phosphatase receptor type O
RGC	Retinal ganglion cell
RGS	Regulator of G protein signalling
RIP	Regulated intramembrane proteolysis
RIPA	Radioimmunoprecipitation assay
RNA	Ribonucleic Acid
RTK	Receptor tyrosine kinase
SAM	Sterile alpha motif
SDF-1	Stromal derived factor 1
SDS	sodium dodecyl sulphate
SH2	Src-homology domain 2
SH3	Src-homology domain 3
Shh	Sonic Hedgehog
SPAR	SP-A recognition protein
ß-ME	ß-Mercaptoethanol
STAT	Signal transducers and activators of transcription
TBE	Tris-Borate-EDTA
TCA	Trichloroacetic acid
TE	Tris EDTA
Tlx	T-cell leukemia translocation
tRNA	Transfer ribonucleic acid
UV/Vis	Ultraviolet-visual spectrum
v-Src	Viral Src
wt	Wild type

Chapter One: Introduction

Chapter One: Introduction

Embryonic development is a delicately orchestrated program in which tissue morphogenesis is precisely modulated, both temporally and spatially, through the mastered use of signaling molecules, ultimately resulting in an intricate organism. Antithetical to this process is cancer, where the degeneration of tissue organization and loss of signaling control leads to progressive dedifferentiation and uninhibited growth of cancer cells. Many of the signaling molecules involved in embryonic development are also implicated in oncogenesis (1), suggesting that understanding of their functions in proper developmental programs may be transferable to the understanding of their participation in cancer and of how these impact the disruption of normal tissue architecture. The panel of molecular suspects in cancer and development is vast, however this thesis focuses on a molecular pairing directly implicated in cellular guidance during development, the Eph and ephrin system (2, 3), and will examine the actions of transmembrane ephrin molecules in the putative signaling pathways that may lead to the observed effects they have when overexpressed in chick embryos.

1.1 Eph and Ephrin System Overview

Eph receptor tyrosine kinases (RTK) and their membrane-bound ligands, the ephrins, work in concert to mediate cell-cell instructive cues in a variety of developmental programmes including the guidance of migrating cells and axonal processes, angiogenesis, as well as serving other distinct functions in tissue

morphogenesis (4, 5). The Eph-ephrin system has been conserved throughout evolution as evidenced by their presence in *C. elegans* (6) and *Drosophila* (7).

The first Eph receptor was discovered in a screen for novel tyrosine kinases involved in cancer and its cDNA was cloned from the namesake erythropoietin-producing hepatocellular carcinoma cell line (8). Subsequently, other Eph receptor family members were discovered and there are now 15 members, that comprise the largest family of RTKs. Eph receptors were long considered 'orphan receptors' since their ligands were expected to be soluble as observed in RTK signaling (9). Eventually, ephrinA1 was found to be the ligand for an Eph receptor and it was thus realized that the ligands had to be membrane-bound (10). More Eph-receptor ligands were discovered by expression of the extracellular domains of Eph receptors as fusion proteins with immunoglobulin or alkaline phosphatase to detect ligands (9). In 1997, due to widespread incongruence of both ligand and receptor names, an international nomenclature committee coined the family of receptors 'Eph' and the ligands 'ephrin' (Eph-receptor interacting proteins) (11).

It is now apparent that there are two classes each of receptors, EphA (A1-A9) and EphB (B1-B6), and ligands, ephrinA (A1-A6) and ephrinB (B1-B3). The distinction of the classes is based on sequence similarity and also corresponds to ligand-receptor class binding preferences (12). In general, EphA receptors bind ephrinA ligands, and EphB receptors preferentially bind to ephrinB ligands (**Figure 1.1**). There is selectivity between specific Eph-ephrin members as well as widespread promiscuous binding within classes and cross-class binding (12). The two classes of ephrins are also further

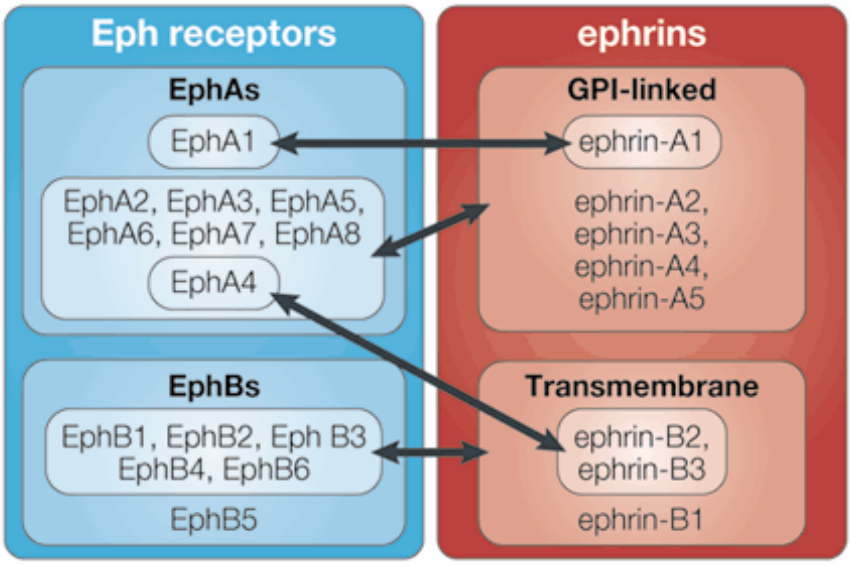

Figure 1.1: Eph receptor and ephrin ligand family members.

Black arrows indicate preferential binding affinities. Adapted from Wilkinson, *Nat Rev Neurosci.*, 2001.

distinguished by their mode of membrane attachment; the A-class is tethered to the membrane via a glycosylphosphatidylinositol (GPI)-anchor and the B-class has a transmembrane domain and short cytosolic tail (**Figure 1.2**).

It became apparent from both genetic and biochemical experiments that the ephrins were more than just ligands since they could also transduce a signal when stimulated by Eph receptors. Thus, a unique aspect of the Eph-ephrin system is the ability of both components to propagate a signal into their respective cells, a process coined 'bi-directional signaling' (**Figure 1.2**). The signal initiated by Eph receptors is termed 'forward' signaling, and those by the ephrins 'reverse' signaling. The receptors and ligands do not function as diffusible components but instead operate *in vivo* exclusively when membrane clustered. This was further evidenced by the observation that unlike artificially clustered ectodomains, monomeric ectodomains of ligands are unable to initiate signals into Eph receptor cells (13). The crystal structure of complexed receptor-ligand pairs has shown that they interact in an anti-parallel orientation (14). Because of this latter attribute, Eph receptors and ephrins are well-suited to provide cell-cell contact cues in many developmental processes.

Ephs and ephrins are abundantly expressed during all phases of embryogenesis in specific spatial and temporal patterns (12). Together they have been described to participate in angiogenesis and vasculogenesis (15, 16); tissue morphogenesis in intestinal crypts (17); eye field formation (18); somite formation (19, 20); neural crest cell migration (21, 22); axon guidance (23); urorectal development (24); T-cell activation (25, 26); synaptic plasticity (27); and hindbrain segmentation (28). For the purpose of this introduction, we focus on a few of their functions in neural development.

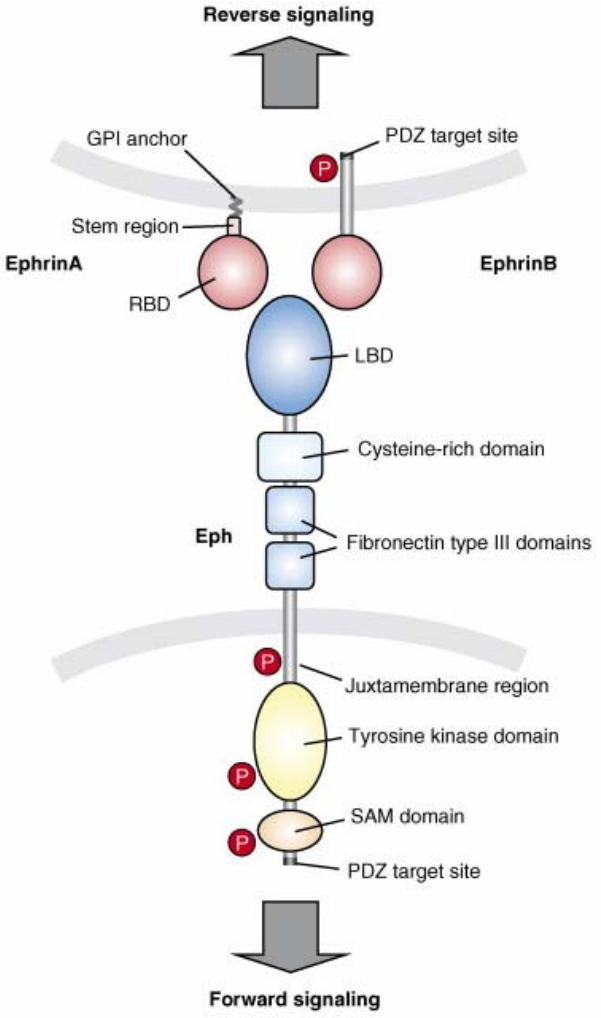

Figure 1.2: General domain structure of Eph receptors and ephrin ligands. Adapted from Egea and Klein, *Trds Cell Bio*, 2007.

1.2 Eph Receptor and Ephrin Structure

1.2.1 Eph Structure

All Eph receptors conform to the structure of RTKs. They have an extracellular N-terminal glycosylated ligand binding domain, a single membrane-spanning domain, and a cytoplasmic region with a tyrosine kinase domain (**Figure 1.2**). The extracellular glycosylated region harbours the N-terminal ligand binding domain, a cysteine-rich segment thought to function in receptor-receptor oligomerization (29), and two fibronectin type III repeats. From a structural standpoint, the ~180 amino acid (aa) N-terminal ligand binding domain of Eph receptors topologically resembles that of lectins (30) however shares no significant sequence similarity to other known proteins (31). The ligand-binding domain exhibits a jellyroll folding topology (14) and the ligand-binding site is formed by the D-E, G-H, and J-K loops (32). The H-I loop of the ligand-binding domain exhibits the most class-specific attributes of Eph receptors and is thought to function in lower-affinity ephrin-binding interactions (33).

The intracellular tyrosine kinase domain of Eph receptors bears stronger similarity to non-receptor tyrosine kinase domains with regards to key catalytic amino acid residues (34). The cytoplasmic domain of Eph receptors contains other key regions such as a juxtamembrane region that is involved in signal activation, a highly conserved tyrosine kinase domain, a sterile α motif (SAM) domain, thought to function in hetero- and homo-oligomerization of proteins, and a PDZ binding motif (PSD-95 post-synaptic density protein, Discs large, Zona occludens tight junction protein) within the carboxy-terminus able to mediate interactions with PDZ-domain containing proteins.

1.2.2 Ephrin Structure

Ephrin ectodomains commonly have a conserved ~20 kDa N-terminal ephrin domain involved in Eph receptor interactions, followed by an ~40 amino acid unstructured spacer that links the domain to the membrane (**Figure 1.2**). The ephrin domain has a primary sequence that shares no similarity with any other known protein however shares structural homology to the cupredoxin-phytocyanin family of Cu^{2+}-binding proteins (35). The ephrin domain structure is an eight stranded β-barrel, with three α helices connecting the strands, and two conserved buried disulfide bonds stabilizing the structure (35). Amino acids identified to be candidate class determinants of the ligands are located in one particular loop, the G-H loop, which is involved in Eph receptor interactions (14). Not surprisingly, the crystallized structure of G-H loops between ephrinA5, ephrinB1 and ephrinB2, ectodomains differ from each other (35-37). These structural differences could translate into Eph-ephrin binding preference and recognition. EphrinB2's G-H loop also has been found to be responsible for homodimerization of this ligand (35), but not for ephrinB1's (36) or ephrinA5's (36). Ephrins are also N-glycosylated at different sites even within classes. These glycosylations likely further refine the structures of the ligands and hence possibly also modulate Eph-ephrin interactions.

1.2.2.1 Cytoplasmic Structure of B-class Ephrins

The three currently known *ephrinB* genes (B1-B3) all possess a transmembrane domain as well as an ~85 residue cytoplasmic domain. The cytoplasmic tail has a stretch

of 33 amino acids at the carboxy-terminus which represents the most highly conserved region between all three B-ephrins, exhibiting a 90-100% identity (**Figure 1.3**). This stretch has no sequence similarity to other proteins. Within this region lie five conserved tyrosine residues that, when phosphorylated, may recruit phospho-tyrosine binding proteins. A short polyproline stretch may recruit SH3-domain binding proteins while a PDZ-binding motif lies at the extreme carboxy-terminus.

A well-packed ß-hairpin structure with high conformational stability occurs in ephrinB2 residues 301-322 (analogous residues in ephrinB1 are 314-335), located in the highly conserved 33 aa C-terminus of ephrinBs (38, 39), when the three tyrosine residues found therein are unphosphorylated. This highly stable structure is abolished when these tyrosines are phosphorylated (38), thus this β-hairpin is thought to function as a cryptic site to mediate phosphotyrosine interactions with proteins, such as the adaptor Grb4 (38, 40-42).

1.2.3 Formation and Structure of Eph/Ephrin Complex

Three Eph-ephrin complex crystal structures have been resolved: ephrinB2 and EphB2 (14), ephrinA5 and EphB2 (43), and ephrinB2 and EphB4 (44). These studies reported that the ligand and receptor are juxtaposed on opposite sides of a plane. This structure is in agreement with Eph and ephrins meeting head-to-head at sites of cell-cell contact. An extensive high-affinity interface results when Eph and ephrins interact that thermodynamically drives the binding interaction: the G-H loop of the ephrin bends and inserts into a deep channel on the surface of the Eph receptor; which then undergoes a

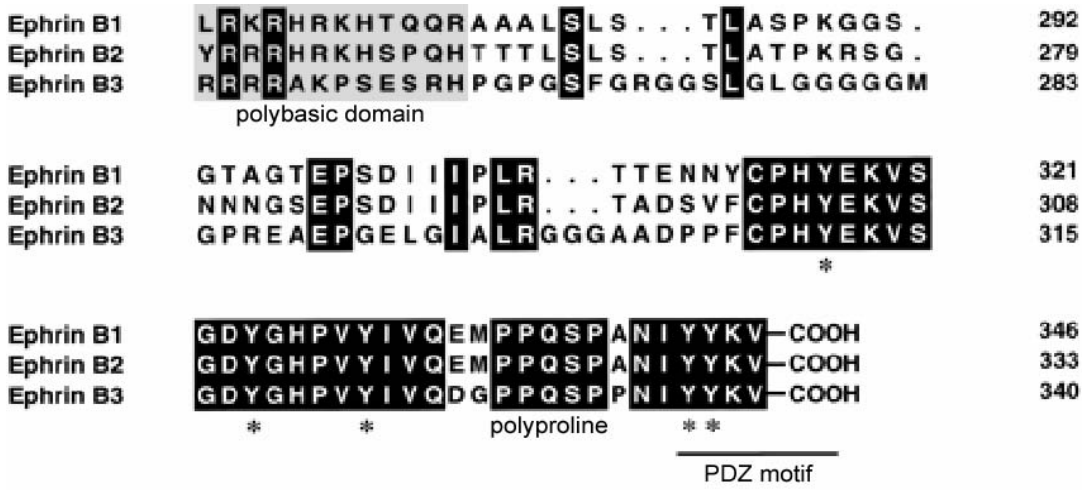

Figure 1.3: Cytoplasmic domain sequences of human B-class ephrins.

Conserved residues are in black boxes, conserved tyrosines are marked by an asterisk, PDZ motif is underlined, grey box highlights the polybasic domain. Adapted from Lin *et al*, *J Biol Chem*, 1999.

conformational change resulting in a hydrophobic interaction pocket that wraps around the ephrin's G-H loop . No other major conformational changes in protein structure of the ephrin or Eph-receptor ligand-binding domains occur following their interaction. Thus, exactly how the extracellular binding of these domains is transduced into a cytoplasmic signal is likely based on homo- or multimerization of the receptor or ligand on the plasma membrane.

The ephrinB2-EphB2 complex structure further demonstrated that although the high-affinity 1:1 heterodimer was the predominant species, these could further associate and form a cyclic 2:2 hetero-tetrameric structure (**Figure 1.4**). This is a novel arrangement not seen with any other described receptor-ligand structures (45). The tetramer forms a planar ring structure, thus enabling one receptor to interact with two ligands, and one ligand to interact with two receptors (14). A second interface between receptor and ligands of much lower affinity is presumed to mediate the assembly of the heterodimers into the tetramer. For effective bi-directional signaling, two molecules of both the receptor and the ligand must be clustered on their respective cells in order to transmit a signal, thus the tetrameric structure provided an attractive solution for this quandary. In contrast, neither the ephrinA5-EphB2 or ephrinB2-EphB4 complex structures yielded arrangements other than the 1:1 heterodimer. This points to intricate interactions between Eph and ephrins that likely help tailor signaling responses.

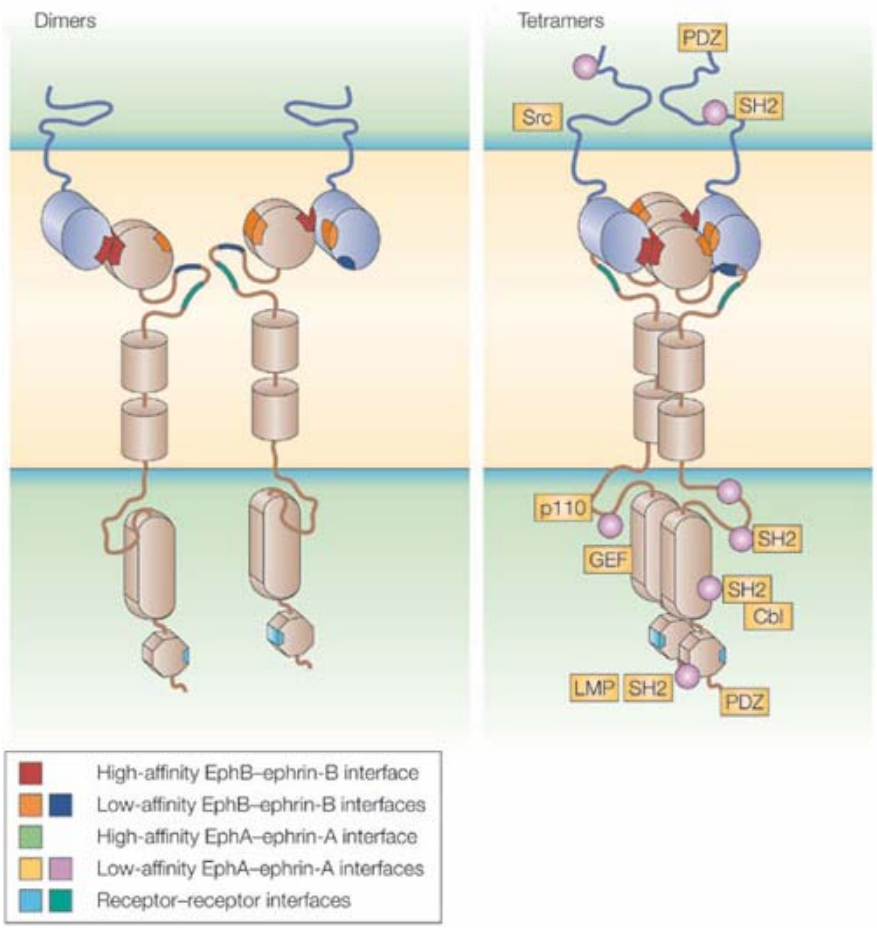

Figure 1.4: Structural Eph-ephrin ectodomain interactions.

Adapted from Pasquale, *Nat Rev Mol Cell Biol*, 2005.

1.3 Signalling Modalities of Eph receptors and ephrin ligands

1.3.1 Receptor-ligand promiscuity

Though there are preferential ligand/receptor interactions, it was discovered early on that ephrins and Eph RTKs displayed promiscuous binding within classes (12). The promiscuous binding of Ephs and ephrins further present a challenge in terms of functional redundancy in genetic studies (5). There are also a few examples of cross-class binding partners including EphA4 which binds to both ephrinB2 (12) and ephrinB3 (46). The latter interaction is physiologically important for establishing proper neuronal circuits involved in controlling walking (47). Recently, ephrinA5 has been found to stimulate EphB2 receptor activation and co-crystalize with this receptor (43). As discussed above, the finite differences in structure of ephrins and Eph receptors likely translates into overall binding preferences. The typical dissociation constant (K_d) of Eph-ephrin interactions is in the subnanomolar to nanomolar range (12). These K_d values were obtained in solution, thus there may exist greater promiscuity of interactions *in vivo* where membranes would permit pre-clustering of receptors or ligands on adjacent membranes (48), allowing interactions between receptor-ligand pairs with lower affinity interactions, such as ephrinA5 and EphB2, to occur.

1.3.2 Spatial Arrays of Ephs and Ephrins Impact their Signaling

Another important facet of Eph and ephrin bi-directional signaling is their required clustering. As described previously, ephrins and Ephs bind in a 1:1 heterodimer

as revealed through the crystal structure. Monomeric ephrin ectodomains added exogenously to Eph expressing cells were not able to induce signaling nor phosphorylation of the Eph receptor (13), however, ephrin ectodomain dimers led to phosphorylation of the Eph receptor and subsequent signaling. Furthermore, neuronal axons were repelled by clustered ligand-fusion proteins but not monomeric ones (49). Thus, there is a minimal requirement of dimerization of Eph and ephrin during signaling, which likely functions to bring into proximity sufficient adaptor proteins to tranduce downstream signals.

Interestingly, differences in downstream signaling have been observed in cells where the degree of multimerization of Ephs and ephrins has been modulated. For example, Stein *et al.* (50) were able to show that tetrameric-clustered ephrinB1 ectodomains, but not dimeric- or other higher-order multimerized ones, could lead to the specific recruitment of low-molecular-weight phosphotyrosine phosphatase (LMW-PTP) to EphB1 in cells and ultimately mediate cell attachment to fibronectin via integrin modulation (51). In these experiments, no differences were seen in the amount of phosphorylation of the EphB1 receptors in response to the different degrees of multimerized ephrinB1 ectodomains. A mutation in the SAM domain (implicated in hetero- and homo-oligomerization of proteins) of EphB2 abrogated the recruitment of LMW-PTP to EphB1 following tetrameric-ephrinB1 engagement and integrin-mediated attachment (51). Thus, the spatial array of ephrins may promote the assembly of specific configurations of Eph SAM domains that may define subsequent signaling steps. Ephrins and Ephs are commonly expressed in gradients, such as in the developing tectum and retina (52), and cells and axonal processes which pathfind through these regions must

interpret these gradients. The above studies provide clues as to how the spatial arrangement of ephrins may elicit appropriate cellular responses.

Eph and ephrin density on cell membranes can likely be modulated to establish tissue gradients of these molecules. A large proportion of PDZ-domain containing proteins are involved in synaptic functions (53). The Eph receptors and ephrins can bind and be clustered by PDZ-domain containing proteins such as syntenin and PICK1 (54). It is believed that PDZ-domain containing proteins connect cell surface proteins to the cytoskeleton and that they may also aid in the organization of large signal transduction complexes at synapses (55, 56). In addition, both the extracellular cysteine-rich domain (57) and the intracellular SAM domains (58) of Eph receptors have been implicated in ligand-independent receptor-receptor oligomerization.

1.3.3 Bi-directional Signalling

1.3.3.1 Eph Receptor 'Forward' Signaling

When Eph receptors are clustered by ephrin ectodomains, this leads to transphosphorylation of the Eph receptor juxtamembrane region (59-61). The phosphorylation of several conserved tyrosine residues in the juxtamembrane region results in the removal of an inhibitory interaction between the juxtamembrane region and the kinase domain. This allows a conformational change in the kinase domain that increases affinity for substrate binding. The inhibitory release also allows the phosphorylated juxtamembrane region to act as an SH2-docking site for proteins, such as the non-receptor tyrosine kinase Src (62), that can also phosphorylate Eph receptors (63),

Ras GTPase activating protein (RasGAP) (64) and Nck, which lead to integrin activation (65). LMW-PTP modulates integrin-mediated attachment through Nck specifically in response to multimerized, activated Eph receptors but not dimeric ones (50). However, unlike other RTKs, Eph receptors are poor activators of Ras/ERK/MAPK (extracellular-signal-regulated kinase/mitogen-activated protein kinase) (5), correlating with their lack of mitogenic effects. In fact, they tend to downregulate Ras/ERK/MAPK pathways in a tyrosine kinase dependent manner which leads to neurite retraction (66). Eph receptor signaling also impinges on the janus kinase/signal transducers and activators of transcription (Jak/STAT) pathway at neuromuscular junctions. Auto-phosphorylated EphA4 can activate JAK2 which in turn phosphorylates STAT1 and STAT3 (67).

Eph receptor propagated signaling pathways generally tend to converge on cytoskeletal remodeling. For example, Ephexin is a guanine nucleotide exchange factor for Rho GTPases (RhoGEF) that binds specifically to EphA receptors C-termini, irrespective of ligand-binding, and acts as a mechanistic link between these receptors and the cytoskeleton (68, 69). In extending EphA4-expressing growth cones, Ephexin contributes to the activation of RhoA, Rac1, and cdc42, resulting in overall extension of the process. When ephrinA1 ligand is encountered, Ephexin is tyrosine phosphorylated suppressing its activity towards Rac1 and cdc42, and enhancing it towards RhoA, resulting in growth cone retraction. Ephexin1 is required for proper guidance of EphA-expressing retinal ganglion cell (RGC) in mice (68). In another example, the Rac-specific GTPase-activating protein (Rac-GAP) alpha2-chimaerin also mediates EphA4-triggered growth cone collapse in response to ephrinB3 (70, 71). Alpha2-chimaerin binds activated EphA4 receptor and then inactivates Rac, which normally acts as a positive

regulator of axonal process extension. The modulation of the ephrinB3/EphA4 interactions by alpha2-chimaerin are important in motor-circuit formation in the developing spinal cord. Modulation of the cytoskeleton following EphA4 activation also involves a Rap GTPase, spine-associated Rap GTPase-activating protein (SPAR), which interacts with EphA4 via a PDZ-based interaction (72). EphrinA1-mediated activation of EphA4 in cultured hippocampal neurons led to the SPAR-mediated inactivation of Rap1 and resulted in growth cone collapse.

Eph/ephrin interacting complexes can be downregulated on the cell surface in a unique fashion via trans-endocytosis. This process involves one cell endocytosing full-length proteins from the interacting cell (73, 74) and may be important in glia cell-mediated shaping of neuronal connections (75) (**Figure 1.5**). Evidence suggests that trans-endocytosis is dependent on the C-terminal tail of both ephrin and Eph receptors since C-terminal truncation mutants of these proteins were unable to endocytose each other even though their respective ectodomains were able to interact (74). The intracellular pathways controlling these processes are not well-described. However, Vav2, a Rac-GEF, has been implicated in EphB-mediated endocytosis of ephrinB-EphB complexes (76). This Vav2-dependent process has been found to be required for axon retraction *in vitro*. Downregulation of Eph forward signaling can also be mediated via the protein-tyrosine phosphatase receptor type O (Ptpro) (77). Ptpro is able to dephosphorylate a regulatory juxtamembrane tyrosine on both EphA and EphB receptors. Modulation of Ptpro expression resulted in altered sensitivity of Eph-expressing axons of retinal ganglion cells.

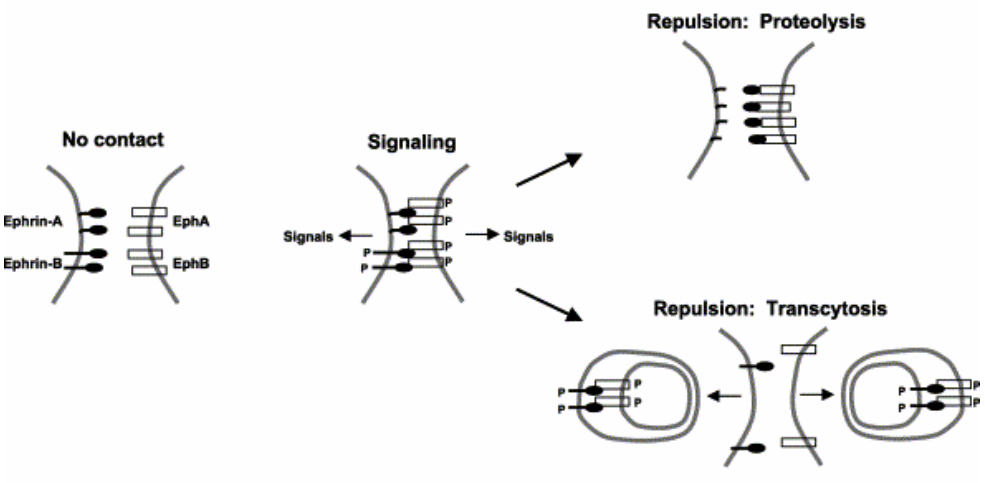

Figure 1.5: Physical methods of Eph/ephrin signal downregulation.
Adapted from Noren and Pasquale, *Cell Signal*, 2004.

There are also Eph receptors, such as A10 and B6, which lack residues for kinase activity and are catalytically inactive. They may function to mediate reverse signaling through ephrins, or possibly function *in trans* to moderate Eph forward signaling. There is precedent for Eph receptor *trans* modulation since EphA7 has two splice variants which lack kinase domains and are expressed in the developing neural tube (78). The catalytically inactive splice variants are able to shift cellular response for the full-length EphA7-expressing cells from repulsion to adhesion when they are co-expressed *in vitro*.

1.3.3.2 EphrinA 'Reverse' signaling

Although initially thought to be unable to transduce signals due to their mode of membrane attachment, GPI-anchored A-class ephrins are able to transduce a signal inside the cell when stimulated by Eph receptors. Genetic studies in *C. elegans* have demonstrated that their ephrin homologues, all of which contain a GPI moiety, have functions independent of their cognate Eph receptor (VAB-1). In this model genetic organism, it has been observed that mutation of ephrins synergizes with VAB-1 kinase domain mutations, and that VAB-1 kinase domain mutants exhibit a weaker mutant phenotype than VAB-1 ligand-binding domain mutants, suggesting that the GPI-tethered ligands can be involved in reverse signaling *in vivo* (6, 79). In addition, we have shown in our lab that ephrinA5 is able to induce a signaling response within the ephrinA5-expressing cell when bound to its cognate Eph receptor (80, 81). Fyn, a member of the Src family of non-receptor tyrosine kinases, is a downstream signaling protein targeted in activated ephrin A5 cells. The physiological consequence to the ephrinA-induced

signaling event is a change in cell adhesion and morphology that is modulated by integrins (80-82). However, the mechanism by which ephrinA signals are transmitted across the plasma membrane is still not understood. A mode of downregulation for A-class ephrin signaling has been proposed that involves the cleavage of these molecules by the Kuzbanian metalloprotease (83) at sites of EphA/ephrinA contact, permitting physical separation of intercellular contact sites (**Figure 1.5**).

1.3.3.3 EphrinB 'Reverse' Signaling

EphrinBs have signaling activities independent from Eph receptors that are required in physiological processes such as the formation of the posterior tract of the anterior commissure (84), cardiac valve development (84), as well as urorectal development (24). The function of ephrinB2 in these processes was shown to be dependent on the presence of its cytoplasmic tail as transgenic mice strains containing an ephrinB2 construct with a large cytosolic truncation in place of the wild type gene exhibited defects in axon pathfinding in the anterior commissure, thickened aortic and pulmonary valves, and hypospadias.

Biochemical evidence supports the ability of membrane-spanning ephrins to participate in bi-directional cell signaling. It has been shown that a total cytoplasmic domain deletion of the the ephrinB1 tail completely disrupts its reverse signal (85). Transmembrane ephrins were initially shown to be tyrosine phosphorylated *in vitro* by v-Src (86), in response to stimulation of cultured cells by either clustered EphB receptor ectodomains, platelet-derived growth factor (PDGF) (86, 87), or Fibroblast Growth Factor (FGF) (88). Src-family kinases have also been implicated in the phosphotyrosine-dependent downstream signaling of ephrinB1 in response to clustered EphB2

ectodomains (86, 87, 89). Multiple *in vivo* tyrosine phosphorylation sites of ephrinB1 and EphB2 have been mapped from developing murine retinal tissues (90). This denotes a physiological significance to the ligand's phosphorylation (86, 90).

To date, only a handful of proteins have been found to interact with the ephrinB cytoplasmic tail, however their signaling does converge on cellular motogenic effects (**Figure 1.6**). Grb4 has been demonstrated to be recruited in a phosphotyrosine-dependent manner to ephrinB1 via its SH2 domain (41). Downstream cytoskeletal changes triggered by this latter association are proposed to be mediated through the adaptor Grb4. The SH3-domain of Grb4 is able to interact with other proteins involved in cytoskeletal regulation, such as Cbl-associated protein (CAP/ponsin) (41). Grb4 is also able to recruit G protein-coupled receptor kinase-interacting protein (GIT) to ephrinB-activated synapses, modulating spine morphogenesis and synapse formation (91). An assortment of PDZ-domain containing proteins interact with ephrinB1's PDZ motif, including protein-tyrosin-phosphatase-basophil like (PTP-BL) (89), glutamate receptor interacting protein (GRIP) (92), and a novel PDZ-domain containing protein with an regulator of heterotrimeric G protein signaling domain (PDZ-RGS3) (93). PTP-BL has been implicated in dephosphorylating ephrinB1 and Src-family kinases following cellular activation of ephrinB1 with clustered EphB ectodomains in cultured cells (89). GRIP, a modular PDZ-domain containing protein, can recruit a serine/threonine kinase to activated ephrinB1 (92). PDZ-RGS3 binds to ephrinB1's cytoplasmic tail following EphB addition (93). This interaction decreased cell migration of cerebellar granule cells towards the chemoattractant Stromal derived factor 1 (SDF-1), through the RGS domain,

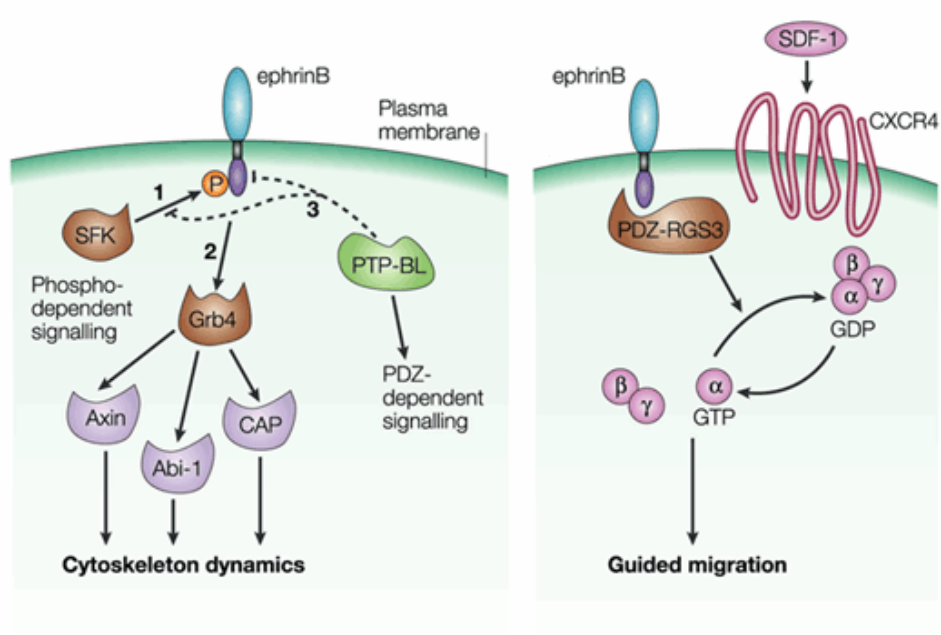

Figure 1.6: EphrinB cytoplasmic tail signaling pathways.

Adapted from Kullander and Klein, *Nat Rev Mol Cell Biol*, 2002.

which promotes GTPase activity of Gα-subunit, thus inhibiting signaling from the chemokine's receptor, CXCR4 (93) (**Figure 1.6**). The cytosolic domain of transmembrane ephrins has been implicated in modulating migration and cell attachment in an integrin-dependent fashion following Eph stimulation implicating the ligands in 'inside-out' signal transduction (94). In addition to PTP-BL dephosphorylating ephrinB1, trans-endocytosis of ephrinB-EphB complexes previously discussed (73, 74) (**Figure 1.5**) is another described mode of ephrinB signal downregulation.

1.3.3.4 Lipid Rafts: Plasma Membrane Signaling Centres used by Ephs and Ephrins

Lipid rafts are liquid-ordered membrane microdomains that represent an assembly of glycosphingolipids and cholesterol (95). These specialized membrane microdomains have a role in a wide variety of processes, including transcytosis (96), alternate route of endocytosis (97), internalization of toxins, bacteria and viruses (98-100), cholesterol transport (101), calcium homeostasis (102), protein sorting (95) and signal transduction (103, 104). It has been hypothesized that lipid rafts can serve as sites of signal integration largely based on the observation that many molecules known to be involved in intracellular signaling are enriched within them (103-105). Examples of these signaling molecules include GPI-anchored proteins, and dually palmitoylated and myristoylated proteins, such as Src-family kinases (106, 107). Growth factor receptors and immune receptors are thought to utilize such membrane compartmentalization to elicit a functional signaling response (105). Regulated signal transduction in these lipid rafts is an attractive strategy for achieving spatial and temporal specificity in Eph/ephrin signaling.

Supporting this theory, both classes of Eph and ephrins have been found to localize to lipid rafts. As is the case for many GPI-anchored proteins (108) ephrinA5 is highly enriched in lipid rafts and its downstream signaling has been found to be initiated from these locales (80, 109). It is clear from recent reports that ephrinB1 association with lipid rafts is important in tailoring its signaling responses as well. EphrinB1's cytoplasmic tail is able to specifically recruit GRIP into lipid rafts when they are expressed together (92). The regulation of tyrosine phosphorylation of ephrinB1 by Src-family kinases was also moderated by lipid rafts (89). Previous studies have demonstrated constitutive lipid raft association of ephrinB1 (89, 92, 110), as well as both classes of Eph receptors. Eph receptors bind to caveolin-1 (111), the quintessential structural protein of caveolae, a specific sub-type of lipid raft discerned as flask-shaped invaginations on the plasma membrane (105). Recently, it was demonstrated that lipid rafts mediate EphA receptor and ephrinA segregation on extending growth cones, enabling both these molecules to act in guidance since this spatial arrangement promotes *trans*- rather than *cis*-interactions (112). Thus, it is clear that lipid rafts are able to mediate spatial regulation of Eph and ephrin signalling.

1.4 Roles of Eph Receptors and Ephrins in Development and Disease

1.4.1 Roles for Ephs and Ephrins in Development

1.4.1.1 Ephs and Ephrins Function in Axon Guidance: Retinotectal Topographic Mapping

A main role for Eph and ephrins is to act as cellular contact cues for guiding axons and migrating cells during embryogenesis. During development, neurons sprout

axons which must migrate over long distances and pathfind their way to their target. Axons are equipped with a highly motile, exquisitely sensitive structure, termed the axon growth cone (113). By responding to short and long range extracellular cues, these axonal growth cones are able to select the correct path towards their target. Similarly, migrating cells, such as neural crest, must crawl over relatively long distances during development relying on a variety of cues in their environment to successfully reach their destination tissue (114). How axonal growth cones and migrating cells respond to and interpret the cues encountered along the way largely depends on the receptors and intracellular downstream signal transducers they express. Eph and ephrins operate in short-range since they must be on the cell surface to work in concert and cluster each other, and have been shown to be required for both axon guidance (23) and neural crest cell migration (21).

Retinotectal topographic mapping is a well-studied system wherein Eph and ephrins work in concert to form complimentary gradients (52), allowing examination of the functions of these proteins in axon guidance. A topographic map is a spatially organized array of projecting neurons that map onto a target field so that the spatial relationship among the neurons is preserved in their connections to the new structure. The prototypical model system to study topographic maps is the retinotectal system. Retinotectal projections involve the topographic mapping of retinal axons to a region of the developing midbrain termed the optic tectum (in chick, frog and fish), or superior collilculus (in mammals) (**Figure 1.7**). The retinal ganglion cells are the output neurons of the retina and it is their axons which form the optic nerve that exit at the rear of the

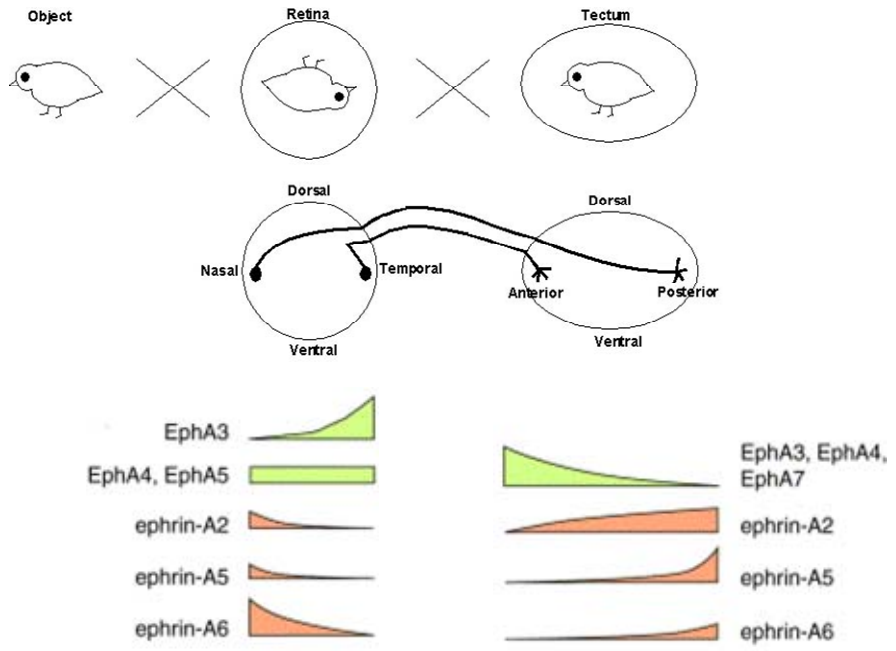

Figure 1.7: Retinotectal topographic mapping along the anterior-posterior axis is mediated by EphA receptors and A-class ephrins.

Levels of expression for the Eph and ephrins in the retina and tectum are depicted. Adapted from Flanagan, *Annu Rev Neurosci*, 1998 and Knoll and Drescher, *Trds Neurosci*, 2002.

eye. In this system, the nasal retinal axons project to the posterior tectum, and the temporal retinal axons project to the anterior of the tectum.

Initially, EphA and ephrinA gradients were described in the retina and tectum at the time mapping occurs, and these gradients were detected by soluble ligand/receptor fusion protein binding (115, 116). It was found that ephrinA5 and A2 were expressed in an anterior-posterior gradient along the tectum providing positional cues for the afferent growth cones, and that EphA3 receptors were expressed in a nasal-temporal gradient in the retina, providing the differential responsiveness in the axons. High-EphA expressing temporal retinal axons project to the tectum and are arrested more anteriorly by low-levels of ephrinAs. Conversely, low-EphA expressing nasal retinal axons are halted more posteriorly by a high-ephrinA expressing-region of the tectum. The importance of EphAs responding to ephrinA cues in the map formation is demonstrated in the ephrinA2-/- and ephrinA5-/- double knockout mice which have severe defects in retinotectal projections in the antero-posterior axes (117). Stripe assays of retinal axons have shown that ephrinA2 and A5 act as repulsion cues for retinal axons (118, 119). However, ephrinAs cannot simply be acting as repulsive cues in this scheme as the retinal axons would not enter the tectum to begin with if this were so. It is likely that ephrinAs can attract axons at low permissive levels or that they work in concert with other attractants (52). Thus, the axon and growth cone interpret the ephrinA gradients and surrounding cues.

This initial model of EphA and ephrinA in retinotectal mapping proved to be too simplistic. EphrinAs were found to also be expressed in the retina in a temporo-nasal gradient, that is in an opposing gradient to the EphA expression initially described in this tissue (12). Similarly EphA receptors were found to be expressed in a posterior-anterior

gradient in the tectum (118). These are thought to act further in refining positional cues in the anterior-posterior mapping and how this occurs is currently being investigated.

The discussion of retinotectal topographic mapping has been limited to the antero-posterior axis mapping in the tectum, however the antero-posterior mapping in the tectum illustrates how ephrins and Ephs function in axon guidance and provide positional cues in complementary gradients.

1.4.1.2 Ephs and Ephrins Mediate Cell Sorting: Hindbrain Segmentation

Hindbrain segmentation is another developmental process where ephrin and Ephs are well-studied and showcases the ability of these proteins to mediate cell sorting. Boundary formation during development prevents cells that form different parts of the embryo from intermingling and also provides positional information to bordering cell populations (120). The transient segmentation of the hindbrain appears as a series of seven bulges in the developing embryo along the anterior-posterior axis (**Figure 1.8**) (121). These constrictions coincide with the boundaries of the rhombomeres, the term used to describe these metameric units of the rhombencephalon, also known as the developing hindbrain. Boundaries are formed between rhombomeres, in a stereotypical fashion and is thought to be mediated through adhesion molecules, since cells obtained from odd-numbered rhombomeres do not mix with those from even-numbered rhombomeres (122), however even- and odd-numbered rhombomere cells are able to intermix with each other (123). Rhombomeres, numbered from 1 through 7 along the antero-posterio axis, acquire distinct identities that are important for subsequent steps of

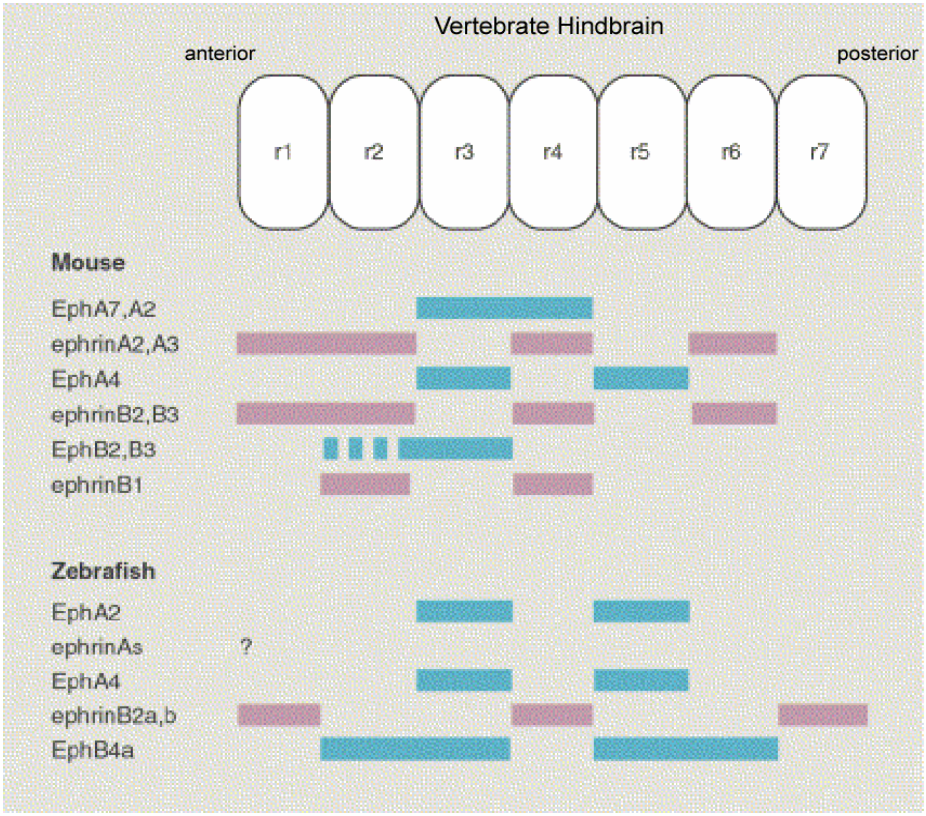

Figure 1.8: Eph and ephrin expression in hindbrain segmentation.

r: rhombomere. Adapted from Tepass *et al.*, *Curr Opin in Gene Dev*, 2002.

hindbrain development including neuronal differentiation and axonal projections, as well as neural crest specification (120).

Molecules involved in specifying this cell sorting include Eph and ephrins several members of which are expressed during and after boundary formation (**Figure 1.8**). Rudimentarily, it has been found that EphA4 receptors are expressed in the odd-numbered rhombomeres 3 and 5, and ephrinB2 proteins are expressed in the even-numbered rhombomeres 2, 4, and 6 (28). The ligand- and receptor-expressing cells mediate repulsion at the boundaries between rhombomeres as knock-down of certain key EphA4 receptor (124), or deletion in the cytoplasmic domains of the molecules, results in some intermixing and less sharpened boundaries (123). Thus, the sorting of rhombomeres is found to be directed by bi-directional signaling between Eph and ephrins. Although these experiments support a role for Eph and ephrins in restriction of cell intermingling between rhombomeres, the exact mechanism this occurs by, either through repulsion and cytoskeletal collapse, or cell-affinity differences, has not been clearly established.

1.4.2 A Role for Ephs and Ephrins in Cancer

EphA1, the first Eph receptor described, was cloned from the erythropoietin-producing hepatoma cell line, in which it was overexpressed by 10-fold (8). Since then, all Eph receptors have been found to be over-expressed or dysregulated in different types of human tumours (125) and is often associated with increased malignancy. Ephrins as well are dysregulated in certain cancers such as ovarian (125). Given the involvement of Eph and ephrins in cell migration and angiogenesis, it is not surprising that these

molecules have been implicated in this disease (2, 125). Eph and ephrins are involved in angiogenic sprouting and thus may mediate new blood vessel formation in tumours (126). Due to their role in cytoskeletal dynamics and association with increased malignancy, the expression of Eph and ephrins may mediate dissemination of cells away from the tumour. In contrast, Ephs and ephrins may also function by sorting out tumour cells from the surrounding tissues. They have been shown to do this in colorectal cancer and the sorting restricts the spreading of the tumour (127).

The recent advances in understanding the structure of Eph/ephrin binding also initiated the investigations into therapeutics which would antagonize their interaction. Many peptides that interact with the Eph receptor ligand-binding cleft have been developed that abolish interactions with ephrins (32, 128-130). Azurin, a member of the cupredoxin protein family to which ephrin folds are structurally similar (35), can also interfere with EphB2 activation and inhibit cancer growth (131). Azurin is a soluble protein which can enter cancer cells wherein it stabilizes the tumour suppressor p53 and increases its intracellular levels, leading to cancer regression (132). Ideally, the study and development of these peptides and proteins will yield novel anti-angiogenic or anti-tumourigenic therapeutics that target aberrant Eph/ephrin signaling.

1.4.3 Craniofrontonasal Syndrome is Associated with EphrinB1 Mutations

EphrinB1 mutations have been linked to Craniofrontonasal Syndrome (CFNS) (133, 134). This syndrome is characterized by body asymmetry such as hypertelorism, polydactyly, and skeletal and dermatological abnormalities (135). A number of sporadic and familial mutations have been described for ephrinB1 (**Figure 1.9**) occuring all along

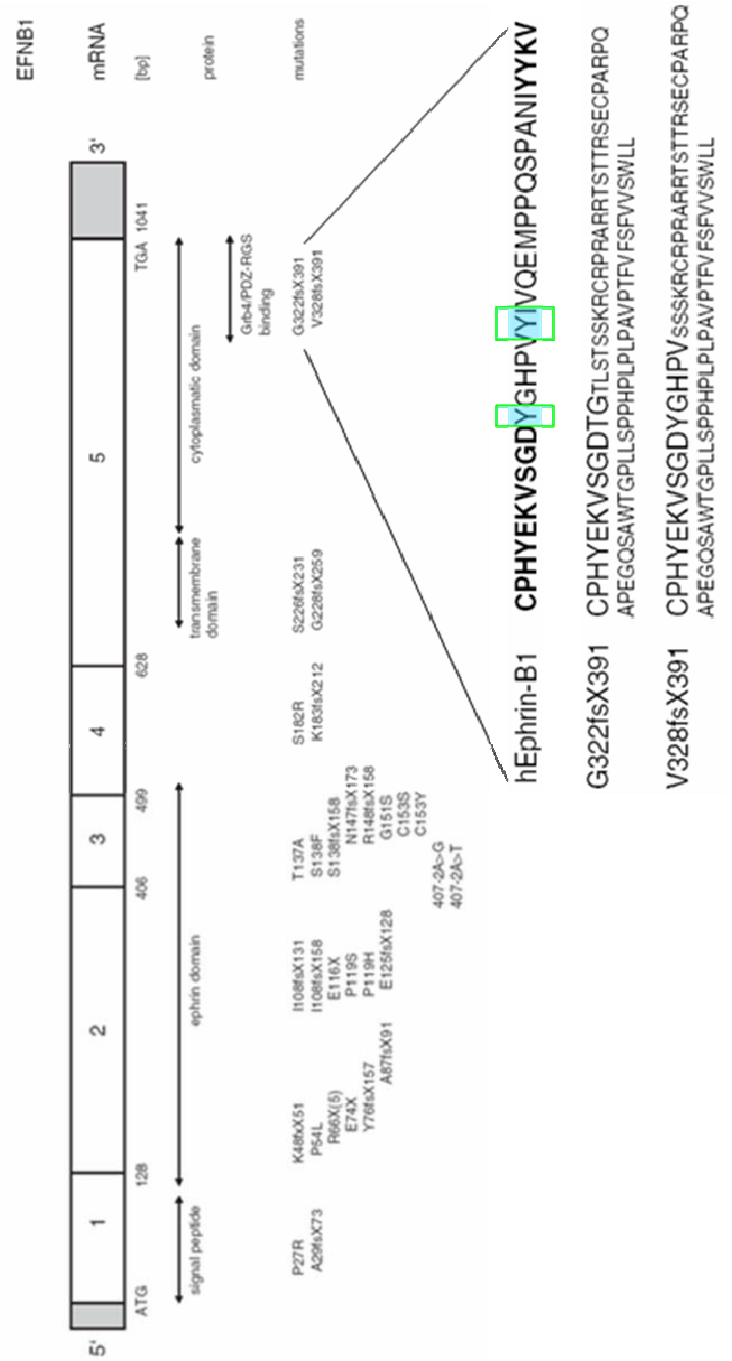

Figure 1.9: Summary of ephrinB1 mutations characterized in Craniofrontonasal syndrome.

Frameshift mutations near the C-terminus of EphrinB1 ablate the conserved carboxy-terminus. Adapted from Wieland *et al.*, *Hum Mutat*, 2005.

the gene (133, 134, 136, 137). Most of the mutations have been mapped to the ephrin fold, a number of which occur within the G-H loop, likely abrogating Eph/ephrin high affinity binding. One mutation predicts a truncated protein which is likely secreted from the cell as a soluble ephrinB1 ectodomain. Finally, two frameshift mutations result in a novel C-terminus of ephrinB1, ablating the highly conserved C-terminus, thus disrupting any links to downstream signaling.

CFNS is an unusual X-linked inheritable disorder in which females are most affected with obligate male carriers showing little manifestation. This pattern of inheritance, along with similar phenotypic manifestations, are observed in X-linked ephrinB1 gene knock-out mice (138, 139). The more severe phenotypes observed in the heterozygous females has been attributed to ephrinB1-positive and negative expressing cells sorting out from each other.

1.5 Study Aims

EphrinBs have signaling activities independent from Eph receptors that are required in physiological processes such as the formation of the posterior tract of the anterior commissure (84), cardiac valve development (84), as well as urorectal development (24). EphrinBs cytoplasmic tail was shown to be required to mediate these processes as in its absence, these processes were severely disturbed (24, 84). There is further evidence in humans of the importance of ephrinB1's cytoplasmic tail in mediating its signalling and function, as a mutation disrupting this area is associated with Craniofrontonasal Syndrome (137). The highly conserved 33 aa carboxy-terminus has

been demonstrated to interact with several proteins *in vitro* however, little is known concerning the exact signaling pathways ephrinB ligands employ *in vivo*. The **overall goal** of this thesis is to further **investigate signaling from ephrinB's cytoplasmic tail** through the following aims:

1) To characterize the regions of the ephrinB1 cytoplasmic tail that are involved in regulating signaling
2) To examine if proteolytic processing of ephrinB1 results in fragments that could possess biological activity
3) To determine the role of ephrinB proteins in neural tube development in the chick

Chapter Two: Materials and Methods

Chapter Two: Materials and Methods

2.1 EphrinB1 cDNA Constructs

For the *in vitro* characterizations of the cytosolic regions involved in ephrinB1 signaling, ephrinB1 constructs were cloned into pBabe expression vector (gift from M McMahon, see **Figure 2.1** for vector map). Primers which annexed 5'XhoI and 3'ClaI restriction enzyme sites at the ends of the ephrinB1wt, ephrinB1Δ1, ephrinB1Δ4, ephrinB1Δ12, and ephrinB1Δ33 constructs were used to PCR the corresponding coding regions of human ephrinB1 originally obtained from pJE14/h-Elk-L (Regeneron, Tarrytown, NY) (see **Table 1** for primer sequences). The 3'primers for ephrinB1Δ1, ephrinB1Δ4, ephrinB1Δ12, and ephrinB1Δ33 also appropriately inserted a new stop codon. The resulting fragments were first ligated into pGEMT (Promega) and subsequently transferred into pBABE using XhoI and ClaI (all restriction enzymes used herein were obtained from New England Biolabs).

EphrinB1ΔKLR, ephrinB1ΔIV, ephrinB1ΔECD, and HA/Myc ephrinB1wt were subcloned via PCR in two or three separate parts per construct (see **Figure 2.2**) using pJE14/h-Elk-L as the template. 5'XhoI and 3'ClaI sites were annexed at the respective ends of the full constructs. Each part of a construct however also possessed appropriately annexed restriction enzyme sites at the intervening 5' and 3' ends to allow for directional cloning of the separate parts into the full cDNA construct (see **Figure 2.2** and **Table 1** for primer sequences and annexing restriction enzymes used). Following PCR,

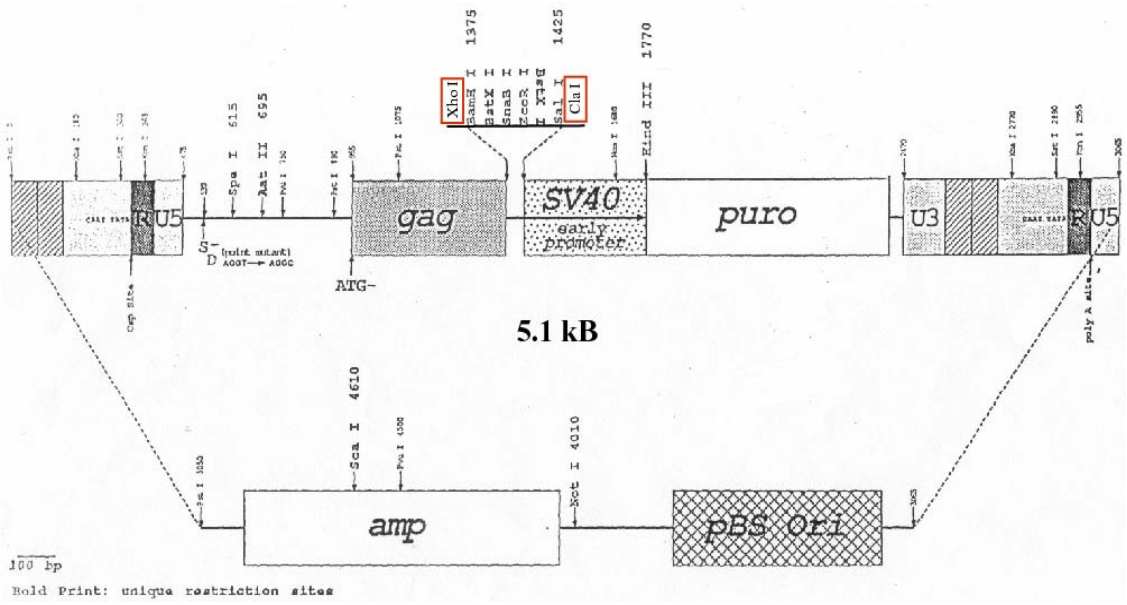

Figure 2.1: pBabe expression vector map.

Red boxes highlight the restriction enzymes sites used to insert the ephrinB1 constructs.

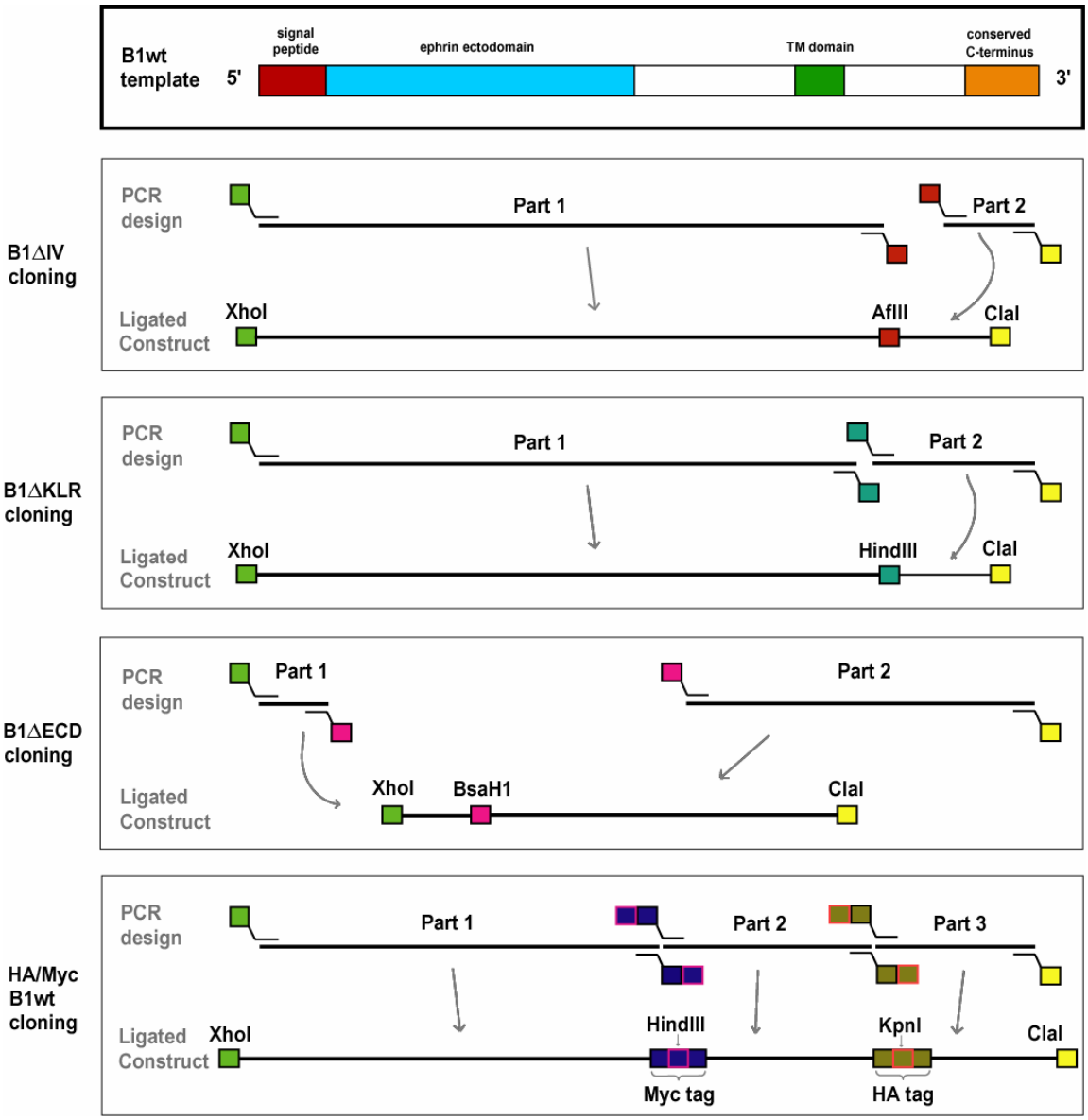

Figure 2.2: Schematic design of multi-part cloning for EphrinB1ΔIV, ΔKLR, ΔECD, and HA/MycB1wt into pBabe.

Coloured boxes indicate non-basepairing overhang of annexed restriction enzyme sites at ends of primers, and in the HA/MycB1wt construct also coloured boxes also indicate non-basepairing sequence of primer coding for the antigenic Myc and HA tags inserted. Appropriate primers and restriction enzymes used for ligations are detailed in Table 2.1.

Table 1: Primers for Cloning pBabe EphrinB1 Constructs

Construct	Parts	RE	5'Primer Name & Sequence	3'Primer Name & Sequence	Base Pairs	aa
ephrinB1wt	1 of 1		ephrin B1 wt 5 (5'XhoI site)	ephrinB1 wt 3 (3'ClaI site)	1038	346
			CCGCTCGAGGGAAGATGGCTCGGCCT	ATCGATTCAGACCTTGTAGTAGATGTT		
ephrinB1Δ1	1 of 1		ephrin B1 wt 5 (5'XhoI site)	ephrinB1 c-term 1 – 3 (3'ClaI site)	1035	345
			CCGCTCGAGGGAAGATGGCTCGGCCT	ATCGATTCACTTGTAGTAGATGTTCGC		
ephrinB1Δ4	1 of 1		ephrin B1 wt 5 (5'XhoI site)	ephrinB1 c-term 4 – 3 (3'ClaI site)	1028	342
			CCGCTCGAGGGAAGATGGCTCGGCCT	ATCGATTCAGATGTTCGCCGGGCTCTG		
ephrinB1Δ12	1 of 1		ephrin B1 wt 5 (5'XhoI site)	ephrinB1 c-term 12 - 3 (3'ClaI site)	1002	334
			CCGCTCGAGGGAAGATGGCTCGGCCT	ATCGATTCACATCTCTTGGACGATGTA		
ephrinB1Δ33	1 of 1		ephrin B1 wt 5 (5'XhoI site)	ephrinB1 c-term 33 - 3 (3'ClaI site)	939	313
			CCGCTCGAGGGAAGATGGCTCGGCCT	ATCGATTCAGTAGTTGTTCTCTGTAGT		
ephrinB1ΔIV	1 of 2		ephrin B1 wt 5 (5'XhoI site)	3intrvdel (3'AflII site)	843	321
		AflII	CCGCTCGAGGGAAGATGGCTCGGCCT	CTTAAGAGGGCAGCCGCCCGCTGCTG		
	2 of 2		5intrvdel (5'AflII site)	ephrinB1 wt 3 (3'ClaI site)	120	
			CCTTAAGGACTACAGAGAACAACTAC	ATCGATTCAGACCTTGTAGTAGATGTT		
ephrinB1ΔKLR	1 of 2		ephrin B1 wt 5 (5'XhoI site)	3juxtaPB (3'HindIII site)	783	337
		HindIII	CCCGCTCGAGGGAAGATGGCTCGGCCT	AAGCTTCAGTAGTAGGACCGTCAGGAA		
	2 of 2		5KLR (5'HindIII site)	ephrinB1 wt 3 (3'ClaI site)	210	
			AAGCTTCGGGCCGGCTGCCCTCTCGCTC	ATCGATTCAGACCTTGTAGTAGATGTT		
ephrinB1ΔECD	1 of 2		ephrin B1 wt 5 (5'XhoI site)	3'BSAH1-B1 SP (3'BsaH1 site)	81	179
		BsaH1	CCGCTCGAGGGAAGATGGCTCGGCCT	GGCGTCGCGAGCCGGCACAGCGCCAC		
	2 of 2		5'BsaH1-B1 Stb (5'BsaH1 site)	ephrinB1 wt 3 (3'ClaI site)	456	
			GACGCCGGCCCCCTGGTAGTCGGGGGCTCC	ATCGATTCAGACCTTGTAGTAGATGTT		
HA/MycB1wt	1 of 3		ephrin B1 wt 5 (5'XhoI site)	corr 3myc primer (3'HindIII site)	540	367
		HindIII	CCGCTCGAGGGAAGATGGCTCGGCCT	AAGCTTCTGCATTGATGCCTCAGGCGT		
	2 of 3		5'Myc primer (5'HindIII site)	3'HA one KpnI (3'KpnI site)	384	
		KpnI	AAGCTTATCTCAGAGGAGGACCTGCAG	GGTACCTCGTATGGGTAGCCCTTGGGA		
	3 of 3		5'HA primer (5'KpnI site)	CTGGCCAGGGTACTGAG	177	
			GGTACCAGATTACGCTGGCAGTGGCAC	ephrinB1 wt 3 (3'ClaI site)		
			AGCGGGCACCGAGCCC	ATCGATTCAGACCTTGTAGTAGATGTT		

Note: RE indicates the intervening restriction enzyme(s) for those constructs subcloned in two or more parts; Base Pairs indicates the expected size of the PCR product with the specified primers; aa indicates the total number of amino acids in the final construct

individual segments were first individually cloned into pGEMT then the two or three parts of each construct were co-ligated together in pGEMT by virtue of the engineered-intervening restriction enzyme sites. Subsequently, the resulting full constructs were transferred into pBabe using XhoI and ClaI sites.

PCR reactions were assembled as follows: 40ng of pJE14/h-Elk-L template, 100 pmol of each appropriate 5' and 3' primer, 1x PCR buffer (Gibco-BRL), 1.5 mM $MgCl_2$ (Gibco-BRL), 0.2 mM deoxynucleotide (dNTP) mix (Invitrogen), 0.25 µl Taq polymerase (Gibco-BRL), and ddH_2O to 50 µl. The PCR reactions were submitted to the following cycles in a Perkin Elmer GeneAmp 2400 PCR System:

1 cycle	94ºC	5 min
25 cycles	94ºC	30 sec
	60ºC	30 sec
	72ºC	2 min
1 cycle	72ºC	7 min
1 cycle	4ºC	∞

EphrinB1Δ3K→R was generated via site-directed mutagenesis by exchanging the three juxtamembrane lysine (K) residues at positions 264, 267, and 271 to arginines (R). Three rounds of site-directed mutagenesis were completed using pBabe/ephrinB1wt as the template. Each round of PCR amplification involved a unique set of phosphorylated complementary and non-complementary primers (see **Table 2**) that consecutively targeted one of the three lysine sites by introducing a base pair mutation for the coding lysine (A<u>A</u>G) to arginine (A<u>G</u>G). The product of each round of site-directed mutagenesis

Table 2: Primers for Site-Directed Mutagenesis Cloning of EphrinB1Δ3K→R

Target Site	Complementary and Non-Complementary Primer Names and Sequences
Lysine 264	K-R -1: GTCCTACTACTGA**G**GCTACGCAAGCGG
	compl K-R -1: CAGGATGATGACT**C**CGATGCGTTCGCC
Lysine 267	K-R -2: CTGA*G*GCTACGCA**G**GCGGCACCGCAAGC
	compl K-R -2: GACT*C*CGATGCGT**C**CGCCGTGGCGTTCG
Lysine 271	K-R - 3: A*G*GCGGCACCGCA**G**GCACACACAGCAGC
	compl K-R -3: T*C*CGCCGTGGCGT**C**CGTGTGTGTCGTCG

Note: bold letters indicated targeted base pair to be mutagenized in current round, italicized letters indicate base pairs mutagenized in previous round

was used as the template for the subsequent round. The mutagenesis reactions were assembled as follows: 50 ng pBabe/ephrinB1wt template, 5 µl 10x PFU buffer (final 200 mM Tris.HCl pH 8.8, 2 mM $MgSO_4$, 100 mM KCl, 100 mM $(NH_4)_2SO4$, 0.1 % TritonX-100, 0.1 mg/ml nuclease-free BSA) (Stratagene), 1 µl PFU enzyme (Stratagene), 4 µl dNTP, 150 ng of each appropriate complementary and non-complementary primers, 1.25 µl DMSO, 5µl 5x Q solution (Qiagen), and ddH_2O to 25 µl. The PCR reactions were submitted to the following cycles:

1 cycle	95ºC	30 sec
18 cycles	95ºC	30 sec
	65ºC	1 min
	68ºC	13 min (2 min/kb)
1 cycle	68ºC	13 min
1 cycle	4ºC	∞

The reactions were digested with DpnI for 2 hr at 37ºC then transformed into competent bacteria. Plasmids from positive transformants were isolated with the use of a Mini-Prep kit (Qiagen) and sequenced to confirm the mutagenesis.

All constructs described herein were DNA sequenced in pBabe with appropriate primers to ensure no mutations were introduced during the cloning.

EphrinB1wt, ephrinB1Δ33, and ephrinB1ΔECD constructs used in the *in ovo* studies were sublconed into pCIG2 expression vector (gift from Dr. Franck Polleux (140), see **Figure 2.3** for vector map). pCIG2 is based on the pCI vector (Invitrogen) and possesses an internal ribosome entry site (IRES) for Green Fluorescent Protein (GFP) that

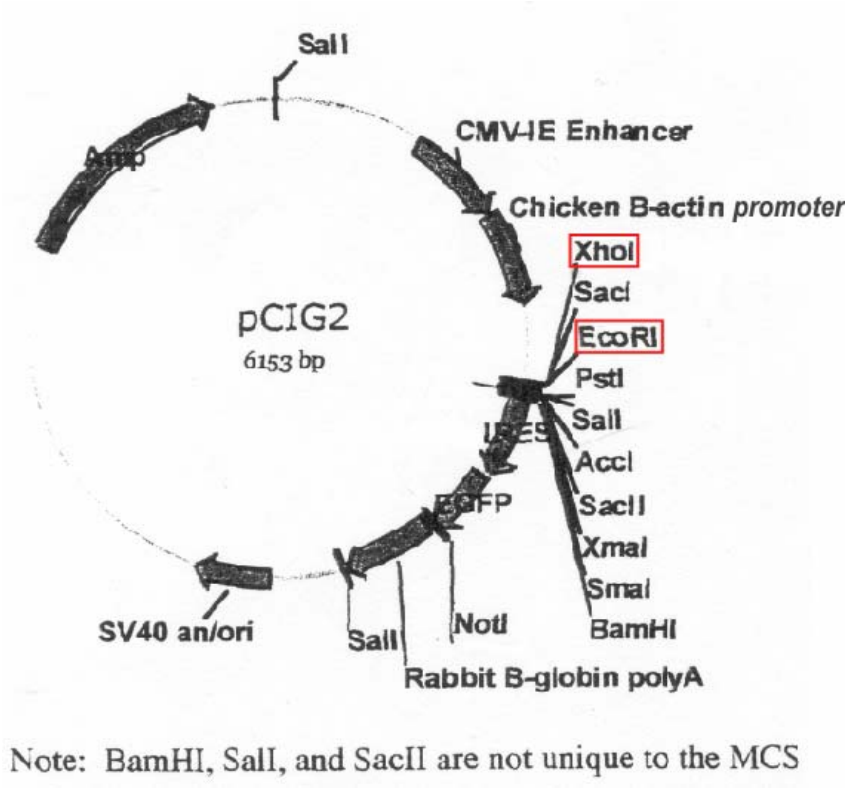

Figure 2.3: pCIG2 expression vector map.

Red boxes highlight the restriction enzymes sites used to insert the ephrinB1 constructs.

can be used to easily monitor expression of the introduced transgene. 5'XhoI and 3'EcoRI restriction enzyme sites were annexed at the ends of each construct for directional ligation into pCIG2. The primers used are listed in **Table 3** and pJE14/h-Elk-L was used as the template for ephrinB1wt and ephrinB1Δ33, while pBabe/ephrinB1ΔECD served as the template for ephrinB1ΔECD into pCIG2. The constructs were generated via PCR with the same reaction conditions as described in section **2.1**, than similarly ligated into pGEMT. The constructs were finally transferred into pCIG2 by the use of XhoI and EcoRI and the DNA sequences of the inserts verified via sequence analysis using appropriate primers.

2.2 Retroviral Stock Generation of pBabe/EphrinB1 Constructs

pBabe/ephrinB1 constructs, or vector alone, were transfected into Bosc 293T cells and the resulting viral supernatant collected after 24 hours as per Robbins *et al.* (106). Briefly, Bosc 293T cells were cultured in Dulbecco's modified Eagle minimal media (DMEM) (Gibco-BRL) supplemented with 10 % heat-inactivated Fetal Bovine Serum (FBS) (Gibco-BRL). These were transfected with a mixture of 275 µl Optimem (Gibco-BRL), 7 µl Fugene-6 (Roche), and 15 µl (1 µg) of pBabe ephrinB1 constructs or vector alone, per 10 ml of media. Two days later, the supernatant was collected and centrifuged at 1000 g for 5 min to remove cells and debris then filtered through a 0.45 µm membrane (PALL Corporation), and stored at -80ºC.

Table 3: Primers for Cloning pCIG2 EphrinB1 Constructs for Chick Studies

Construct	Primer Name and Sequence		Insert Size (bp)	Total Size (aa)
	5' Primer	3' Primer		
ephrinB1wt	ephrin B1 wt 5 (5'XhoI site)	3'EcoRI-B1wt	1038	346
	CCGCTCGAGGGAAGATGGCTCGGCCT	GAATTCGGGAAGATGGCTCGGCCTGGG		
ephrinB1Δ33	ephrin B1 wt 5 (5'XhoI site)	3'd33-EcoRI	939	313
	CCGCTCGAGGGAAGATGGCTCGGCCT	GAATTCTCAGTAGTTGTTCTCTGTAGT		
ephrinB1ΔECD	ephrin B1 wt 5 (5'XhoI site)	3'EcoRI-B1wt	537	179
	CCGCTCGAGGGAAGATGGCTCGGCCT	GAATTCGGGAAGATGGCTCGGCCTGGG		

2.3 Establishment and Culturing of Stably Expressing pBabe/EphrinB1 Cell Lines

NIH3T3 (clone 7) cells, cultured in 10 % FBS/DMEM, were infected for 48 hr with a mixture of 0.2 µg/µl polybrene and 400 µl of viral supernatant of pBabe ephrinB1 constructs or vector alone, per 4.5 ml culture media. The infected cells were then selected with 2 µg/ml of puromycin (Sigma) supplemented to their media. The selected NIH3T3 cells were cultured as a pooled population in 10 % FBS/DMEM with 2 µg/ml of puromycin (Sigma).

Presenilin (PS) 1,2 +/+ wt and PS1,2 -/- knock-out mouse embryonic fibroblasts (MEFs) (kind gift from Dr. Bart de Strooper) were cultured in 10 % FBS/DMEM. PS cells stably expressing ephrinB1wt or vector alone were established via retroviral transfection as described above. PS cells were also selected with 2 µg/ml of puromycin and cultured as a pooled population.

MDCK cell lines expressing pBabe/ephrinB1wt and pBabe/ephrinA5wt were a kind gift from Alan Box. These were cultured in 10 % FBS/DMEM with 1-2 µg/ml of puromycin.

2.4 EphB2-Fc Cellular Staining and Detection by Flow Cytometry

NIH3T3 cells stably expressing ephrinB1 constructs or vector alone, were washed once with phosphate-buffered saline (PBS). The cells were de-adhered from culture plates with 2 ml of PUCKS•EDTA (5.4 mM KCl (Sigma), 137 mM NaCl (Sigma), 4.9 mM $NaHCO_3$ (Sigma), 5.6 mM glucose (Sigma), 1 M Hepes pH 7.3 (Sigma), 1 mM EDTA(Sigma)), then resuspended and transferred to 2 ml DMEM supplemented with 0.5

% cosmic calf serum (CCS). The cells were pelleted at 1000 g in a tabletop centrifuge. The cells pellets were resuspended with 0.5 % CCS/DMEM containing 0.1 µg/ml EphB2-Fc (R&D Systems Inc.) and incubated for 45 min at 4ºC. The cells were then washed three times with 5 ml of PBS. After the washes, the cell pellet were resuspended in 250 µl 0.5 % CCS/DMEM with 1:200 Alexa-488 Fluor conjugated goat anti-human IgG antibody (2mg/ml, Molecular Probes) and incubated for 30 min at room temperature in the dark. The cells were then washed three times with PBS and the cell pellet resuspended in 500 µl of PBS and analysed with a Becton Dickinson FACScan equipped with a 488 Argon Laser. Appropriate secondary antibody alone controls were also performed.

2.5 SDS-Polyacrylamide Gel Electrophoresis and Western Blotting

Proteins were subjected to electrophoresis using 10 % polyacrylamide gels that were run for 1000 V•hr. Following electrophoresis, proteins were transferred onto 0.45 µm nitrocellulose membrane (Whatman) in transfer buffer (25 mM Tris (Sigma), 192 mM glycine (Sigma), 20% methanol (EMD Science), 0.1% SDS (Roche)) using a Hoefer TE Series Transphor Electrophoresis Unit for 2 hr at 800 mA. The blocking conditions and wash buffers used for the subsequent steps of Western blotting are listed in **Table 4**. Briefly, the membranes were blocked for 1 hr in 5 % BSA (Roche) or skim milk powder in the appropriate wash buffer (low wash buffer: 1xTBS (137 mM NaCl, 27 mM KCl, 25 mM Tris.HCl pH 7.5) with 0.1 % Tween-20 (Sigma) and 0.1% NP-40 (Fluka Biochemika); extra low wash: 1x TBS with 0.1 % Tween-20). The membranes were then

Table 4: Antibodies and their Dilutions for Western Blotting

Primary Antibody	Manufacturer	Dilution	Block	Wash Buffer	Secondary Antibody
anti-ephrinB (C-18)	Santa Cruz Biotechnology Inc.	1:1000	milk powder	low wash	anti-rabbit HRP
anti-ephrinB (PAN)	Zymed Laboratories	1:1000	milk powder	low wash	anti-mouse HRP
anti-phospho-ephrinB	Cell Signaling Technology	1:1000	BSA	extra low wash	anti-rabbit HRP
anti-actin	Oncogene Sciences	1:2500	milk powder	low wash	anti-mouse HRP
anti-cyclinD1	NeoMarkers-Medicorp Clone Sp4	1:250	milk powder	low wash	anti-rabbit HRP
anti-syntenin	Synaptic Systems	1:200	BSA	low wash	anti-rabbit HRP
12CA5	in house	1:1000	milk powder	low wash	anti-mouse HRP

probed with appropriately diluted primary antibody in 5 % block/wash buffer for 1 hr at room temperature. The membrane was washed three times for 10 min with wash buffer then probed with 1:10000 of the appropriate horseradish peroxidase (HRP)-conjugated secondary antibodies. Subsequently, the membrane was washed three times with wash buffer prior to incubation in enhanced chemiluminescent (ECL) reagent. The membrane was then wrapped in plastic wrap, placed in a film cassette, and then exposed to film (Kodak X-OMat-BT-Film) prior to development.

2.6 Sample Preparation of Equal Protein Loaded Blot

NIH3T3 cells expressing the ephrinB1 constructs or vector alone were lysed in 1 % NP-40 lysis buffer (50 mM Hepes pH 7.5, 150 mM NaCl, 10 % glycerol, 1.5 mM $MgCl_2$, 1mM EGTA, 100 mM NaF, 1 mM PMSF (EMD Biosciences), with 10 µg/ml each of aprotonin (Roche) and leupeptin (Roche) (A/L), 1 mM Na_3VO_4 (Sigma)) on ice for 15 min, then homogenized using a Wheaton dounce homogenizer. An aliquot of the lysates, and BSA standards, were used with the BCA Protein Assay Kit (Pierce) to determine the protein concentration in the lysates. A Beckman DU530 UV/Vis spectrophotometer was used to quantify the assay. 100 µg of each protein lysate was loaded onto an SDS-PAGE gel then analysed via Western blotting with appropriate antibodies.

2.7 Lipid Raft Isolation by Sucrose Density UltraCentrifugation

NIH3T3 cells expressing ephrinB1wt or vector alone, were serum starved overnight. Cells were then stimulated with 0.1 – 1.0 µg/ml EphB2-Fc for 20 min at 37ºC.

Cells were then lysed in 1 ml cold 1 % TritonX-100(Sigma)/MBS lysis buffer (25mM MES pH 6.0 (Sigma), 150 mM NaCl, with 1 mM PMSF, 10 µg/ml A/L, 1 mM Na_3VO_4) and then dounce homogenized. Then, an equal volume of 80 % sucrose in lysis buffer was added to the lysate to bring it to a final concentration of 40 % sucrose. The lysate was transferred to an ultracentrifuge tube (Beckman No. 344059) and overlayed with a 30 to 5 % linear sucrose gradient in MBS. The samples were centriguged at 37 000 rpm in a Beckman Sw41Ti rotor at 4ºC for 18 hrs. The top 7 ml of the gradient, containing the buoyant lipid rafts, was transferred into a new ultracentrifuge tube and mixed with 15 ml MBS buffer with 1 mM sodium orthovanadate. This was then centrifuged at 37000 rpm at 4ºC for 1 hr to pellet the lipid rafts. The supernatant was decanted and the pelleted lipid rafts resuspended in 60 µl of 1x sample loading buffer.

2.8 N-Glycolytic Treatment of Live Cells

NIH3T3 expressing ephrinB1wt, ephrinB1Δ4 or vector alone were lifted from culture plates with PUCKS•EDTA, washed once with 0.5 % CCS/DMEM, then resuspended in media at a density of $2x10^7$ cells/ml. $2.2x10^6$ cells (110 µl) were treated with 12.2 µl 10x G1 buffer (50 mM sodium citrate pH 6.0, New England Biolabs) and with 2 µl PNGaseF (100 U, New England Biolabs), then incubated at 37ºC for 2hrs. PNGaseF is an N-encoglycolytic that hydrolyzes nearly all N-linked glycosylations directly at the asparagines residue. The cells were pelleted at 3000 g for 3 min, washed once in PBS. The cell pellets were lysed directly in 100 µl of 2x sample buffer that was pre-warmed to 80ºC.

2.9 Cellular Stimulation and Inhibitor Treatment Conditions

NIH3T3 cells expressing ephrinB1 constructs or vector alone, equally seeded in 24-well culture plates were serum starved overnight. Cells were stimulated with 0.5 - 4 µg/ml EphB2-Fc, or with 30-50 ng/ml PDGF-AB, or PDGF-BB (Upstate, Lake Placid, NY) as indicated. In the transient stimulation of cells with EphB2-Fc, cells were treated with EphB2-Fc for 10 min, then washed once with 0.5 % CCS/DMEM, and the cells were reincubated with fresh 0.5 % CCS/DMEM for up to 2.5 h. Cells stimulated with 1 mM sodium orthovanadate were treated for 60 min.

DAPT (10 µM final concentration; EMD Biosciences) and MG132 (5 µM final concentration; EMD Biosciences) were dissolved in DMSO and added to cells ~16 hours (+/- 4 hr) prior to cellular stimulations when indicated. Epoxomycin (1 µM final concentration; EMD Biosciences) and γ-Secretase Inhibitor X (50 µM final concentration; EMD Biosciences) were added to cells 4 hours prior to cellular stimulations when indicated. PP2 (10µM final concentration; EMD Biosciences) was added to cells ~15 min prior to cellular stimulations when indicated.

In all time courses and treatments, cells were lysed directly in 200 µl of 2x sample buffer that was pre-warmed to 80ºC.

2.10 Particulate Fractionation of Cells by Hypotonic Lysis

Following appropriate stimulation, cells were rinsed and then lysed with a cold hypotonic lysis buffer (1 mM EGTA, 1 mM EDTA, 2 mM $MgCl_2$, 10 mM KCl, 10 mM Tris pH 8.0, 0.1% ß-ME, 1 mM PMSF, 10 µg/ml A/L, 1 mM Na_3VO_4) on ice. The lysates were then dounce homogenized and 85.6 mg sucrose and 2 µl of 0.5 M EDTA

were added per ml of lysate. The lysates were then centrifuged at 3000 g and an aliquot of the resulting resuspended pellet was loaded onto the final gel. The resulting supernatant was then centrifuged at 100,000 g for 1 hour to precipitate the particulate fraction of cells. The supernatants from this centrifugation, which represents the soluble fraction of cells, was adjusted to 10% final volume with TCA and incubated on ice for 30 min to precipitate proteins. The precipitated proteins were resuspended in 75 µl 2x sample buffer and 75 µl unbuffered 1M Tris. The pellet from the high speed centrifugation, which encompasses the particulate fraction of cells, was washed once with lysis buffer and pelleted at 13000 g for 20 min at 4ºC, then resuspended in 150 µl 2x sample buffer. Equal volumes (75 µl) of each soluble and particulate fractions of the cells were loaded onto the gel.

2.11 Immunoprecipitations and Peptide Pulldowns

2.11.1 Anti-HA immunoprecipitations

NIH3T3 cells expressing HA/Myc ephrinB1wt or vector alone appropriately stimulated were lysed in RIPA buffer (0.1% SDS, 0.1% TritonX-100, 1 % sodium deoxycholate (Sigma), 10% glycerol, with 1 mM PMSF, 10 µg/ml A/L, 1 mM Na_3VO_4), incubated on ice for 15 min, and then dounce homogenized. The lysates were centrifuged at 13000 g at 4ºC for 10 min. The supernatant were incubated with 50 µl of a 50 % Protein-G bead slurry in PBS (Sigma) for 1 hr while rocking at 4ºC. The beads were pelleted and the pre-cleared supernatant was transferred to a new microfuge tube with 2 µl 12CA5 (mouse anti-HA monoclonal antibody serum) and rocked for 1 hr at 4ºC. 50 µl of a 50 % Protein-G bead (Sigma) slurry in PBS were added and the samples were

incubated for 1 hr at 4ºC with gentle agitation. The beads were then pelleted and washed three times with lysis buffer. Sample buffer without ß-ME that was pre-warmed to 80ºC was added to the beads and the entire samples were loaded onto a gel and then blotted with appropriate antibodies.

2.11.2 EphrinB Immunoprecipitation from Chick Tissue

Chick limbs were crudely dissected from embryonic (E) day 6 embryos. Approximately four full sets of limbs were used for each immunoprecipitation. The limbs were incubated in a final volume of 1 ml of Howard's Ringer buffer (62 mM NaCl, 0.8 M $CaCl_2$, 2.5 mM KCl, pH 7.2) and treated with 1 mM sodium orthovanadate for 1 hour while rocking at room temperature. At the end of the incubation, the limbs were quickly centrifuged to collect the tissue in the bottom of the microfuge tube and the supernatant aspirated. 1% TritonX-100 lysis buffer (1% TritonX-100, 150 mM NaCl, 10 mM NaPPi, 20 mM NaF, 50 mM Tris pH7.5, 1 mM PMSF, 10 µg/ml A/L, and 1 mM Na_3VO_4) was added to the limbs, dounce homogenized and incubated on ice for 15 minutes. The lysates were treated and immunoprecipitated 1 hr with 4 µl of anti-ephrinB (PAN) antibody (0.5 mg/ml, Zymed Laboratories), or with or with a mouse IgG1 isotype control antibody (0.5 mg/ml, BD Pharmingen), in a new microfuge tube. 100 µl of a 50 % Protein-G bead slurry in PBS (Sigma) was added to the supernatants for 1 hr with continued rocking at 4ºC. The beads were then pelleted and washed three times with cold lysis buffer. Sample buffer without ß-ME that was pre-warmed to 80ºC was added to the beads and the entire samples were loaded onto a gel and then blotted with appropriate antibodies.

2.11.3 EphrinB1 C-terminal Peptide Generation and Pulldown

The biotinylated ephrinB1 C-terminal peptide encompasses the following sequence: (biotin)-GPHYEKVSGDYGHPVYIVQEMPPQSPANIYYKV-CO_2H The peptide (File No. CS3714) was generated by the Alberta Peptide Institute, University of Alberta, Edmonton, Alberta. It was synthesized with an Applied Biosystems 430A Peptide Synthesizer using their standard method. The peptide purity was determined by HPLC.

NIH3T3 cells were lysed in 1 % NP-40 lysis buffer and incubated on ice for 15 min, then dounce homogenized. The lysates were centrifuged at 13000 g for 10 min at 4ºC. The supernatant was transferred to a new microfuge tube and incubated with 75 µl of Streptavidin beads (Pierce) for 1 hr with rocking at 4ºC. The beads were pelleted and the pre-cleared supernatant transferred to a new microfuge tube with 20 µl of biotinylated peptide (1 µg/µl in ddH_2O) then rocked at 4ºC for 1 hr. 75 µl of Streptavidin beads were added to the supernatant and then reincubated for 1 hr at 4ºC. The beads were then pelleted, washed three times with lysis buffer, then finally treated with 2x sample buffer that was pre-warmed to 80ºC and loaded onto a gel.

2.12 Silver Staining of SDS-Polyacrylamide Gel Electrophoresis (PAGE) and Mass Spectrometric Analysis

The following silver stain protocol is based on Rabilloud *et al.* (141) and Blum *et al.* (142). Following electrophoresis, the SDS-polyacrylamide gel was fixed 1 – 24 hrs in a solution of 10 % acetic acid (EMD Sciences)/30 % ethanol. The gel was then equilibrated in three 20 min incubations with 30 % ethanol and quickly incubated with

0.2 g/L sodium thiosulfate (Sigma) for 1 min before rinsing quickly in ddH_2O three times for 20 sec. The gel was then incubated with 0.2 % $AgNO_3$ (Sigma) with 0.3 % formaldehyde stock (Sigma) for 20 min, then washed with ddH_2O three times for 20 sec. The gel was developed by incubating twice for 5 min or longer in 6% Na_2CO_3 (Sigma), 0.2% formaldehyde, and 0.4mg/100ml of sodium thiosulfate. The development reaction was stopped by adding 3.5 ml of glacial acetic acid (Sigma) in the developer and then incubated with shaking for an additional 10 min. The gel was finally rinsed four times for 30 min each in ddH_2O. Silver stained bands of interest were cut out for the gel and frozen immediately at -80ºC until analysis.

Peptide extracts were analyzed on a Bruker REFLEXII (Bremen/Leipzig, Germany, Serial #: FM 2413) time of flight mass spectrometer using MALDI in positive ion mode. Peptides were fragmented using MALDI MS/MS analysis done on a PE Sciex API-QsTAR pulsar (MDS-Sciex, Toronto, Ontario, Canada, Serial # K0940105). The obtained sequence information was used to identify the protein(s).

2.13 Chick Specific Protocols

2.13.1 Large Scale DNA Preperation with CsCl Gradient Centrifugation

A 250 ml overnight culture of appropriate expression vector was grown overnight at 37ºC with rapid shaking in Luria broth (LB) supplemented with 0.1 mg/ml ampicillin (amp). The bacteria were pelleted at 5000 rpm for 10 min at 20ºC in a Sorvall SLA 1500 rotor. The pelleted bacteria were resuspended in 5 ml of solution I (50 mM glucose, 10 mM EDTA pH 8.0, 25 mM Tris.HCl pH 8.0) containing 1 mg/ml of lysozyme (Sigma)

and incubated at room temperature for 10 min. To the mixture was added 7.5 ml of freshly prepared solution II (0.2 N NaOH, 1% SDS) which was then swirled and incubated for 5-10 min. Then 7.5 ml of cold Solution III (3 M potassium acetate, 2 M glacial acetic acid) was added and incubated on ice for an additional 10 min. The bacterial lysate was centrifuged at 9000 rpm for 15 minutes at 4ºC in a Sorvall SS-34 rotor. The supernatant was transferred to a new centrifuge bottle and mixed with 0.6 volumes (~13.5 mls) of propan-2-ol (EMD Sciences), then incubated at room temperature for 20-30 min to precipitate the DNA. The DNA was pelleted by centrifuging at 9000 rpm for 20 minutes at 20ºC in a Sorvall SS-34 rotor. The pellet was rinsed with 70 % ethanol, centrifuged at 9000 rpm for 5-10 min, air-dried and finally resuspended in 3.8 ml of TE buffer (10 mM Tris, 1 mM EDTA pH 8.0) by vortexing.

3.8 g of CsCl and 0.3 ml ethidium bromide solution (10 mg/ml) were dissolved in the DNA solution. The resulting solution was loaded into an ultracentrifuge tube (Beckmann No. 362185) and centrifuged at 55000 rpm overnight at 20ºC in VTi 65.2 rotor. The plasmid band was extracted using a 1 ml syringe attached to a 20-21 gauge needle and then transferred to a microfuge tube. The ethidium bromide was extracted from the plasmid by washing several times with butan-1-ol (EMD Sciences) saturated with 5 M NaCl via vigorous shaking and brief centrifugation. The resulting DNA solution was dialysed in Spectra/Por dialysis tubing (Spectrum Laboratories, Inc.) in TE buffer overnight.

The dialysed DNA solution was diluted with 3 volumes of ddH_2O to which 1/10 volume of 3 M NaoAc was added and then mixed with 2.5 volumes of ethanol and precipitated on ice for 20-30 min. The DNA was pelleted by centrifugation at 9000 rpm

for 20 minutes at 4ºC in a Sorvall SS-34 rotor. The pellet was rinsed with 1-2 ml of 70% ethanol by vortexing, then repelleted by centrifugation at 9000 rpm for 5 minutes at 20ºC. The pellet was air-dried at room temperature and resuspended in an appropriate volume of sterile TE buffer overnight at 4ºC.

2.13.2 In ovo electroporation

Fertilized Hubbard broiler hen eggs (Klaas and Elvina Itjsma, Airdrie, AB) were incubated at 38°C and embryos staged according to the method of Hamburger and Hamilton (143).

In ovo electroporation was performed as previously described (144). Purified pCIG2 ephrinB1 constructs described in section **2.1** were prepared via the CsCl method described in section **2.13.1** and resuspended in sterile TE buffer at a concentration of 1-1.7 µg/µl. One twentieth volume of 0.1 % Fast Green FCF (Sigma) was added to the DNA to facilitate the visualization of the injected sites (see **Figure 2.4**). Taped eggs were cut open to reveal the embryo. With the use of Zeiss Stemi 2000 microscope, the purified plasmid DNA was injected into HH 9-12 staged embryos via a glass needle and the Pneumatic Picopump PV820 (World Precision Instruments, Stevenage, Hertfordshire, England). Electroporation of the neural tube lumen results in the specific transfer of a DNA construct, which is negatively charged, to the half of the neural tube that is positioned next to the positive electrode. The contralateral side of the neural tube does not receive electroporated DNA and serves as an internal, paired negative control. Following successful injections, the embryos were electroporated with the following electroporation parameters: 25-35 V in 7-10 pulses of 25 msec, with 1 sec intervals

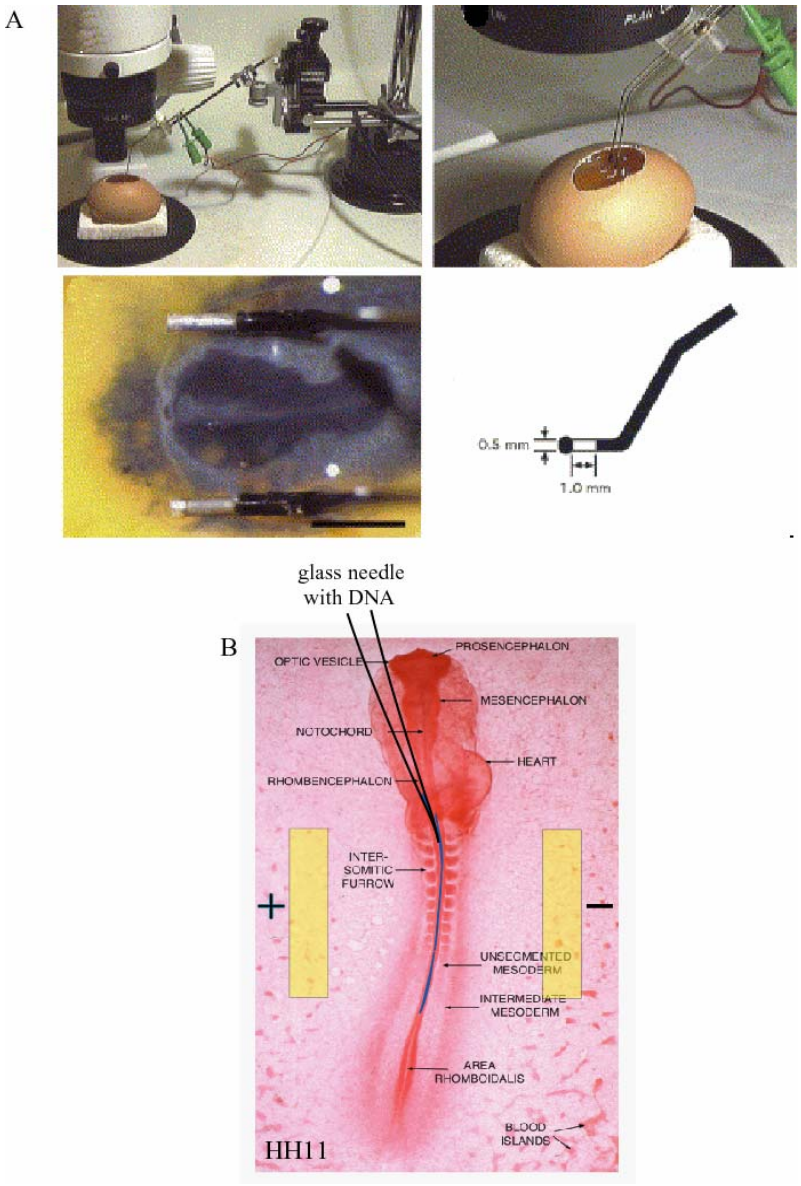

Figure 2.4: *In ovo* electroporation set-up.

The general set-up of the microscope and electrodes used during electroporation are shown in (A). The targeted delivery of DNA (in blue) via a glass needle into an HH 11 embryo, as well as the relative positioning of the electrodes (yellow bars), are shown in (B). Adapted from Nakamura *et al.*, *Mech Dev*, 2004 and Hornbruch, *Methods Mol Biol*, 1999 (145).

between pulses, delivered by the ElectroSquarePorator ECM 830 (BTX Harvard Apparatus, Holliston, MA, USA). Following electroporations, embryos were resealed with tape and reincubated for an additional 24-48 hours at 38ºC.

Whole chick embryos were then removed from the egg and partially dissected in Howard's Ringer prior to fixation in cold 4% paraformaldehyde (PFA; Sigma) in 0.1 % diethyl pyrocarbonate (DEPC)-treated PBS (Sigma) overnight at 4ºC.

2.13.3 Synthesis of Digoxigenin-Labeled RNA probe

A reaction was mixed in the following order at room temperature: 8.5 µl of sterile DEPC-treated ddH_20, 4 µl of 5x Transcription Optimized buffer (final 40 mM Tris.HCl pH 7.9, 6 mM $MgCl_2$, 2 mM spermidine, 10 mM NaCl, Promega), 2 µl of 0.1 M DTT (Promega), 2 µl of 10x digoxigenin (DIG) Nucleotide mix (pH 8.0) (Roche), 2 µl of linearised plasmid template (0.5 µg/µl) (*Tlx-3* template previously described in (146)), 0.5 µl of Placental ribonuclease inhibitor (40 U/µl) (Roche), and 1 µl of SP6, T7 or T3 RNA polymerase (10 - 20 U/µl) (Promega). The reaction was incubated at 37^o C for exactly 2 h. A 1 µl aliquot was removed and ran on 1.5 % agarose (Invitrogen)/0.5x TBE (final 0.45 mM Tris, 0.45 mM boric acid, 1 mM EDTA) ribonuclease free gel containing 0.5 µg/ml ethidium bromide to ensure the proper transcription of the RNA probe. 2 µl of ribonuclease-free DNase 1 (10 U/µl) (Roche) was added to the remainder of the probe and incubated at 37^o C for 15 min. 100 µl DEPC-treated ddH_20 and 10 µl of 4 M LiCl (DEPC-treated) were subsequently mixed with the RNA, then 300 µl ethanol was added to precipitate the RNA on ice for 30 min. The RNA was pelleted at 13000 g for 15-20

min and then washed with 70 % ethanol (in DEPC-treated ddH_2O), and repelleted. The ethanol was removed and the pellet was air-dried and resuspended in DEPC-treated ddH_2O at approximately ~0.1 μg/μl and stored at -20^oC.

2.13.4 Wholemount in situ *Hybridization*

Wholemount *in situ* hybridization of intact embryos was performed using a DIG-labeled *Tlx-3* RNA probe (146). The following protocol is based on Wilkinson's (147) except that the RNAse step was omitted.

PFA-fixed embryos were washed twice in PBT (DEPC-treated PBS with 0.1 % Tween-20). The embryos were dehydrated via a series of washes with rocking of the following solutions: 25 % methanol (EMD Sciences)/75 % PBT for 15 min, 50 % methanol/50 % PBT for 15 min, 75 % methanol/25 % PBT for 15 min, 100 % methanol for 10 min twice. The embryos were subsequently rehydrated by rocking at room temperature with the following series of washes: 75 % methanol/25 % PBT for 10 min, 50 % methanol/50 % PBT for 10 min, 25 % methanol/75 % PBT for 10 min, PBT for 10 min twice. The embryos were bleached with 6 % hydrogen peroxide (Sigma) in PBT for 1 hr, then washed three times with PBT. The specimens were treated with 10 μg/ml proteinase K (Roche) in PBT for an appropriate time (HH 17 for 10 min, HH 21 for 15 min). The embryos were rinsed twice with PBT for 10 min and then post-fixed with 0.2 % gluteraldehyde (Sigma)/4 % PFA in PBT for 20 min.

After three 10 min washes with PBT, the embryos were incubated with pre-heated hybridzation solution (50 % formamide (EMD Biosciences), 50 μg/ml yeast tRNA (Roche), 1% SDS, 50 μg/ml heparin (Sigma), in 5x SSC pH 4.5 (final 0.75 M NaCl, 75

mM sodium citrate)) without riboprobe and incubated at 72ºC for 1 hr. The solution was then replaced with hybridization solution containing approximately 1 µg/ml of DIG-labeled *Tlx-3* RNA probe, previously described in (146), and incubated at 72ºC overnight. The specimens were washed twice with Solution 1 (50 % formamide, 5x SSC pH 4.5, 1 % SDS) for 30 min at 72ºC and then twice with Solution 3 (50 % formamide, 2x SSC pH 4.5) at 67ºC. The embryos were then washed three times with TBST (1x TBS with 1 % Tween-20) supplemented with fresh 2 mM levamisole (Sigma) for 15 min at room temperature.

The embryos were then incubated in a pre-block solution of 10 % goat serum (Gibco-BRL) in TBST for 60-90 min at room temperature. During this time, 0.5 ml of TBST with 3 mg of embryo powder was heated to 70ºC for 30 min, then cooled on ice. To this solution were added 5 µl of goat serum and 1 µl anti-DIG antibody conjugated to alkaline phosphatase (AP) (Roche) in order to preabsorb the antibody for 1 hr at 4ºC. This mixture was microfuged at 13000 g for 10 min and the supernatant diluted to a final volume of 2 ml with 1 % goat serum in TBST. The pre-block solution was removed from the specimens and replaced with the preabsorbed anti-DIG-AP antibody solution and rocked overnight at 4ºC.

The embryos were washed three times for 15 min with TBST, and then washed hourly throughout the day at room temperature and then overnight at 4ºC. The specimens were washed three times for 15 min with freshly prepared NTMT (100 mM NaCl, 100 mM Tris.HCl pH 9.5, 50 mM $MgCl_2$, 0.1 % Tween-20, 2 mM levamisole). The wash solution was exchanged with NTMT containing 3.5 µl/ml each of nitroblue tetrazolium chloride (NBT) and 5-bromo-4-chloro-3-indoyl-phosphate (BCIP) (Roche) and the

samples covered in foil, placed in a dark place at room temperature and left to develop to the desired intensity. To stop the reaction, samples were washed with PBT supplemented with 20 mM EDTA. Specimens were refixed using 4 % PFA in PBS before subsequent immunohistochemistry, sectioning and/or storing.

2.13.5 Wholemount Immunohistochemistry

The following protocol for wholemount immunohistochemistry of chick is based on that described by Davis *et al.* (148). The primary antibodies and dilutions used in immunohistochemistry, along with the secondary antibodies used for their detection, are listed in **Table 5**. Secondary biotinylated or HRP-conjugated rabbit and mouse IgG antibodies (Jackson ImmunoResearch Laboratories Inc., West Grove, PA) were used where appropriate and were later visualized with or without Vectastain (Vector Laboratories, Burlingame, CA) and DAB (Sigma).

PFA-fixed embryos were washed three times with PBS then treated with methanol:DMSO (4:1) overnight at 4ºC. Endogenous peroxidases were subsequently blocked and the specimens bleached via treatment with methanol:DMSO:30 % peroxide (4:1:1) for 4-5 hrs at room temperature. The embryos were rehydrated by rinsing sequentially in 50 % methanol for 45 min, 15 % methanol for 45 min, and PBS for 30 min. After being washed twice in PBSMT (2 % skim milk powder, 0.1 % TritonX-100 in PBS) for 1 hr at room temperature, the specimens were incubated 3-5 days at 4ºC with primary antibody appropriately diluted in PBSMT + 0.04 % sodium azide (Sigma). The embryos were then washed twice for 2 hrs at 4ºC with PBSMT, followed by three more washes at room temperature with PBSMT, and then incubated 1-2 days with appropriate

Table 5: Antibodies and their Dilutions for Chick Wholemount Immunohistochemistry

Primary Antibody	Manufacturer	Dilution	Secondary Antibody
anti-ephrinB (PAN)	Zymed Laboratories	1:10000	1:500 biotinylated anti-mouse IgG1
anti-LIM1/2 (4F2)	Developmental Studies Hybridoma Bank	1:5	1:200 anti-mouse HRP
anti-ß-tubulin (Tuj1)	Covance Research Products Inc.	1:200	1:500 biotinylated anti-mouse IgG2a
anti-GFP	Molecular Probes	1:1000	1:200 anti-rabbit HRP
Mouse IgG1 Isotype Control	BD Bioscience Pharmingen	1:10000	1:500 biotinylated anti-mouse IgG1

secondary antibody diluted in PBSMT. The specimens were again washed twice for 2 hrs at 4ºC with PBSMT, followed by three more washes at room temperature with PBSMT.

For HRP-conjugated secondary antibodies, the embryos were incubated with 0.5 mg/ml inactive DAB in PBT (0.2 % BSA, 0.1 % TritonX-100 in PBS) for 20 min covered in foil. Fresh DAB in PBT activated by 0.03 % peroxide was added to the embryos which were developed to the desired colour density for approximately 20 min. The reaction was stopped by the addition of PBT + 0.04 % sodium azide.

For biotinylated-coupled secondary antibodies, embryos were washed for 20 min in PBT at room temperature. The embryos were incubated overnight in 0.1 % TritonX-100 in PBS supplemented with 2 µl/ml Vectastain ABC solution. The embryos were then washed twice for 2 hrs at 4ºC with PBSMT, followed by three more washes at room temperature with PBSMT, and then developed with DAB as described above.

Embryos were then stored in 4 % PFA in PBS at 4ºC prior to subsequent analysis and/or sectioning.

2.13.6 Vibratome Sectioning

Following wholemount *in situ* hybridization and/or immunohistochemistry, selected embryos were embedded in a mixture of gelatin and albumin (27 % albumin (from chicken egg white, Sigma), 4.5 % gelatin (Sigma), 18% sucrose (Sigma) in PBS + 0.04 % sodium azide) and transverse sectioned at 25-50 µm using a Leica VT100S vibratome (Leica Microsystems). Sections were then dehydrated with ethanol and xylene (Fisher) and mounted under coverslips with Entellan mounting medium (EMD Science).

2.13.7 Confidence Interval Calculation

The confidence interval of manipulated chick neural tubes that exhibited a phenotype in our samples was calculated to estimate the proportion of chick neural tubes in the population that would exhibit a phenotype (149).

In our calculation, the variable y_i was an indicator, where $y_i=1$ if the neural tube exhibited a phenotype, and $y_i=0$ if it did not. Letting p (an estimate) denote the proportion in the sample with a phenotype:

$$p = \frac{1}{n}\sum_{i=1}^{n} y_i$$

The variance was estimated as follows:

$$\mathrm{var}(p) = \frac{p\ (1-p)}{n-1}$$

Finally, the 95% confidence interval was determined as follows:

$$p \pm t_{\alpha/2,\,n-1}\sqrt{\mathrm{var}(p)}$$

Sample calculation: ephrinB1wt overexpression resulted in 9/19 neural tubes exhibiting a phenotype following the manipulation; p=0.473, n=19, var = 0.0139, $t_{\alpha/2,n-1}$=2.101, confidence interval (0.226, 0.721).

The p and confidence intervals for each ephrinB1 construct were graphed using the program R (150).

Chapter Three: Cell-Based Analysis of EphrinB1 Signaling

Chapter Three: Cell-Based Analysis of EphrinB1 Signaling

3.1 Introduction

EphrinBs have signaling activities independent from Eph receptors that are required in physiological processes such as the formation of the posterior tract of the anterior commissure (84), cardiac valve development(84), as well as urorectal development (24). The function of ephrinB2 in these processes was shown to be dependent on the presence of its cytoplasmic tail as transgenic mice strains containing an ephrinB2 construct with a large cytosolic truncation in place of the wild type gene exhibited defects in axon pathfinding in the anterior commissure, thickened aortic and pulmonary valves, and hypospadias.

The ephrinB cytosolic domain has a highly conserved 33 aa sequence at the C-terminus. In this conserved stretch are five tyrosine residues, that when phosphorylated, may act as phosphotyrosine dependent binding sites, a short polyproline stretch that may mediate SH3-based interactions, and a PDZ-motif at the carboxy end that may mediate interactions with PDZ-domain containing proteins. Cellular ephrinB proteins are tyrosine phosphorylated following treatment with clustered EphB receptor ectodomains or PDGF (87). The tyrosine phosphorylation of B-class ephrins is thought to modulate downstream signaling from these proteins. Src-family kinases have been implicated in the tyrosine phosphorylation of ephrinBs, and their downstream signaling, in response to EphB (87, 89). To date, only a handful of proteins have been shown to interact with the cytoplasmic tail of ephrinB. These include the adaptor protein Grb4, which is recruited via SH2-based interactions to the cytoplasmic tail of ephrinB (41), and PTP-BL (89),

PDZ-RGS3 (93), and GRIP (92) via PDZ-based interactions. These proteins modulate ephrinB cellular responses *in vitro* and its tyrosine phosphorylation following treatment with clustered EphB receptors. Although effects of ephrinB function and signal propagation are dependent on its cytosolic tail, little is known concerning the specific signaling pathways ephrinBs employ to mediate cellular signaling.

Spatial regulation of ephrinB proteins on the plasma membrane may be involved in regulating their signaling(109). Lipid rafts are plasma membrane microdomains enriched in cholesterol and glycosphingolipids and are thought to act as highly specialized signaling centers as certain signaling proteins are concentrated within them (105). EphrinBs are biochemically associated with lipid rafts in cell lines and in both embryonic and adult mouse brain tissues (89, 92, 110). It has been demonstrated in our laboratory that soluble EphB receptor ectodomains can stimulate ephrinB1 to translocate into a lipid raft fraction in NIH3T3 fibroblasts transfected with this protein (151), suggesting ephrinB1 may localize to lipid rafts transiently when activated by EphB receptors. It is clear from recent reports that ephrinB1 association with lipid rafts is important in tailoring its signaling responses. EphrinB1's cytoplasmic tail is able to specifically recruit GRIP, a modular PDZ-domain containing protein, into lipid rafts when they are expressed together (92). An uncharaterized GRIP-associated serine/threonine kinase was also recruited to the ephrinB1/GRIP complexes (92). The regulation of tyrosine phosphorylation of ephrinB1 by Src-family kinases was also moderated by lipid rafts (89), as was ephrinB1 modulation of ß1-integrins (152). Lipid rafts have also been implicated in the downregulation of ephrinB1 tyrosine phosphorylation by PTP-BL (89). Deletion of the majority of ephrinB1's cytosolic tail

abrogated its association with these specialized microdomains (92) suggesting the presence of an intracellular mechanism responsible for the intracellular localization of ephrinB1. Taken together, lipid rafts may facilitate temporal and spatial B-class ephrin signaling via modulation of signal complex formation or downregulation and thus ultimately contribute in mediating their cellular responses.

Based on the evidence provided in our lab and others (92, 110, 153), it was hypothesized that **the cytoplasmic domain of ephrinB1 contains specialized regions for inducing signaling events and that lipid rafts are involved in mediating these responses**. The specific aims undertaken to examine this hypothesis were:

1. To construct ephrinB1 cytoplasmic domain mutants
2. To characterize the ability of the ephrinB1 cytoplasmic domain mutants:
    i. to translocate to lipid rafts upon stimulation with clustered EphB2 receptor ectodomains
    ii. to be tyrosine phosphorylated in response to clustered EphB2 receptor ectodomains
    iii. to be tyrosine phosphorylated in response to PDGF
3. To identify ephrinB1 cytoplasmic tail interacting proteins

3.2 Results

3.2.1 Construction of EphrinB1 Cytoplasmic Domain Mutants and Establishment of their Stably-Expressing NIH3T3 cell lines

3.2.1.1 Experimental Design of EphrinB1 Cytoplasmic Domain Mutants

To characterize cytoplasmic regions of ephrinB1 required for its translocation to lipid rafts, as well as to mediate its tyrosine phosphorylation response to EphB receptors and PDGF, a series of deletion mutants were designed and constructed using human wild type (wt) ephrinB1 as the template (**Figure 3.1**).

The first construct was full-length or wild type ephrinB1 protein (B1wt), while the second construct was missing the carboxy-terminal amino acid valine (B1Δ1). It has previously been demonstrated that mutation of this residue eliminates the interactions of ephrinB1 with PDZ-domain containing proteins such as PTP-BL (154). Although deletion of this terminal amino acid may not abolish all PDZ interactions of ephrinB1, generally PDZ domains prefer to bind to hydrophobic amino acids at the C-terminus (155). Complete ablation of ephrinB1's YYKV PDZ-binding motif defines the third construct (B1Δ4). In the B1Δ12 construct, the PDZ-motif as well as the polyproline stretch were eliminated. All of the highly conserved carboxy-terminal 33 amino acids (aa), and thus potential PDZ-based, phosphotyrosine, or polyproline interactions, were ablated within the B1Δ33 construct.

A putative juxtamembrane polybasic domain in the cytoplasmic portion of ephrinB1 was condensed in the B1ΔKLR construct. This deletion removed nine of the

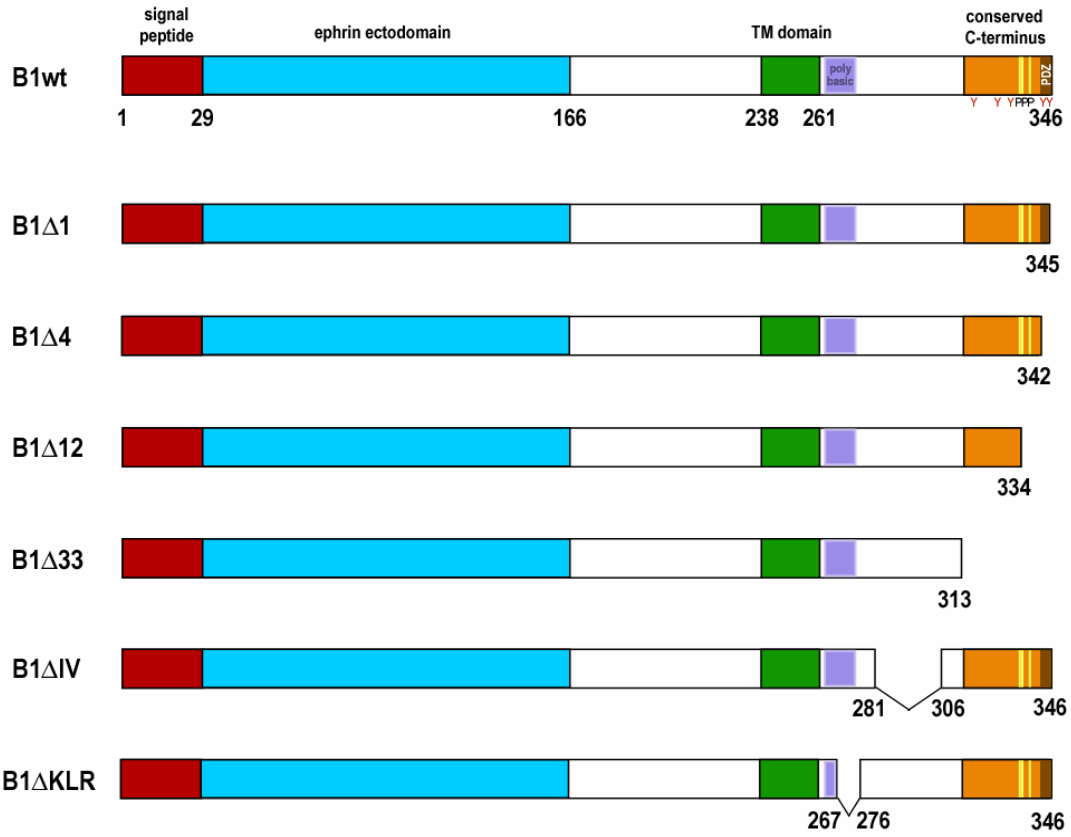

Figure 3.1: Schematic of EphrinB1 Cytoplasmic Mutant Constructs.

Purple box indicates polybasic domain; yellow lines and PPP indicate poly-proline positions, brown box indicates PDZ motif; red Y indicate positions of conserved tyrosine residues; TM indicates transmembrane domain. Numbers below schematics indicate relevant amino acid positions.

thirteen amino acids in this stretch. A few basic residues were conserved to ensure appropriate membrane topology of B1ΔKLR. B1ΔKLR and ephrinB1wt membrane topologies were compared with five different membrane topology prediction programs: MEMSAT (156), HMMTOP (157), TopPred2 (158), TMHMM (159), and TMpred (160), which unanimously indicated the constructs possessed identical topologies. Although the exact sequence of residues among all three ephrinB proteins may differ, the polybasic nature of this juxtamembrane sequence was conserved (**Figure 1.3**). The protein MARCKS (161), syndecan-4 (162, 163), and Tubby (164), are examples of proteins which harbour a polybasic domain by which they interact with phosphatidylinositol 4,5-bisphosphate ($PI(4,5)P_2$ or PIP_2) to mediate interactions with other proteins (165). Cdc42 is a protein containing a small polybasic domain that functions in homodimerization of Cdc42 molecules to increase their intrinsic GTPase activity (166), and similarly, syndecan-4 multimerization is also dependent on its polybasic domain (163). In light of the functions mediated by polybasic domains in other proteins, ephrinB1's polybasic domain may be required for certain aspects of its signaling, such as protein-protein interactions, multimerization of ephrins, or PIP_2 interactions. PIP_2 phospholipids are enriched in lipid rafts (167) and thus interactions with them may target ephrinB1 to these microdomains. Thus by mutating ephrinB1's polybasic domain novel regulatory signaling functions may be uncovered.

The final construct generated was B1ΔIV. Song *et al.* (39) reported that residues 253-300 of ephrinB2, which span the polybasic domain but excludes the last highly conserved 33 aa, were found to form aggregates. The corresponding region of ephrinB1 are residues 266-313, which have a 60% identity to ephrinB2. It is not clear from this

study whether the aggregation was due to the polybasic domain, or to the sequence which intervenes the polybasic region and the conserved carboxy 33 aa. To assess whether the intervening (IV) sequence may have an important function in signaling, such as multimerization of ephrinBs, the B1ΔIV construct was designed wherein a large portion of the intervening sequence was ablated.

3.2.1.2 Establishment of NIH3T3 Cell Lines Stably Expressing EphrinB1 Cytoplasmic Mutant Constructs

NIH3T3 fibroblasts expressing the ephrinB1 constructs were established in order to characterize the cytosolic region of ephrinB1 involved in regulating its EphB-mediated lipid raft translocation and tyrosine phosphorylation responses to EphB receptors and PDGF. NIH3T3 cells used herein have been used previously to characterize ephrinB1 signaling (87, 89). The ephrinB1 constructs described above were subcloned and transfected into NIH3T3 cells to establish pooled population cell lines.

To confirm cell surface expression of the ephrinB1 constructs, EphB2-Fc receptor body staining of their cell lines was assessed by flow cytometry (**Figure 3.2**). EphB2-Fc receptor bodies are fusion proteins composed of EphB2 receptor ectodomains and the Fc portion of the human Immunoglobulin (Ig) class G_1 gene (168). These fusion proteins result in dimerization of EphB2 receptor ectodomains thus enabling them to bind and cluster ephrinB1 on cells. Receptor-bodies, like EphB2-Fc, are also used to study activation of ephrin cellular responses. From the flow cytometry analysis, it was ascertained that the 3T3 cell lines expressing ephrinB1 constructs were positively stained

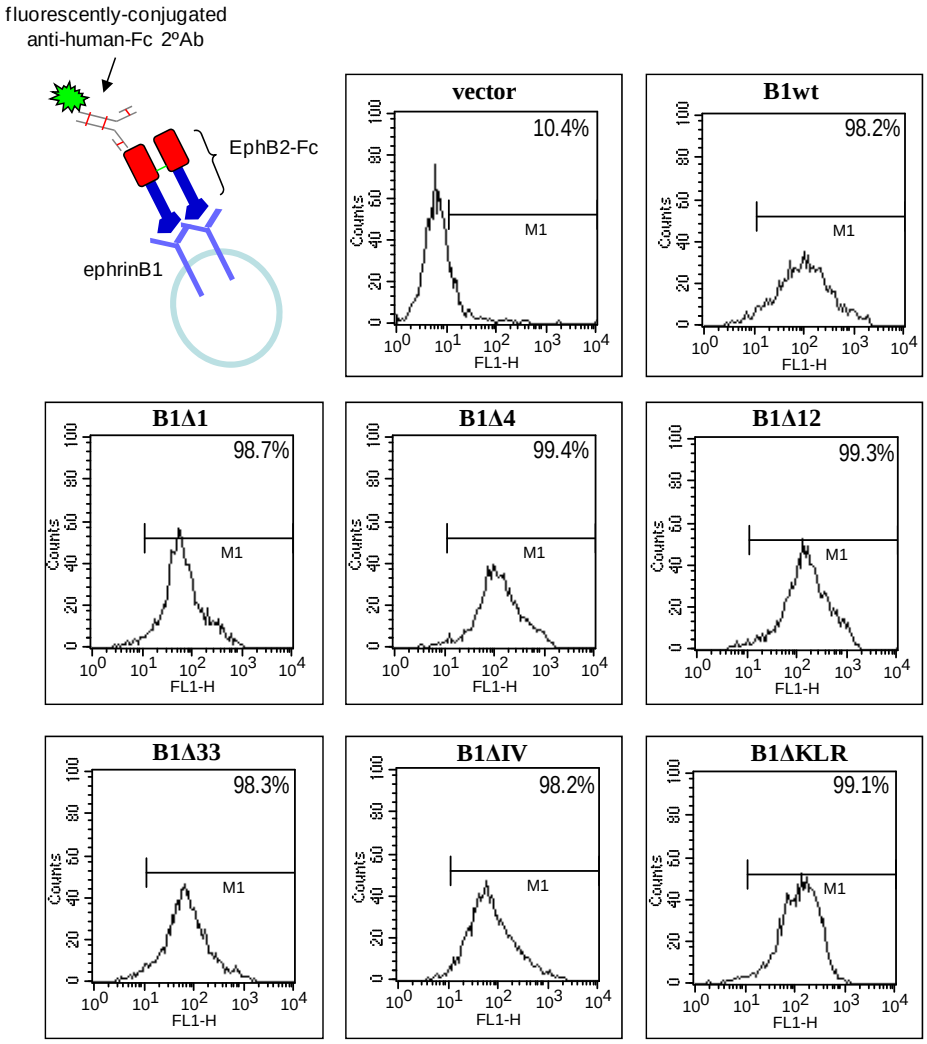

Figure 3.2: Positive cell surface expression of ephrinB1 constructs in stably NIH3T3 cells.

Cells expressing the ephrinB1 constructs or vector alone were stained with EphB2-Fc receptor bodies detected by anti-human-Fc Alexa-488 fluorescently conjugated secondary antibody (see diagram). The staining was assessed by flow cytometry (fluorescence on x-axis) and the percentage of gated cells are indicated in the top right hand corner for each construct. (n=1)

by EphB2-Fc (**Figure 3.2**), indicating cell surface expression of properly-folded ephrinB1 ectodomains for all constructs. The vector control cells were not stained by EphB2-Fc.

Cellular expression of the constructs was also confirmed by anti-ephrinB immunoblotting (**Figure 3.3**). Equal amounts of lysate protein, as confirmed by the loading control actin, were compared. Anti-ephrinB Western blotting analysis confirmed expression of all constructs except B1Δ33. The commercial anti-ephrinB antibody used reportedly detects an epitope in the carboxy-terminus of the protein. Due to our inability to detect B1Δ33, it is likely that this antibody's epitope lies more specifically in the region between amino acid positions -11 and -32 relative to the C-terminus. As discerned from the Western blot, there were differences in molecular weight and expression level between the constructs expressed in 3T3 cells (**Figure 3.3**). B1ΔKLR was slightly smaller in molecular weight relative to ephrinB1wt by ~1 kDa, which corresponds to its expected molecular weight decrease of ~1.2 kDa. The expression of B1ΔKLR was very low relative to ephrinB1wt. B1ΔIV was observed at a smaller molecular weight relative to B1wt by ~3 kDa, correlating with its predicted decrease in molecular weight by ~2.8 kDa. B1ΔIV expression levels were similar to those of ephrinB1wt, while those of B1Δ4 were relatively higher, and those of B1Δ12 slightly lower.

The cytosolic mutants with deletions in the PDZ-motif, B1Δ4 and B1Δ12, demonstrated an unexpected increase in molecular weight of ~3 kDa, where a decrease of ~0.5 kDa and ~1.4 kDa, respectively, were anticipated (**Figure 3.3**). A 3 residue YKV deletion in the PDZ-motif of ephrinB1 by Palmer *et al.* (89) also resulted in a similar size

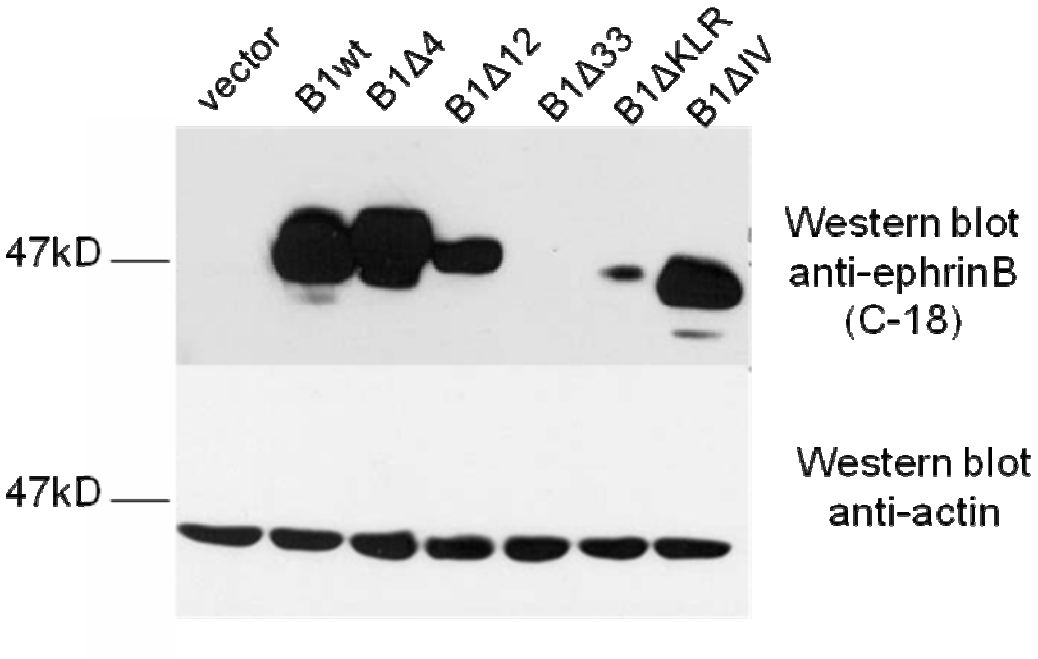

Figure 3.3: Protein Expression of EphrinB1 constructs in NIH3T3 cells.

Equal amounts of protein (100µg) were loaded (n=3). The epitope for the anti-ephrinB1 antibody lies in the last 33 amino acid, a region completely ablated in B1Δ33, thus this particular construct is undetectable by Western blotting.

increase of their mutant relative to ephrinB1wt. The relative increase in molecular weight may have been due to a conformational change or a post-translational modification(s). Since PDZ interactions are known to be involved in sorting of proteins (169-171), it is possible that ephrinB1wt and B1Δ4 may be differentially sorted and this may have translated into differences in their glycosylations. EphrinB1 possesses one N-glycosylation site in its extracellular domain. Differences in N-glycosylation between B1wt and B1Δ4 were determined by treating cell lysates with PNGaseF, a glycolytic enzyme that cleaves the entire N-glycolytic modification from proteins. B1wt and B1Δ4 both decreased in molecular weight in equal proportion following PNGaseF treatment (**Figure 3.4**). Thus it is apparent their N-glycosylations are approximately the same relative size and are not responsible for the difference in molecular weight observed between the proteins. Another type of post-translational modification, such as phosphorylation, or a conformational change may have been responsible for the observed size differences between ephrinB1wt and of B1Δ4 and B1Δ12.

From these experiments, it was confirmed that the NIH3T3 cells expressed the ephrinB1 constructs and that the mutant constructs were able to interact with EphB2 receptor ectodomains. Thus, by establishing these cell lines, the function of the cytoplasmic interaction in the regulation of ephrinB1 signaling could next be assessed.

3.2.2 Characterization of the Ability of EphrinB1 Cytoplasmic Domain Mutants to Translocate to Lipid Rafts upon Stimulation with Clustered EphB2 Receptor Ectodomains

Recent reports suggest that lipid rafts play an important role in tailoring ephrinB1

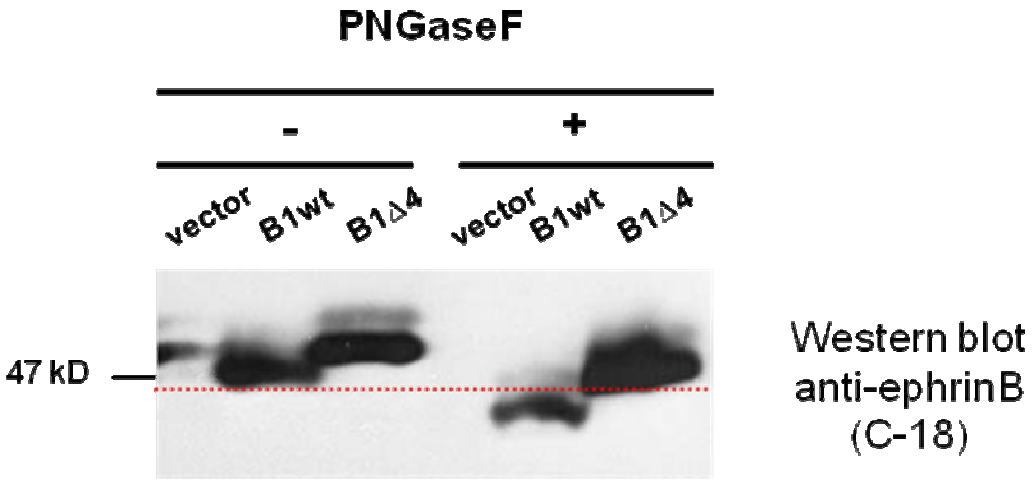

Figure 3.4: Differences in N-glycosylation were not responsible for the molecular weight increase in B1Δ4 relative to B1wt.

NIH3T3 cells expressing the constructs were treated with PNGaseF, an N-glycolytic enzyme (n=2).

signaling responses (89, 92). The translocation of ephrinB1 into lipid rafts was found to be induced by soluble-EphB2 receptor stimulation (151) and the partitioning of B-class ephrins into these microdomains was dependent on its cytoplasmic tail (92). Taken together, these studies suggest the requirement of an intracellular mechanism to mediate the EphB-induced lipid raft translocation of ephrinBs. The NIH3T3 cells lines expressing the ephrinB1 cytoplasmic mutant constructs were used to assess which regions of the protein are required for translocation.

EphrinB1wt-expressing NIH3T3 clonal cell line #9 (B1-9) was previously established in our lab to characterize ephrinB1 lipid raft translocation (151) and was used as a positive control for this experiment. B1wt and the clonal B1-9 cells were treated with 0.5-2.0 μg/ml EphB2-Fc for 20 min prior to lysis in cold, 1% TritonX-100 lysis buffer. Lipid rafts were biochemically isolated from cells based on their insolubility in cold, non-ionic detergents, such as TritonX-100, and their buoyancy in high-density sucrose gradients. The lysates from the cells were centrifuged on a high-density (40-5% w/v) sucrose gradient and the buoyant lipid raft fractions collected were analyzed by anti-ephrinB Western blotting (**Figure 3.5**). An EphB2-Fc dose-dependent translocation of ephrinB1 into lipid rafts was observed in the B1wt-expressing cells and a dose of 0.5 μg/ml of EphB2-Fc was used in subsequent lipid raft experiments.

To assess cytosolic regions required for ephrinB1 lipid raft translocation, NIH3T3 cells expressing the ephrinB1 cytosolic mutants were treated with EphB2-Fc and their lipid raft fractions were isolated and analyzed by anti-ephrinB immunoblotting (**Figure 3.6**). B1Δ4, B1Δ12, B1ΔKLR, and B1ΔIV were able to translocate to lipid rafts

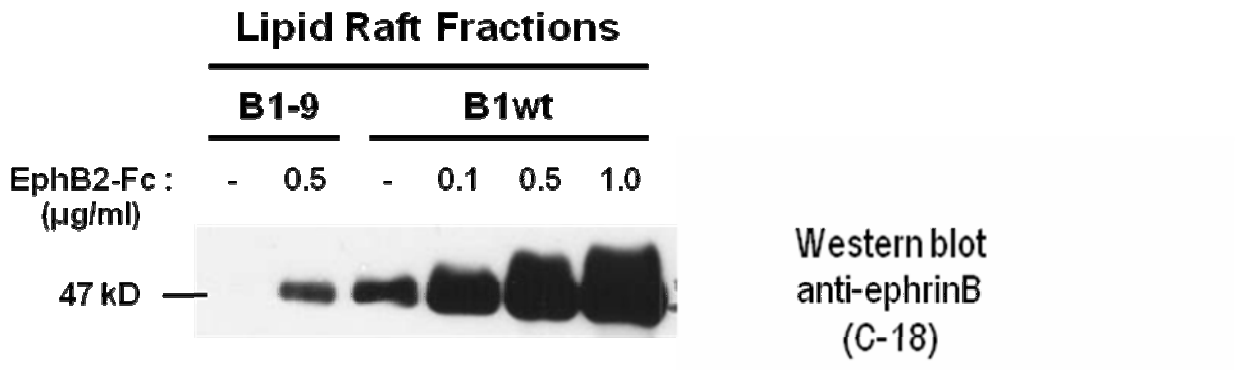

Figure 3.5: EphrinB1wt translocated to lipid rafts following treatment with EphB2-Fc.

EphrinB1wt NIH3T3 cell line and EphrinB1-9 NIH3T3 clonal cell line #9 (B1-9) were treated with the indicated concentration of EphB2-Fc for 20 minutes. The cells were then lysed in cold 1% Triton X-100 lysis buffer and the lipid raft fraction of these lysates were isolated via sucrose density gradient centrifugation. (n=2)

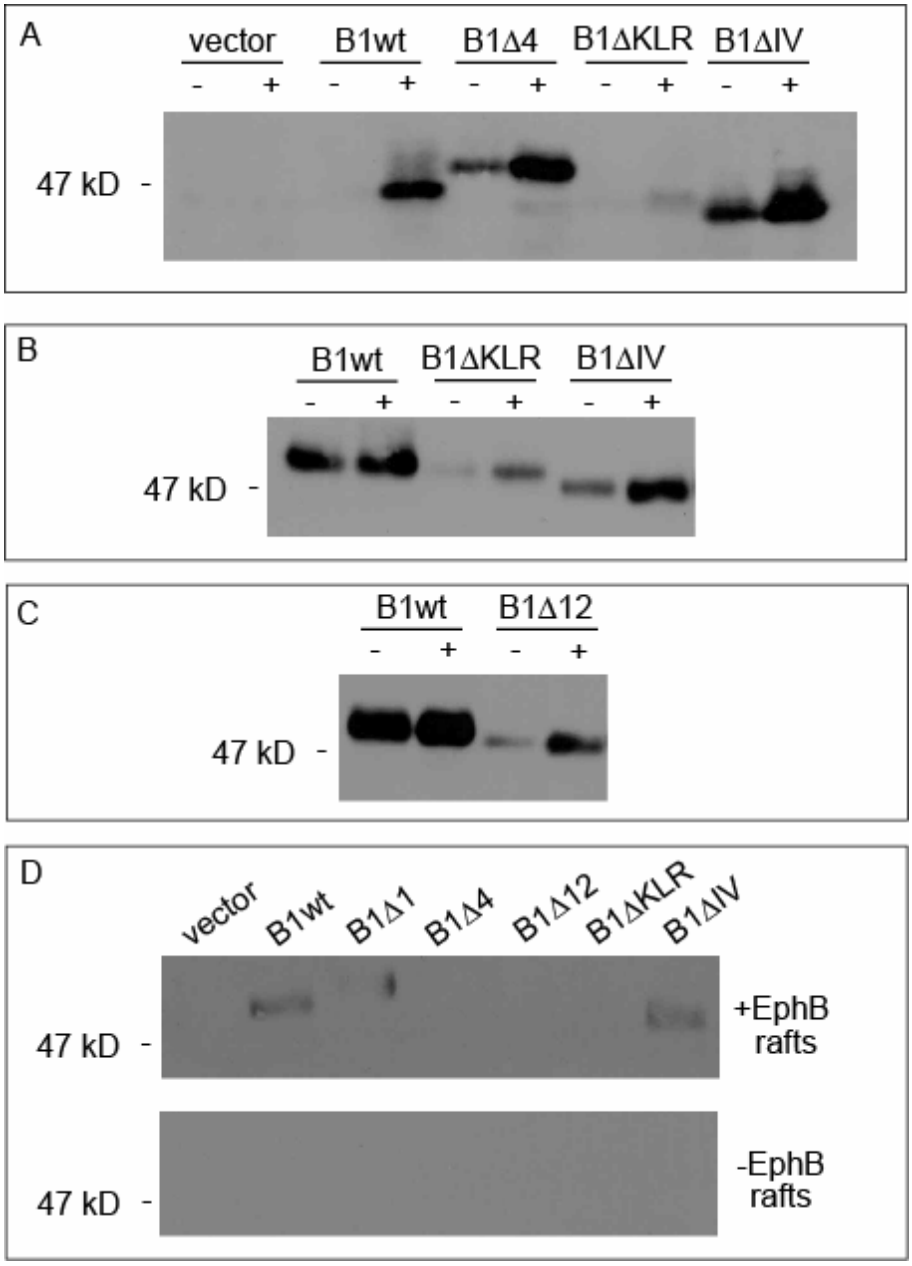

Figure 3.6: EphrinB1 cytoplasmic mutants translocate to lipid rafts.

NIH3T3 cells expressing the indicated ephrinB1 cytoplasmic mutant constructs were treated for 20 minutes with 0.5 µg/ml EphB2-Fc. The cells were then lysed with cold 1% TritonX-100 lysis buffer. The lipid raft fractions were isolated via sucrose density gradient centrifugation. Panels A, B, C, and D represented the results of lipid raft translocation experiments undertaken in this study.

post-stimulation to the same relative extent as the wild type protein. As before, B1Δ33 could not be assessed due to our antibody detection limitations. Differences in basal levels of ephrinB1 in the lipid rafts noted for particular constructs in this experiment reflected slight variations in cultured cell density prior to lysis, as in our hands ephrinB1 expressing cells grown at higher density exhibited increased basal levels of the protein in lipid rafts. From this study, the PDZ-motif, polyproline stretch, polybasic domain, and intervening sequence of ephrinB1 did not appear to be involved in EphB2-Fc-induced lipid raft translocation of ephrinB1 in 3T3 cells. Our experiments are thus consistent with previous studies indicating that the cytosolic stretch uniquely deleted in B1Δ33 may be involved in mediating EphB2-Fc-induced lipid raft translocation.

3.2.3 Tyrosine Phosphorylation of EphrinB1 Cytoplasmic Mutants in Response to Clustered EphB2 Receptor Ectodomains

EphB receptor-induced tyrosine phosphorylation of B-class ephrins are thought to link B-class ephrins to downstream signaling pathways (87). Fibroblasts expressing the ephrinB1 constructs were next employed to describe regions of the ephrinB1 cytoplasmic tail required to mediate tyrosine phosphorylation in response to EphB2-Fc. To investigate this, a commercial anti-phospho-ephrinB antibody, that specifically recognizes phosphorylated tyrosines at positions -18 and/or -23 from the C-terminus of ephrinBs (positions 324 and 329 in ephrinB1), was obtained (89). These tyrosine residues are physiologically relevant since they have been found to be phosphorylated in both tissues and in cell lines (172). With this tool, the tyrosine phosphorylation of the ephrinB1 constructs in response to EphB2-Fc or other stimuli could be assessed.

EphrinB1 proteins detected by this antibody are hereafter referred to as being tyrosine phosphorylated or assumed to be activated.

Cells expressing the ephrinB1 constructs were treated with EphB2-Fc for up to 6 hours and their phosphorylation responses assessed by anti-phospho-ephrinB and anti-ephrinB Western blotting (**Figure 3.7**). The anti-ephrinB antibody detected unphosphorylated ephrinB1wt at ~47 kDa, and the anti-phospho-ephrinB antibody detected the protein at ~55 kDa following EphB2-Fc stimulation, indicating ephrinB1wt underwent a molecular weight increase of ~5-8 kDa following treatment. A similarly sized molecular weight increase of ephrinB1wt in response to EphB2-Fc was previously described (87, 89). The anti-ephrinB antibody was unable to detect the higher molecular weight tyrosine-phosphorylated species and modifications occurring within this antibody's epitope, such as tyrosine phosphorylation, may have obstructed it. This observation indicates the presence of two detectable pools of ephrinB1 in cells, one pool that is unphosphorylated (detected by the anti-ephrinB antibody) and another that is tyrosine phosphorylated at residues 324 and 329 (detected by the anti-phospho-ephrinB antibody). B1ΔIV also displayed an analogously sized molecular weight shift to that of ephrinB1wt following treatment with EphB2-Fc, that is from ~45 kDa to ~52 kDa (**Figure 3.7**). Tyrosine phosphorylated B1Δ4 (~54 kDa) however displayed an increase of only ~2-4 kDa relative to its ~50 kDa non-phosphorylated protein. B1ΔKLR response to EphB2-Fc was inconsistent and not reported herein.

In the ephrinB1wt cells, tyrosine phosphorylation in response to EphB2-Fc was detected at 5 min, peaked at 30 min and was sustained at this level for the remainder

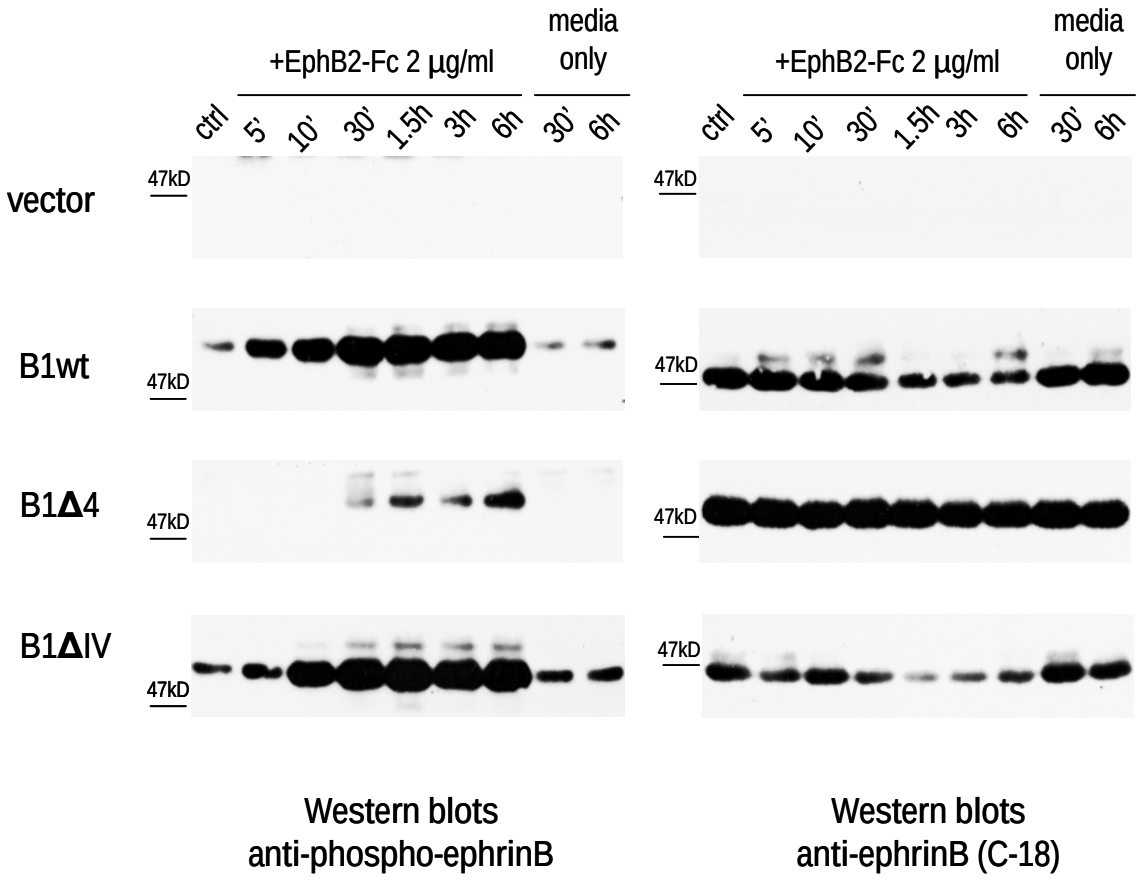

Figure 3.7: PDZ-based interactions were involved in mediating tyrosine phosphorylation of ephrinB1 in response to EphB2-Fc.

NIH3T3 cells expressing the indicated ephrinB1 constructs were serum starved overnight, then treated with 2 µg/ml EphB2-Fc for up to 6 h, or with media alone. The cells were then lysed directly in sample buffer and analyzed by immunoblotting for anti-phospho-ephrinB first, then reprobed with anti-ephrinB (C-18). (n=2)

of the time course (**Figure 3.7**). B1ΔIV displayed similar tyrosine phosphorylation kinetics to ephrin B1wt. B1Δ4 exhibited relatively little activation overall, however its tyrosine phosphorylation was first detected at 30 min and its maximal levels reached at 6h of treatment. Treatment of ephrinB1 construct expressing cells with media only did not result in detectable tyrosine phosphorylation of the constructs (**Figure 3.7**).

Relative levels of non-tyrosine phosphorylated ephrinB proteins during these time courses were analyzed by reprobing the membranes with anti-ephrinB antibody (**Figure 3.7**). From these blots, it was apparent that ephrinB1wt and B1ΔIV displayed lower levels of their non-phosphorylated full-length proteins beginning at 30 min post-treatment with EphB2-Fc. The decrease of non-tyrosine phosphorylated ephrinB1 at these time points correlated with the detected increase of their tyrosine-phosphorylated ephrinB1 species by the anti-phospho-ephrinB antibody, indicating that the pool of unphosphorylated ephrinB1 in the cell is depleted over time in response to EphB2-Fc. In line with this observation, B1Δ4, which is not activated by EphB2-Fc, did not exhibit a change in the amounts of its non-tyrosine phosphorylated protein detected over this time course.

From these experiments it was found that ephrinB1wt and B1ΔIV elicited similar EphB2-Fc induced tyrosine phosphorylation responses, and a correlative decrease in their unphosphorylated ephrinB1 levels was also discerned. The B1Δ4 mutant however was impaired in its tyrosine phosphorylation response to EphB2-Fc. This represents the first demonstration that a PDZ-based interaction was involved in mediating tyrosine phosphorylation of ephrinB1wt following treatment with EphB2-Fc.

3.2.4 Tyrosine Phosphorylation of EphrinB1 Cytoplasmic Mutants in Response to Transient Stimulation with Clustered EphB2 Receptor Ectodomains

The previous experiment succeeded in studying the induction of tyrosine phosphorylation of ephrinB1 constructs in response to EphB2-Fc however a downregulation of their responses was not observed over the time course. Therefore, a transient EphB2-Fc stimulation of ephrinB1 construct expressing cells was used to evaluate which regions of ephrinB1's cytosolic domain are required to downregulate its tyrosine phosphorylation response to this stimulus.

Cells expressing ephrinB1 constructs were treated for 10 min with EphB2-Fc, rinsed with media thus removing the majority of the agonist, and fresh media was added to the cells which were then incubated for up to 2.5 h, and their responses analyzed by immunoblotting with anti-phospho-ephrinB antibody (**Figure 3.8**). EphrinB1wt peak tyrosine phosphorylation occurred at 10 min post-EphB2-Fc removal which then decreased at 30 min post-EphB2-Fc removal and was sustained at this level for 2.5 h. The downregulation of ephrinB1wt phosphorylation B1ΔIV displayed similar kinetics to those of ephrinB1wt although its peak phosphorylation at 10 min post-EphB2-Fc removal was relatively less marked. Tyrosine phosphorylation of B1Δ4 and B1Δ12 was not detected during the course of the transient treatment with EphB2-Fc. The levels of non-phosphorylated ephrinB1 proteins detected by the anti-ephrinB antibody were also analyzed (**Figure 3.8**). B1Δ4 and B1Δ12 did not exhibit any changes in these protein levels during the experiment. EphrinB1wt and B1ΔIV exhibited a small gradual loss of their non-phosphorylated proteins during the transient EphB2-Fc stimulation beginning at 30 min post-EphB2-Fc removal.

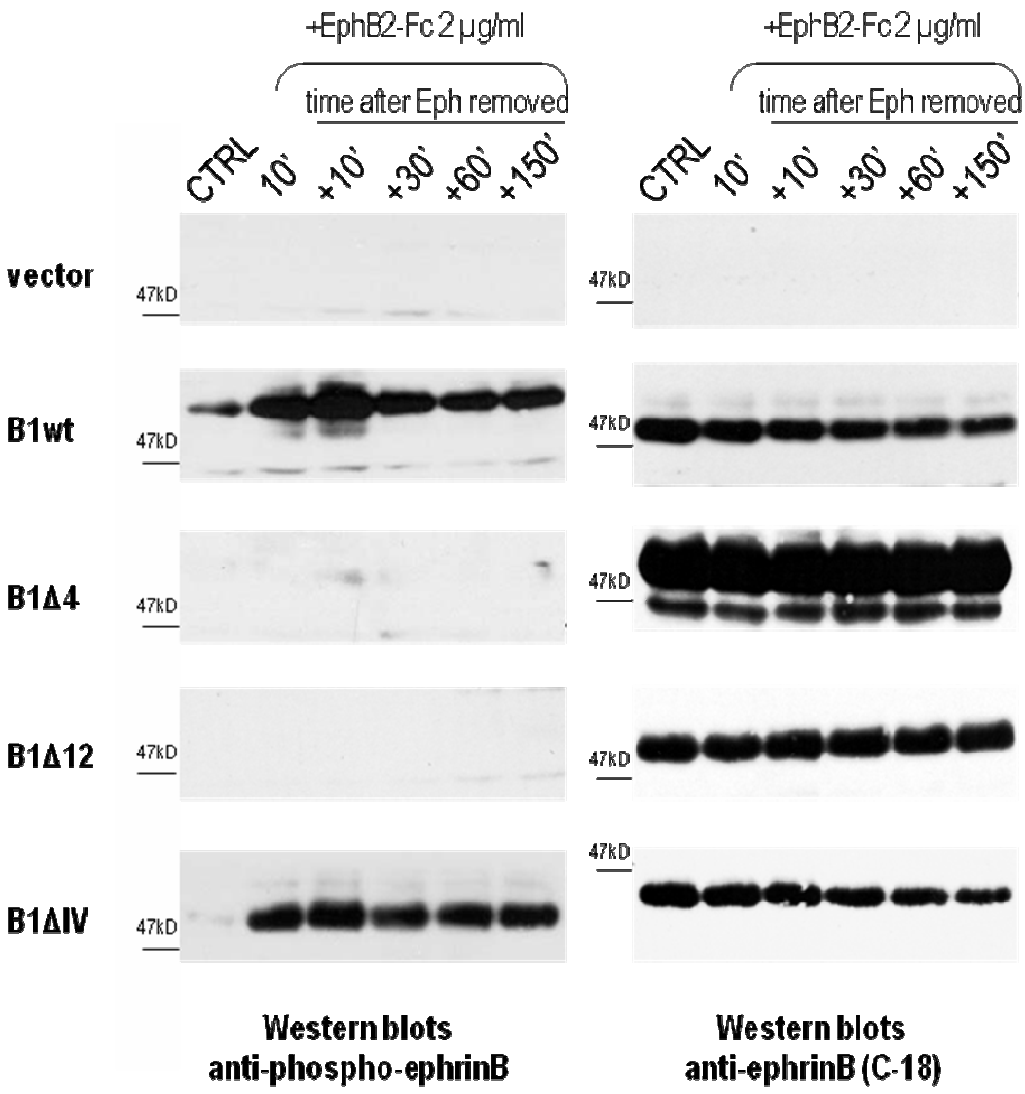

Figure 3.8: The intervening sequence of ephrinB1 is not required to mediate downregulation of ephrinB1 tyrosine phosphorylation in response to transient EphB2-Fc stimulation.

NIH3T3 cells expressing the indicated ephrinB1 constructs were serum starved overnight, then treated with 2 µg/ml EphB2-Fc for 10 min. The cells were then rinsed with media, and reincubated with fresh media for up to 2.5h. The cells were then lysed directly in sample buffer and analyzed by immunoblotting for anti-phospho-ephrinB first, then reprobed with anti-ephrinB (C-18). (n=2)

These experiments showed that ephrinB1wt and B1ΔIV responded similarly to the EphB2-Fc transient stimulation indicating the non-conserved intervening sequence is not required to effect dephosphorylation. The B1Δ4 and B1Δ12, constructs that share a PDZ-motif deletion, were not phosphorylated in response to EphB2-Fc and therefore their downregulation to this stimulus was not assessed.

3.2.5 Tyrosine Phosphorylation of EphrinB1 Cytoplasmic Mutants in Response to PDGF

In addition to stimulation by clustered EphB receptors, ephrinBs can be tyrosine phosphorylated in response to cellular treatment with PDGF (87) and FGF (88). Like ephrinBs, PDGF receptor (PDGFR) signaling has been shown to be important in both developmental and pathological angiogenesis (173, 174), thus there is precedent for a physiological significance to PDGFR signaling to cross-activate B-class ephrins. The tyrosine phosphorylation responses of the ephrinB1 constructs to PDGF were used to characterize the cytoplasmic regions of ephrinB1 involved in mediating this process.

Cells expressing ephrinB1 constructs were treated with PDGF for up to 60 min and their tyrosine phosphorylation levels were characterized by anti-phospho-ephrinB Western blotting (**Figure 3.9**). EphrinB1wt and B1ΔIV peak tyrosine phosphorylation occurred at 15 min post-treatment with PDGF, which then gradually decreased to the end of the time course. The B1ΔKLR tyrosine phosphorylation response to PDGF was inconsistent and therefore not reported herein. There was no discernable change in unphosphorylated ephrinB1 protein level of the constructs during the course of the PDGF

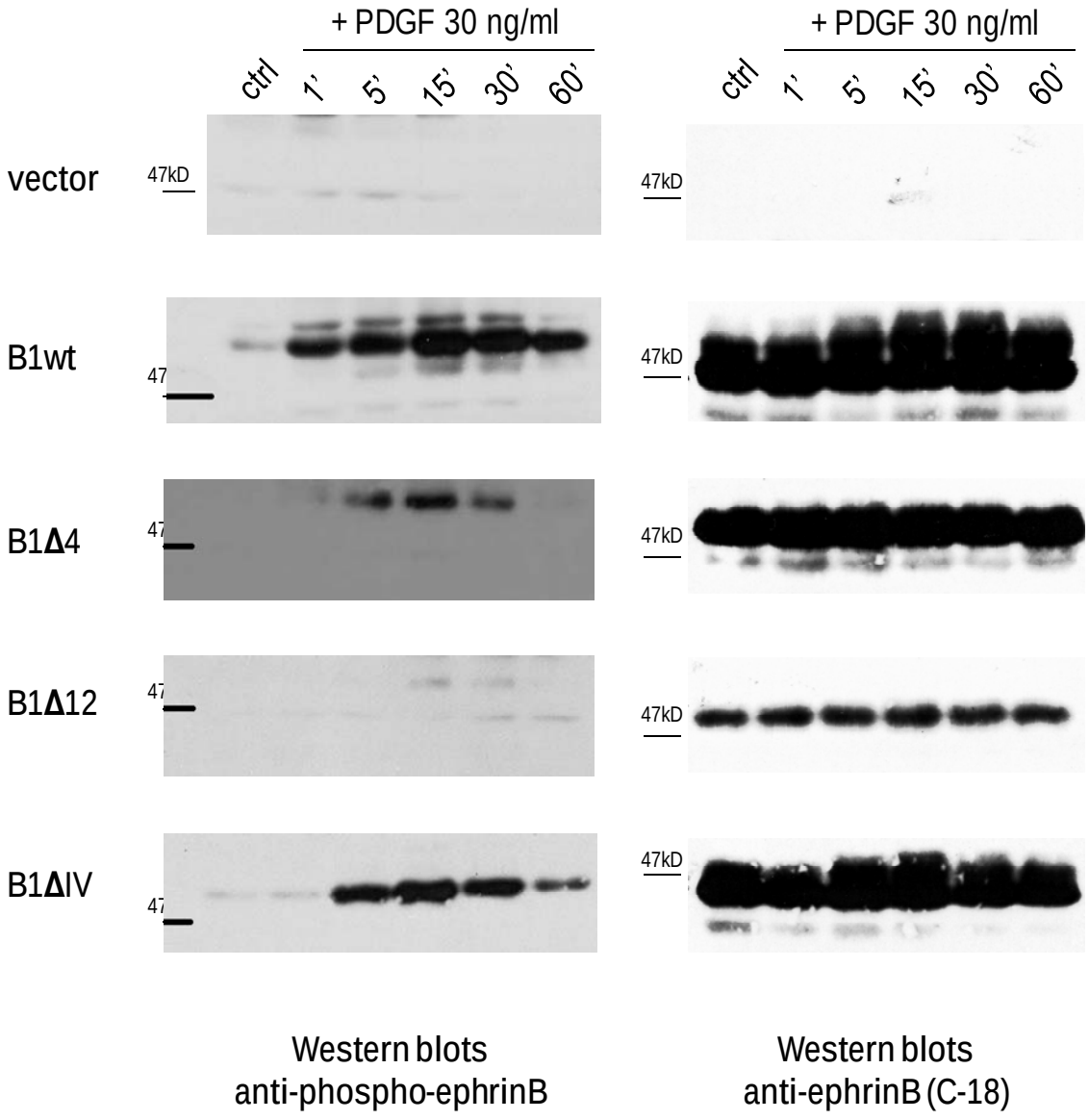

Figure 3.9: PDZ-based interactions are involved in mediating tyrosine phosphorylation of ephrinB1 in response to PDGF.

NIH3T3 cells expressing the indicated ephrinB1 constructs were serum starved overnight, then treated with 30 ng/ml of PDGF-BB for up to 60 min. The cells were then lysed directly in sample buffer and analyzed by immunoblotting for anti-phospho-ephrinB first, then reprobed with anti-ephrinB (C-18). (n=2)

stimulation as assessed by anti-ephrinB immunoblotting.

In response to PDGF, tyrosine phosphorylated ephrinB1wt and B1ΔIV proteins exhibited a ~5-8 kDa increase in molecular weight relative to their unphosphorylated respective proteins, and B1Δ4 and B1Δ12 exhibited an increase of ~2-4 kDa (**Figure 3.9**) In agreement with our study, Bruckner *et al.* (87) have also described a ~5-8 kDa increase in molecular weight of ephrinB1wt associated with its PDGF- mediated tyrosine phosphorylation. The molecular weight increases resulting from PDGF-induced tyrosine phosphorylation of the ephrinB1 constructs were of the same size as those characterized following their EphB2-Fc-induced responses (**Figures 3.7 and 3.8**).

From these experiments, ephrinB1wt, B1Δ4, B1Δ12, and B1ΔIV proteins were found to exhibit similar temporal tyrosine phosphorylation profiles in response to PDGF. However, the PDZ-motif mutants, B1Δ4 and B1Δ12, were not as robustly phosphorylated relative to ephrinB1wt. This observation is the first demonstration that a PDZ-based interaction was required to mediate efficient PDGF-mediated tyrosine phosphorylation of ephrinB1 in response to PDGF.

3.2.6 Identification of EphrinB1 Cytoplasmic Tail Interacting Proteins

It is clear from our experiments that ephrinB1 signaling in NIH3T3 fibroblasts involved its cytoplasmic tail since it was tyrosine phosphorylated within this region following EphB2-Fc or PDGF stimulation and its carboxy PDZ-motif was found to be required to efficiently mediate these processes. To identify cytosolic proteins that bind to ephrinB1's conserved C-terminus and regulate its signaling and function in these cells, an N-terminal biotinylated peptide of the carboxy 33 aa of ephrinB1 was used in pull-down

experiments with NIH3T3 cells lysates. The biotinylated peptide was incubated with NIH3T3 cell lysates and then precipitated, along with interacting proteins, via the addition of Streptavidin-coated beads. The pulldowns were analyzed by polyacrylamide gel electrophoresis and silver staining. A ~30 kDa was specifically precipitated with the peptide (**Figure 3.10**) then excised from the stained gel and identified by mass spectrometry as the PDZ-domain containing protein syntenin (structure shown in **Figure 3.10**). Syntenin, an adaptor-like protein, has previously been established as an ephrinB1 PDZ-binding partner (154). To confirm the mass spectrometry identification of this protein, the peptide pulldown was also analysed by anti-syntenin Western blotting (**Figure 3.10**). Syntenin was detected in the Western blot at ~30 kDa when the peptide was used in the pulldown but not by Streptavidin-beads alone. However, an association between ephrinB1 protein and syntenin was not confirmed in NIH3T3 cells since syntenin was not co-immunoprecipitated with ephrinB1 (data not shown). Nonetheless, our study identified syntenin as a candidate protein involved in ephrinB1 function in NIH3T3 cells.

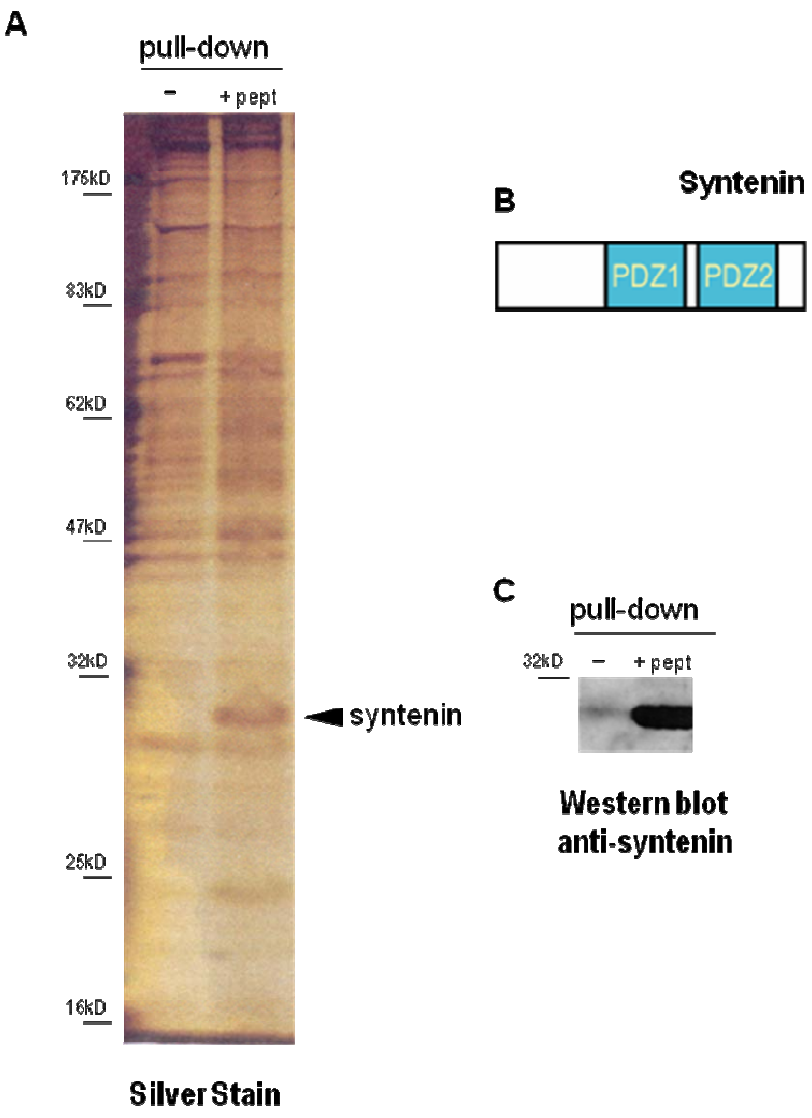

Figure 3.10: Syntenin-1 interacted with a peptide consisting of the conserved C-terminus of ephrinB1.

A N-terminal biotinylated peptide of the carboxy 33 aa of ephrinB1 was used in pull-down experiments of NIH-3T3 cell lysates. Syntenin-1 was identified in the pull-downs by polyacrylamide silver staining (A) (n=4) and subsequent MS analysis, and confirmed by Western blotting (C) (n=1). A schematic of the domain structure of syntenin is shown in (B).

3.3 Discussion

To investigate the function of ephrinB1's cytoplasmic domain in the regulation of its lipid raft association and tyrosine phosphorylation responses to EphB2-Fc and PDGF, several cytosolic mutants of the protein were designed and 3T3 cells expressing them were established. It was found that like ephrinB1wt, the cytoplasmic mutants B1Δ4, B1Δ12, B1ΔKLR, and B1ΔIV translocated to lipid rafts following EphB2-Fc treatment, suggesting that this event may instead depend on a stretch of amino acids uniquely deleted in the B1Δ33 construct that was not assessed due to the removal of the detecting antibody's epitope. It was also determined that B1Δ4 mutant construct (i.e. lacking the PDZ-binding motif) was not efficiently tyrosine phosphorylated in response to EphB2-Fc or PDGF stimulation. This result represents the first demonstration that a PDZ-based interaction is potentially involved in mediating tyrosine phosphorylation of ephrinB1 in response to agonist-stimulation. Furthermore, syntenin-1 was identified as a binding protein of an ephrinB1 C-terminus peptide suggesting that these proteins may interact in NIH3T3 cells. Taken together, our results indicate that PDZ-based interactions are important in mediating ephrinB1 function.

3.3.1 EphrinB1 Cytoplasmic Mutants bind EphB Receptor Ectodomains

To determine whether cytosolic interactions were important for lipid raft association of ephrinB1 and/or mediating tyrosine phosphorylation in response to EphB receptors and PDGF, cytoplasmic deletion constructs of ephrinB1 were designed and constructed (summarized in Figure 3.1), and NIH3T3 fibroblasts stably expressing each

of these constructs were established. EphB2-Fc cell surface staining of each construct as assessed by flow cytometry confirmed their expression and that their respective ephrinB1 ectodomains were properly folded. Expression of each construct was also confirmed by Western blotting. All ephrinB1 constructs were detected except B1Δ33, since the deletion in this construct ablated the detection antibody's epitope. Oddly, B1Δ4 and B1Δ12 were ~3 kDa larger than ephrinB1wt, where a decrease in molecular weight of ~0.5 and ~1.4 kDa respectively were expected for these proteins. The design of the ephrinB1 constructs and establishment of their respective stably-expressing cell lines provided the platform for the ephrinB1 signaling studies subsequently performed.

3.3.2 A Conformational Change or a Post-Translational Modification May Occur in EphrinB1 Mutants with PDZ-Motif Ablations

The ~4 kDa molecular weight difference between ephrinB1wt and both B1Δ4 and B1Δ12 discerned in established cell lines was further investigated. Both B1Δ4 and B1Δ12 possess PDZ-motif ablations and interestingly, a 3 aa deletion in ephrinB1's PDZ motif by Palmer *et al.* (89) also resulted in a size increase of ~3 kDa relative to ephrinB1wt. The size increase associated with the elimination of the PDZ-motif suggests that a constitutive post-translational modification or conformational change is occurring in B1Δ4 and B1Δ12 that may be regulatory and thus possibly important in ephrinB1 signaling.

The molecular weight difference between the PDZ-motif mutants may be due to post-translational modifications, such as phosphorylation on either serine or tyrosine residues, and/or alternatively glycosylation. It was postulated that glycosylation

differences in the PDZ-motif mutants relative to ephrinB1wt may result as PDZ-domain containing proteins have previously been implicated in protein sorting (170, 171). However, N-glycolytic treatment of B1Δ4 and ephrinB1wt proteins indicated that these proteins possessed similarly sized N-glycosylation modifications. In subsequent experiments, it was characterized that B1Δ4 and B1Δ12 are not detected by the anti-phospho-ephrinB antibody and thus are not constitutively tyrosine phosphorylated on residues 324 or 329. However, the mutants may be tyrosine phosphorylated on the third conserved residue they still possess, as tyrosine 317 is not detected by the anti-phospho-ephrinB antibody used in our studies.

The putative role of serine phosphorylation in ephrinB1 function remains largely uncharacterized. Previous studies have indicated that serine phosphorylation of an ephrinB1 cytosolic domain GST-fusion protein resulted when it was incubated with lysates of EphB2-Fc stimulated 3T3 ephrinB1wt expressing cells (89). In addition, ephrinB1 was found to recruit an uncharacterized serine/threonine kinase through an interaction with the PDZ-domain containing protein GRIP (92). Thus, it is possible that if PDZ-motif ablation leads to a post-translation modification in ephrinB1 resulting in a ~4 kDa molecular weight increase, it may involve serine phosphorylation, such as at conserved residue 321. The putative regulatory significance of such an event remains to be characterized.

Alternatively, a conformational change in the cytoplasmic tail of ephrinB1 may have resulted from the ablation of the PDZ-motif in these mutants. EphrinB2 residues 301-322 (analogous residues in ephrinB1 are 314-335) are located in the highly conserved 33 aa C-terminus of ephrinBs and when unphosphorylated form a well-packed

ß-hairpin structure with high conformational stability (38, 39). This highly stable structure is abolished when phosphorylated at any of the three conserved residues found in this stretch (38), thus functioning as a cryptic site to mediate phosphotyrosine interactions with proteins, such as Grb4 (38, 40-42). Conformational changes in other proteins can be discerned as increases in molecular weight by SDS-PAGE (175). It is possible that ablation of the PDZ-motif, which is located next to the highly stable ß-hairpin, may have resulted in a constitutive conformational change by opening the highly stable ß-hairpin which may be discerned by SDS-PAGE as an increase in molecular weight.

3.3.3 A Highly-Conserved 21 Residue Stretch Deleted in B1Δ33 is Likely Involved in Mediating EphB2-Fc Mediated Lipid Raft Association.

Lipid rafts are specialized plasma membrane microdomains that may function to spatially and temporally regulate ephrinB signaling as these proteins are found to associate with them *in vivo* (89, 92, 110). The translocation of ephrinB1 into lipid rafts was found to be induced by soluble-EphB2 receptor stimulation (151) and the partitioning of B-class ephrins into these microdomains was dependent on its cytoplasmic tail (92). Therefore, the ephrinB1 construct expressing NIH3T3 cell lines were used to assess whether cytosolic interactions were required for ephrinB1 translocation to lipid rafts in response to EphB2-Fc. Lipid rafts were biochemically isolated from the cells following treatment with EphB2-Fc and then analyzed by anti-ephrinB immunoblotting. EphrinB1wt and B1Δ4, B1Δ12, B1ΔKLR, and B1ΔIV cytosolic mutant proteins translocated to lipid rafts in response to the stimulation. Thus, ephrinB1 was able to

translocate to membrane microdomains following EphB2-Fc treatment independently of its C-terminal 12 aa (including the PDZ-motif that houses two conserved tyrosine residues), polybasic domain or non-conserved intervening sequence. Due to our antibody detection limitations, the ability of B1Δ33 protein to translocate to lipid rafts was not assessed.

The unique region removed in B1Δ33 relative to the other cytosolic mutants was a highly conserved 21 aa stretch with three tyrosine residues that form the highly stable ß-hairpin structure (38, 39). Since the association of ephrinB1 with lipid rafts in 293T cells was previously found to be abrogated when the majority of its cytosolic domain was ablated (92), it is possible this 21 aa stretch uniquely deleted in B1Δ33 mediates interactions required for ephrinB1 lipid raft association.

Following stimulation with EphB2-Fc, B1Δ4 mutant protein translocated to lipid rafts and was later determined to be inhibited in becoming tyrosine phosphorylated in response to stimulus. From these results, it can be extrapolated that phosphorylation at the two conserved tyrosines detected by the anti-phospho-ephrinB antibody, are likely not required for EphB2-Fc-induced lipid raft association of ephrinB1.

The two tyrosines detected by the anti-phospho-ephrinB antibody are located in B1Δ33's uniquely deleted 21 aa stretch. Thus, it is likely that if this 21 aa stretch mediated lipid raft association it would do so in a manner independent of phosphorylation at tyrosines 324 and 329. If EphB2-Fc mediated lipid raft association of ephrinB1 is related to this 21 aa stretch, phosphorylation of the third conserved tyrosine 317 may be involved in mediating this response. A phosphotyrosine-based interaction with a protein, or a conformational change also leading to novel protein interactions within this stretch,

may recruit ephrinB1 to lipid rafts. Interestingly, the only SH2-mediated interaction described for B-class ephrins to date is with Grb4 (41), and tyrosine phosphorylation at residue 317 is critical for this interaction to occur (40, 42). Thus, it possible an interaction with Grb4 at tyrosine 317 when this residue is phosphorylated may mediate lipid raft translocation of ephrinB1. Alternatively, ephrinB association with membrane microdomains may occur independently of cytoplasmic interactions and instead be mediated by an extracellular mechanism.

3.3.4 PDZ-based Interactions Mediate EphrinB1 Tyrosine Phosphorylation in Response to Clustered EphB2 Receptor Ectodomains and PDGF

Tyrosine phosphorylation of ephrinBs is thought to be important in coupling these proteins to downstream signaling pathways and thus mediate cellular responses following contact with EphB receptors or stimulation with PDGF (87). Recently, this hypothesis was confirmed as phosphotyrosine-dependent interactions in ephrinB1's conserved 33 aa cytosolic tail were found to mediate interactions with signal transducer and activator of transcription 3 (STAT3), leading to its enhanced transcriptional activity (176). This report represents the first description of a cell surface signal by ephrinB proteins being delivered to the nucleus.

To characterize regulatory cytosolic regions required for tyrosine phosphorylation of ephrinB1, the phosphorylation of the ephrinB1 constructs following stimulation with EphB2-Fc or PDGF were characterized. A commercial anti-phospho-ephrinB antibody, which recognizes two conserved tyrosine residues of ephrinB when phosphorylated (89), was used in Western blotting analysis of cell lysates from the stimulated cells. Thus, a

caveat for these experiments is that the tyrosine phosphorylation responses of these proteins was measured specifically for tyrosines at positions -18 and -23 from the C-terminus (positions 324 and 329 in ephrinB1), identified as *in vivo* phosphorylation sites (90), and not for the three other conserved tyrosine residues of ephrinB1's cytoplasmic tail.

A ~5-8 kDa molecular weight increase was observed between phosphorylated ephrinB1wt, detected by the anti-phosphoephrinB antibody, and the unphosphorylated ephrinB protein, detected by the anti-ephrinB antibody, following activation by both EphB2-Fc and PDGF. Similarly sized molecular weight increases can be associated with post-translational modification(s), such as ubiquitination (7 kDa) (177). However, it is also likely that tyrosine phosphorylation together with a conformational change in the ß-hairpin structure (where two of the conserved tyrosine residues detected by the anti-phospho-ephrinB antibody are found) in ephrinB1's conserved 33 aa carboxy-terminus could explain the size shift. As discussed earlier, a ~3-4 kDa increase in molecular weight observed in the B1Δ4 and B1Δ12 mutants may have been due to a constitutive conformational change in the ß-hairpin structure resulting from ablation of ephrinB1's PDZ-motif. B1Δ4 and B1Δ12 mutants, although weakly responding, exhibit a molecular weight increase of ~2-4 kDa following stimulation with either EphB2-Fc or PDGF, as detected by the anti-phospho-ephrinB antibody, suggesting that tyrosine phosphorylation at these two residues results in a ~2-4 kDa increase in molecular weight. Taken together, it is possible that the ~3-4 kDa molecular weight increase proposed to occur following a conformational change in the ß-hairpin structure, and the ~2-4 kDa molecular weight

increase associated with tyrosine phosphorylation in this structural region, could account for the ~5-8 kDa increase observed in ephrinB1wt following treatment with agonists.

From both the stimulations performed with EphB2-Fc and PDGF, it was concluded that the intervening sequence removed in B1ΔIV is not required to mediate ephrinB1 tyrosine phosphorylation or its subsequent downregulation. B1Δ4 however was quite inhibited in its ability to be phosphorylated in response to EphB2-Fc or PDGF, thus presenting the first demonstration that a PDZ-based interaction was required to mediate phosphorylation of ephrinB1 to these agonists. The involvement of the PDZ-based interactions in diminishing EphB2-Fc phosphorylation was not assessed with B1Δ4 as it was not efficiently phosphorylated. PDZ-domain containing proteins may be involved in assembling supramolecular complexes (55). The contribution of ephrinB1 activation in response to growth factor receptor signaling remains to be determined.

3.3.5 Syntenin-1 Binds to the Conserved C-terminus of EphrinB1

To uncover cytoplasmic proteins involved in ephrinB1 signaling, an N-terminally biotinylated peptide compromised of the highly conserved 33 aa C-terminus of ephrinB1 was used to pull-down interacting proteins from NIH3T3 lysates. A ~30 kDa PDZ-domain containing protein, syntenin-1, was pulled-down by the peptide and identified by mass spectrometry. The interaction of syntenin with the peptide was confirmed by anti-syntenin Western blotting analysis of peptide pulldowns. However an intracellular interaction between native ephrinB1 and syntenin proteins was not confirmed by co-immunoprecipitation. Syntenin is widely expressed and previously identified to interact directly with ephrinB1's PDZ-motif (54, 154).

Initially identified as *melanoma differentiation associated* gene 9 (*mda-9*) (178), the enhanced expression of *mda-9*/syntenin is associated with advanced metastatic melanomas (179) as well as increased cell migration in other cancer cell lines (180). Syntenin was also identified as a binding protein for the signaling and trafficking syndecan proteoglycans (171) and was also implicated in cytoskeleton-membrane organization (171, 181). Sytenin can function in neuronal development by acting as a scaffolding protein for the serine/threonine kinase Unc51.1, a gene expressed during early neuronal differentiation, and Rab5 GTPase, a protein involved in regulating endocytosis and functions in axon extension (182). Taken together, syntenin's functions appear characteristically similar to those mediated by ephrinBs and therefore sytenin may be involved in modulating ephrinB signaling.

Syntenin proteins have been proposed to act as detectors of receptor clustering, rather than driving the formation of specific molecular assemblies (183). Thus, EphB2-mediated ephrinB1 clusters may be discerned by syntenin which would subsequently act to recruit signaling proteins to ephrinB1, including tyrosine kinases. Since ephrinBs have been found to associate with activated FGF receptors (88), a similar interaction with the activated PDGF receptor may function to cluster ephrinBs, and thereby act to analogously recruit syntenin.

Overall, through the use of our designed ephrinB1 cytoplasmic deletion constructs expressed in NIH3T3 cells several key ephrinB1 signaling aspects were characterized. First, our studies were able to delineate that a 21 aa conserved stretch uniquely deleted in B1Δ33 is likely involved in mediating EphB2-Fc-induced lipid raft association of

ephrinB1. Our novel experiments were also able to implicate that phosphorylation at tyrosine 324 and 329 were not required for this translocation to occur. A molecular weight increase of ~4 kDa was identified in ephrinB1 mutants possessing PDZ-motif deletions, suggesting a putative regulatory conformational change or post-translational modification occurring on ephrinB1 that is associated with the loss of PDZ-based interactions. The PDZ-motif was also found to be critical for efficient phosphorylation as ephrinB1Δ4 and Δ12 (both lacking the PDZ-binding motif) are inefficiently tyrosine phosphorylated in response to EphB2-Fc and PDGF, thus representing the first documented evidence of PDZ-based interactions being required for this process. Finally, syntenin was identified as a putative binding protein of ephrinB1 in NIH3T3 cells, possibly functioning to sense activated ephrinB1 signaling clusters. Taken together, our studies pointed to a very central function of the PDZ-binding motif in ephrinB1 signaling.

Recently, the *in vivo* significance of ephrinB1 PDZ interactions in mediating physiological responses was demonstrated by the phenotypes observed in mice strains with PDZ-motif truncations of ephrinB1 and ephrinB2. Chimeric mouse embryos with an ephrinB1Δ1 mutation exhibited cleft palate, a phenotype observed in ephrinB1 knock-out mice (138, 139) and the ephrinB2Δ1 knock-in mice die shortly after birth due to chylothorax, that is effusion of chyle from the thoracic duct into the pleural space, related to defects in lymphatic vasculature remodeling (184). Thus, it is clear that PDZ-motif interactions mediate important B-class ephrin physiological functions and our study has aided to characterize the associated molecular mechanisms by which these may be transduced.

3.4 Future Directions

Further defining the role lipid rafts play in ephrinB1 signal regulation should be pursued. Determining whether the 21 aa stretch uniquely deleted in the B1Δ33 mutant is required for lipid raft translocation could be accomplished by selectively deleting this conserved stretch in a new mutant protein, while leaving intact other cytoplasmic regions, and determining if it translocates to lipid rafts following EphB2-Fc treatment. Defining proteins which interact with ephrinB1 in lipid rafts to propagate its signaling could be accomplished by immunoprecipitating ephrinB1, or using the ephrinB1 C-terminus peptide in pull-downs, from the lipid raft fraction of cells. As well, surveying lipid raft proteins following EphB2-Fc stimulation of ephrinB1 expressing cells could identify signaling molecules specifically recruited or displaced in lipid rafts which would likely be involved in ephrinB1 signal regulation.

Determining if syntenin is required to mediate ephrinB signaling in NIH3T3 cells would also be a logical next step in defining ephrinB1 signaling pathway. Syntenin subcellular localization could be monitored via co-immunofluorescence to ascertain if it is recruited to ephrinB1 following agonist stimulation. A tagged-version of syntenin could be co-expressed in ephrinB1 NIH3T3 cells and then immunoprecipitated to determine if the proteins interact, with or without EphB2-Fc stimulation. If an interaction was confirmed, other proteins which bind to syntenin could then be characterized to ultimately describe an ephrinB signaling pathway. The tyrosine phosphorylation response of ephrinB1 to EphB2-Fc and PDGF could be assessed in cells with syntenin expression knocked-down in order to implicate whether syntenin recruits a tyrosine kinase to ephrinB1.

Chapter Four: Proteolytic Processing of EphrinB1

Chapter Four: Proteolytic Processing of EphrinB1

4.1 Introduction

Proteins with Type I membrane topology such as ephrinB1 have an extracellular N-terminus and can be regulated by proteolysis, occasionally resulting in fragments with new biological activity. These fragments can be generated via shedding of their extracellular domain and, in certain cases, are subsequently cleaved by the intramembrane protease gamma-secretase.

Cell surface shedding of proteins is involved in a number of molecular processes including receptor downregulation and signal modulation, and is tied to physiological processes including development, inflammation, and cancer (185-188). Shedding of Type I membrane proteins is largely mediated by transmembrane metalloproteases, such as A Disintegrin And Metalloproteinases (ADAMs) and Matrix Metalloproteinases (MMPs) (189, 190). These proteases target proteins near the plasma membrane surface, resulting in the release of the majority of their ectodomains. How shedding is regulated is largely unknown, as is the selectivity of the proteases. Released soluble domains of cytokine and growth factor receptors that are generated by shedding can modulate the functions of their ligands by acting to antagonize or prevent the formation of active signaling complexes (191). The portion of the protein that remains on the membrane following shedding, often referred to as a carboxy-terminal-fragment (CTF), can have independent signaling activity, such as observed with the Epidermal Growth Factor Receptor (EGFR) family member Erb-B4 (192). Thus, the shedding of membrane-associated proteins can generate fragments with signal modulating abilities.

Following ectodomain-shedding, some Type I membrane proteins are further cleaved within their transmembrane domain by the gamma-secretase complex, an intramembrane aspartyl protease, releasing their intracellular domain (ICD). This process is commonly referred to as regulated intramembrane proteolysis (RIP) and for certain proteins that undergo it, such as Notch receptor (193), Syndecan-3 (194), and p75 Neurotrophin receptor (195), unique signaling can result. The gamma-secretase generated ICD of Notch translocates to the nucleus where it participates in regulation of gene transcription (196, 197). The purpose of gamma-secretase cleavage of Syndecan-3 is to mediate the translocation of its intracellular binding partner CASK from the plasma membrane to the nucleus where it acts as a transcription factor (194). The p75 Neurotrophin receptor ICD has recently been implicated in Rho-family GTPase modulation (195). Thus, as in cell surface shedding, intramembrane proteolysis of Type I membrane proteins also generates protein fragments with novel signaling abilities.

As described in Chapter 3, a phospho-ephrinB specific antibody was employed to characterize phosphorylation kinetics of ephrinB1 constructs in response to the agonists EphB2-Fc and PDGF. Over the course of these studies, it was observed that ephrinB1 may be proteolytically processed following cellular stimulation, a process not previously described for these proteins. From these observations, it was hypothesized that **ephrinB1 is proteolytically processed resulting in the production of (a) signaling competent fragment(s)**. Specific aims for this project included:

1. The characterization of ephrinB1 phospho-carboxy-terminal-fragments
2. The characterization of the proteolytic processing of ephrinB1 phospho-carboxy-terminal fragments

4.2 Results

4.2.1 Phospho-Carboxy-Terminal Fragments are Produced in Connection with Tyrosine-Phosphorylation of EphrinB1

To address whether phosphorylation of ephrinB1 by EphB2-Fc and PDGF was temporally controlled, samples were collected at various time points from NIH3T3 ephrinB1wt or vector control cells and immunoblotted with anti-phospho-ephrinB antibody (**Figure 4.1 and 4.2**). It was noted that the anti-phospho-ephrinB antibody was not limited to detection of full-length tyrosine phosphorylated ephrinB1 proteins. An accumulation of smaller ~25 kDa-sized bands were also detected by the phospho-ephrinB antibody in our ephrinB1wt cells but not in the vector control cells (**Figure 4.1 and 4.2**). As the levels of phosphorylated ephrinB1wt increased during both time courses, so did those of the 25 kDa species leading us to hypothesize that the phosphorylation and accumulation of these 25 kDa bands were tied to the status of ephrinB1 tyrosine-phosphorylation. The 25 kDa bands detected by the anti-phospho-ephrinB antibody were classified as ephrinB1 **phospho-carboxy-terminal-fragments, pCTF**.

Sodium orthovanadate (a tyrosine phosphatase inhibitor) treatment of ephrinB1wt NIH3T3 cells led to accumulation of tyrosine phosphorylation of full-length ephrinB1 as well as pCTF (**Figure 4.3**). Other groups have found that sodium pervanadate (sodium orthovanadate mixed with peroxide) induced shedding of the cell adhesion molecule L1 and this process was mediated by Src-family tyrosine kinase activation (198). In our study, pre-treatment of cells with PP2, a Src-family kinase inhibitor, prior to addition of sodium orthovanadate to the cells inhibited part of the tyrosine phosphorylation of ephrinB1 and less pCTF was produced (**Figure 4.3**). This indicated that Src-family

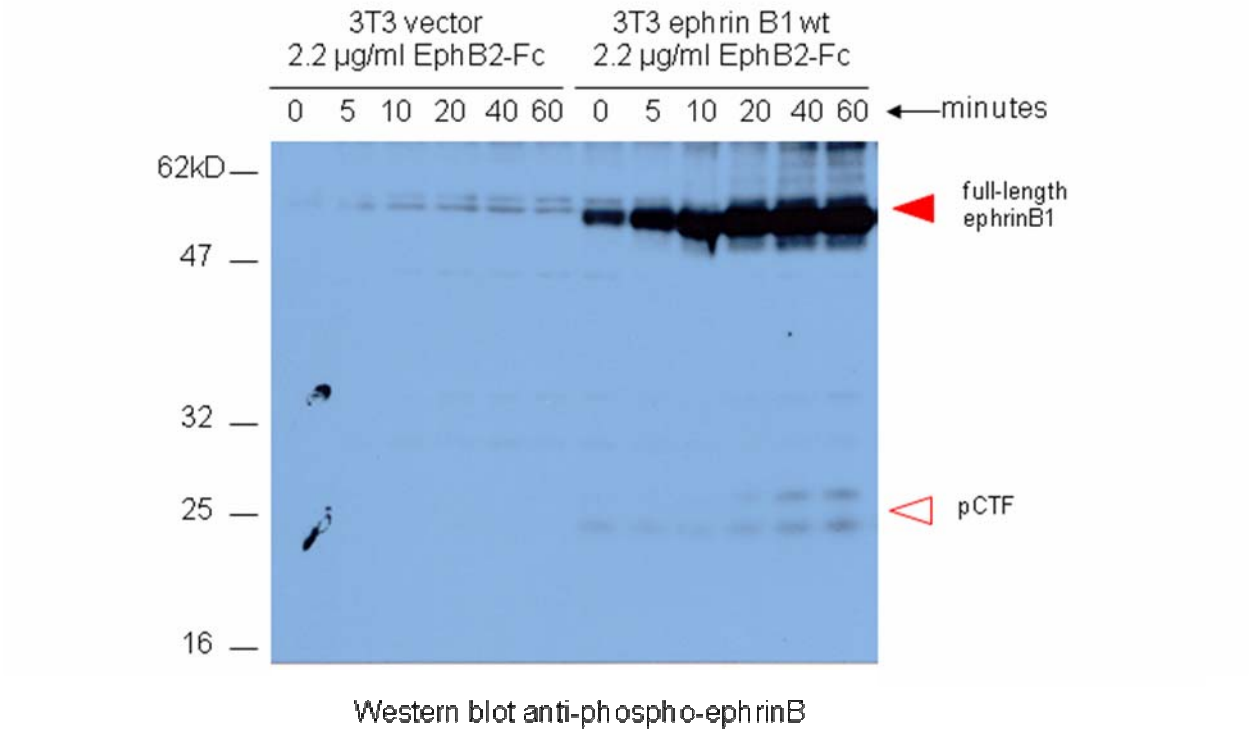

Figure 4.1: EphrinB1 phospho-carboxy-terminal fragment (pCTF) accumulated in response to EphB2-Fc stimulation.

NIH3T3 cells expressing ephrinB1wt or vector alone were stimulated with 2.2 µg/ml of EphB2-Fc for up to 60 min, and then lysed directly in sample buffer. (n=3)

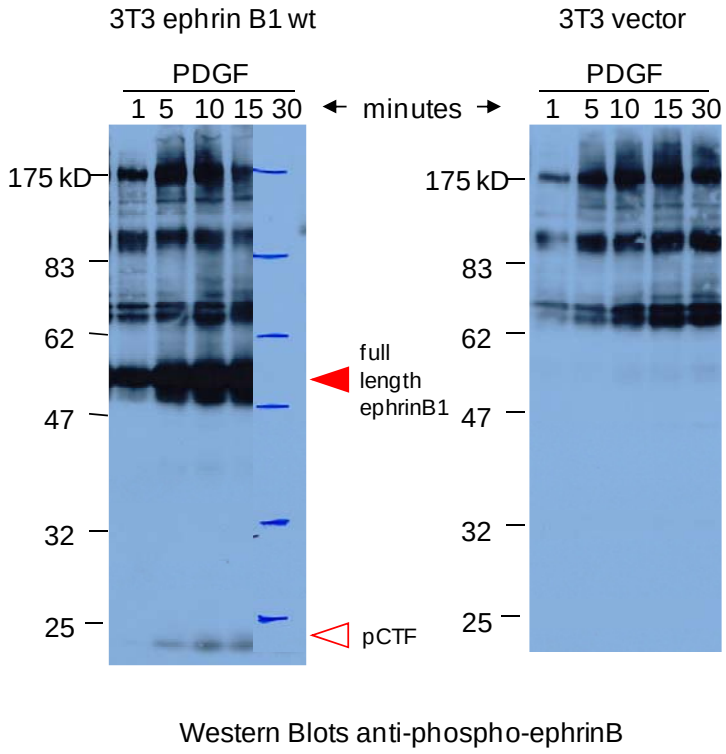

Figure 4.2: EphrinB1 pCTF accumulated in response to PDGF stimulation.

EphrinB1wt NIH3T3 cells were stimulated with 50 ng/ml of the PDGF-AB for up to 30 min, and then lysed directly in sample buffer. (n=6)

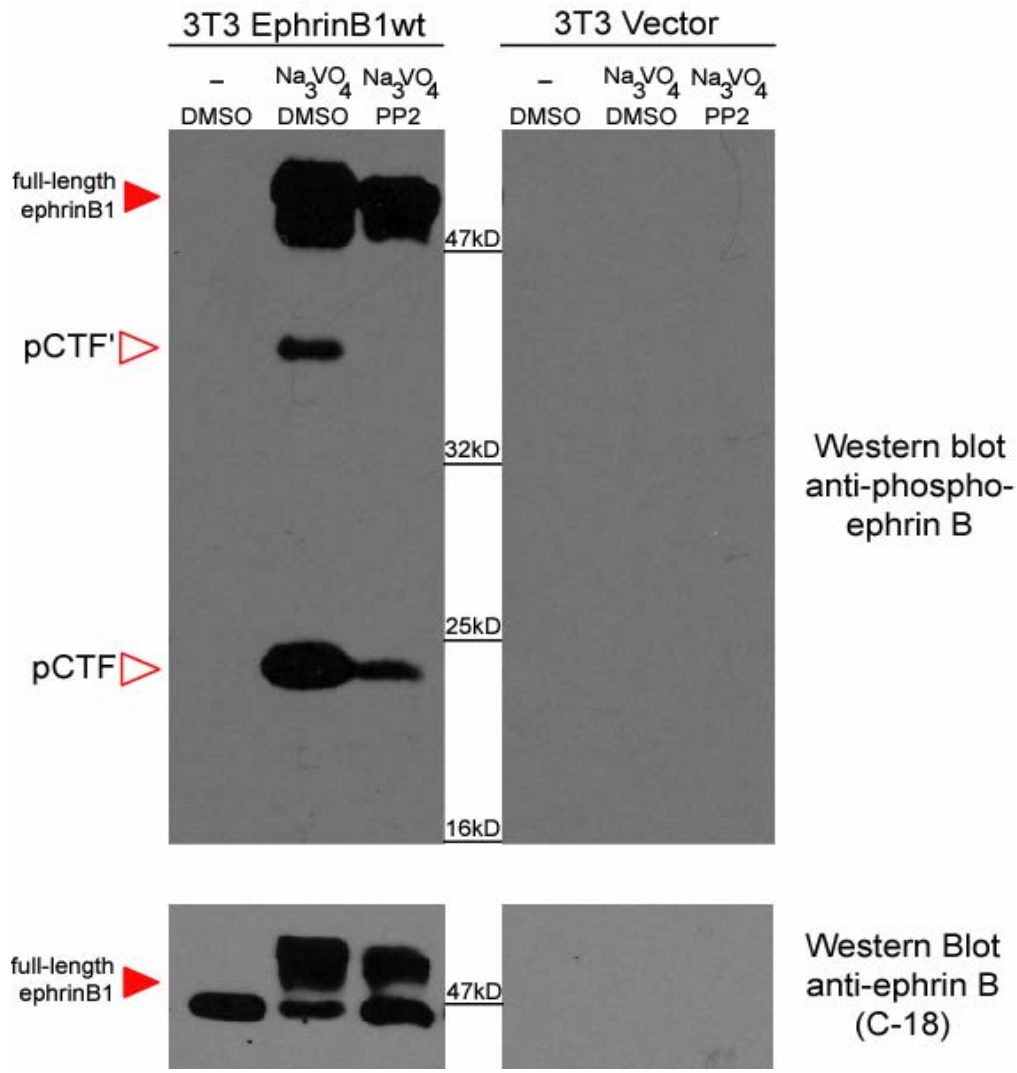

Figure 4.3: Sodium orthovanadate induced pCTF accumulation via Src-family kinase activation.

EphrinB1wt 3T3 cells were pretreated with 10 μM PP2 (n=1), a Src-kinase inhibitor, or DMSO (n=3), for 15 min prior to addition of 1 mM sodium orthovanadate for 1 hr, and then lysed directly in sample buffer. The samples were blotted with anti-phospho-ephrinB, then reprobed with anti-ephrinB1 (C-18).

kinases, implicated in EphB-mediated activation and downstream signaling of ephrinB1 (87, 89), were also involved in mediating tyrosine phosphorylation of ephrinB1 following sodium orthovanadate treatment. In this particular experiment, pCTF of differing sizes were detected by the anti-phospho-ephrinB antibody, including a ~38 kDa band which was more specifically sub-classified as **pCTF′** (**Table 6**). pCTF′ may represent pCTF modified with a post-translational modification, such as ubiquitin, or possibly a dimer of pCTF. Based on the success and reliability of sodium orthovanadate to result in increased pCTF production in comparison to EphB2-Fc or PDGF, it was adopted as the primary treatment in subsequent experiments to study pCTF signaling.

In addition to its accumulation in ephrinB1wt NIH3T3 cells, pCTF was detected in MDCK cells stably expressing ephrinB1wt treated with sodium orthovanadate (**Figure 4.4**), indicating pCTF production occurred in other cell types. Since ephrinB1 has been implicated in limb development (138, 139), and as developing limbs were simple to dissect, endogenous ephrinB proteins were immunoprecipitated from crudely dissected E6 chick limbs treated with sodium orthovanadate prior to their lysis (**Figure 4.5**). This demonstrated that pCTF production occurred *in vivo*.

The ephrinB-antibody had revealed the presence of smaller ephrinB-specific bands of ~16 kDa and ~32 kDa in unstimulated ephrinB1wt expressing 3T3 cells, termed carboxy-terminal fragments CTF and CTF' respectively, were not detected by the phospho-ephrinB antibody (**Figure 4.6)**. CTF and pCTF may play roles in ephrinB1 signaling considering that these experiments demonstrated that production of pCTF was linked to tyrosine phosphorylation of ephrinB1 in both cultured cells and *in vivo*.

Table 6 : Summary of EphrinB1 Carboxy-Terminal-Fragment Species

Fragment Name	Fragment Acronym	Molecular Weight (kDa)	Antibody Detection
carboxy-terminal-fragment	CTF	16	Anti-ephrinB
Carboxy-terminal-fragment′	CTF′	32	Anti-ephrinB
Phospho-carboxy-terminal-fragment	pCTF	25	Anti-phospho-ephrinB
Phospho-carboxy-terminal-fragment′	pCTF′	38	Anti-phospho-ephrinB
HA/Myc EphrinB1wt carboxy-terminal-fragment	HA/Myc CTF′	35	Anti-HA
HA/Myc EphrinB1wt Phospho-carboxy-terminal-fragment	HA/Myc pCTF	28	Anti-phospho-ephrinB
HA/Myc EphrinB1wt Phospho-carboxy-terminal-fragment′	HA/Myc pCTF′	40	Anti-phospho-ephrinB

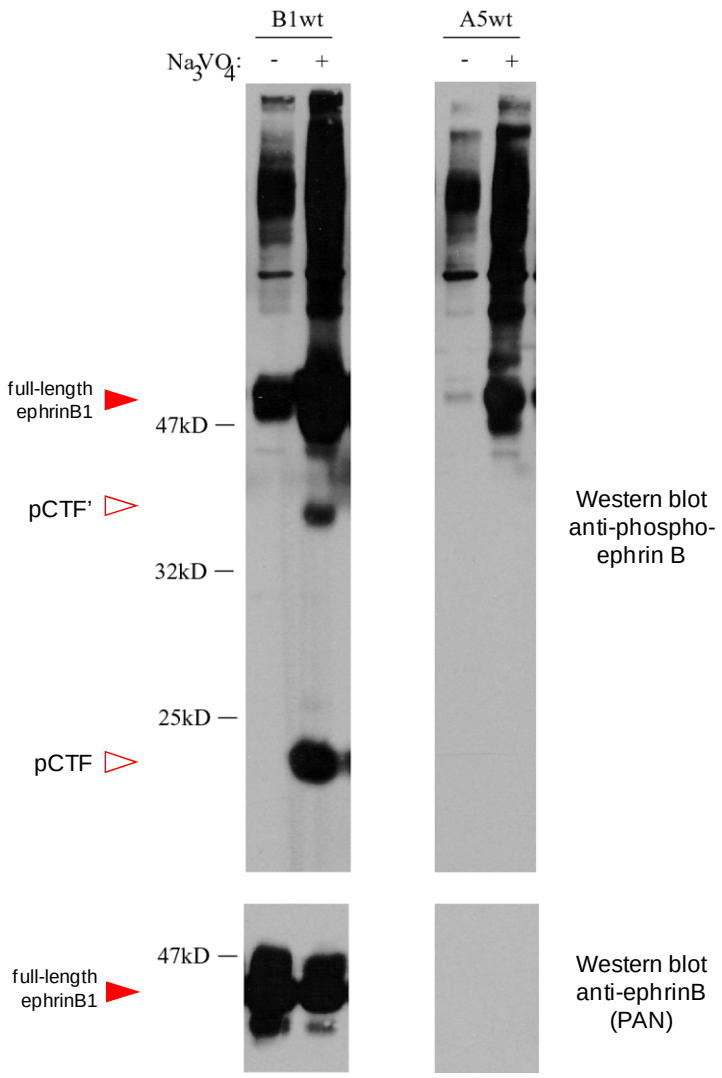

Figure 4.4: EphrinB1 pCTF was produced in MDCK cells following sodium orthovanadate addition.

EphrinB1wt or ephrinA5 (negative control) expressing MDCK cells were treated with 1 mM sodium orthovanadate for 1 hr then lysed directly in sample buffer. The samples were blotted with anti-phospho-ephrinB, then reprobed with anti-ephrinB1 (PAN). (n=2)

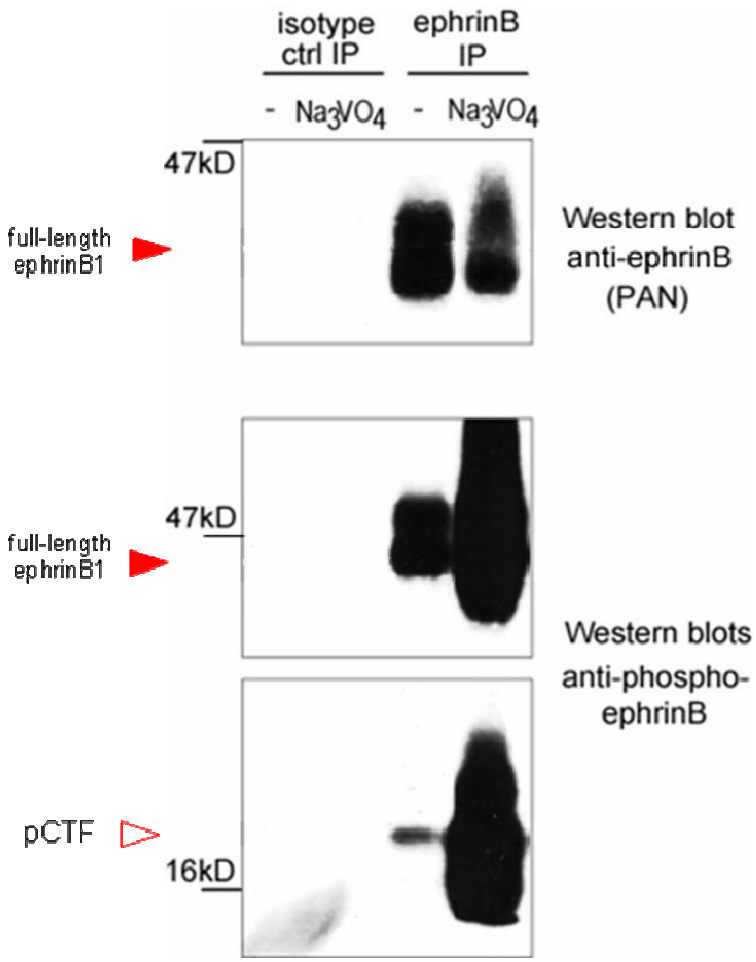

Figure 4.5: EphrinB pCTF were produced in embryonic chick limb tissue following sodium orthovanadate addition.

Crudely dissected E6 chick limbs were treated with 1 mM sodium orthovanadate for 1 hr, then lysed and endogenous ephrinB proteins were immunoprecipitated. The samples were blotted with anti-phospho-ephrinB, then reprobed with anti-ephrinB1 (PAN). (Note: there are two ephrinB gene products in chick, ephrinB1 and B2.) (n=3)

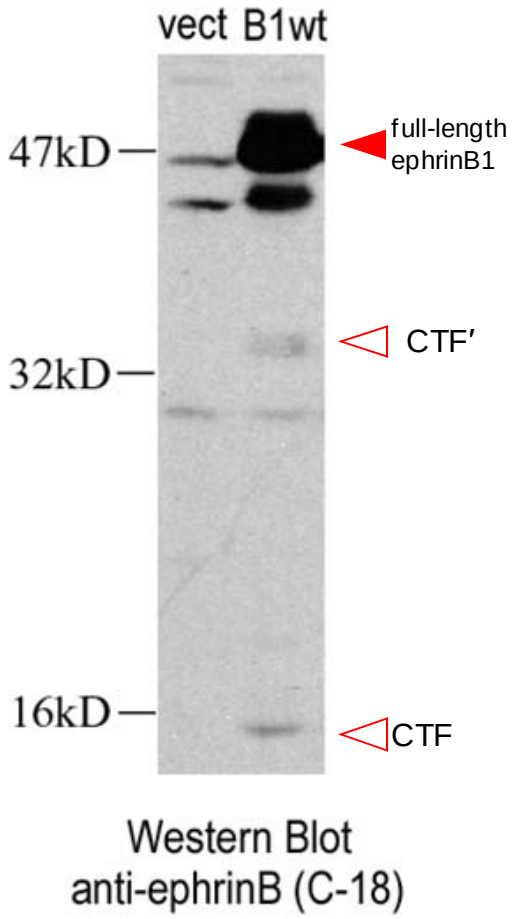

Figure 4.6: EphrinB1 CTF is found in ephrinB1wt expressing 3T3 cells.

Untreated ephrinB1wt or vector expressing cells were lysed directly in sample buffer. (n=3)

Furthermore, tyrosine phosphorylation of pCTF suggested it may possess signaling abilities. CTF, an unphosphorylated version of pCTF, was also be present in unstimulated cells. The molecular weight and characteristics of these fragments are summarized in Table 6.

4.2.2 Phospho-Carboxy-Terminal Fragments are EphrinB1-Specific

The anti-phospho-ephrinB antibody detection of protein bands by immunoblotting was not limited to tyrosine phosphorylated ephrinB proteins (**Figures 4.1, 4.2 and 4.4)**. Therefore, in order to confirm that pCTF was ephrinB1-specific and not an artifact detected by this antibody, a HA/Myc-dually tagged version of ephrinB1wt, termed HA/MycB1wt, was generated and assessed via tag-specific immunoblotting and immunoprecipitation. A PCR-based subcloning approach was used to insert a 12 aa Myc tag following the ephrin ectodomain and a 9 aa HA tag within the cytosolic tail (**Figure 4.7A**). The expected molecular weight increase for inserting these internal tags into ephrinB1 was ~2.5 kDa. NIH3T3 cells stably expressing HA/MycB1wt were established and positive expression of the construct was validated by anti-HA and anti-ephrinB Western blotting of cell lysates (**Figure 4.7B**). HA/MycB1wt ran at a molecular weight of ~55 kDa which is ~5 kDa larger than expected for the presence of the antigenic tags. Immunoblotting for HA antigen confirmed expression of this epitope tag in the HA/MycB1wt construct (**Figure 4.7B**) however similarly blotting for the Myc antigen was unsuccessful (data not shown). In addition to the full-length protein, ~35 kDa CTF′ was also detected in the HA/MycB1wt cells (**Figure 4.7B**). The expression of full-length HA/MycB1wt appeared to be lower than that of ephrinB1wt as grossly characterized by

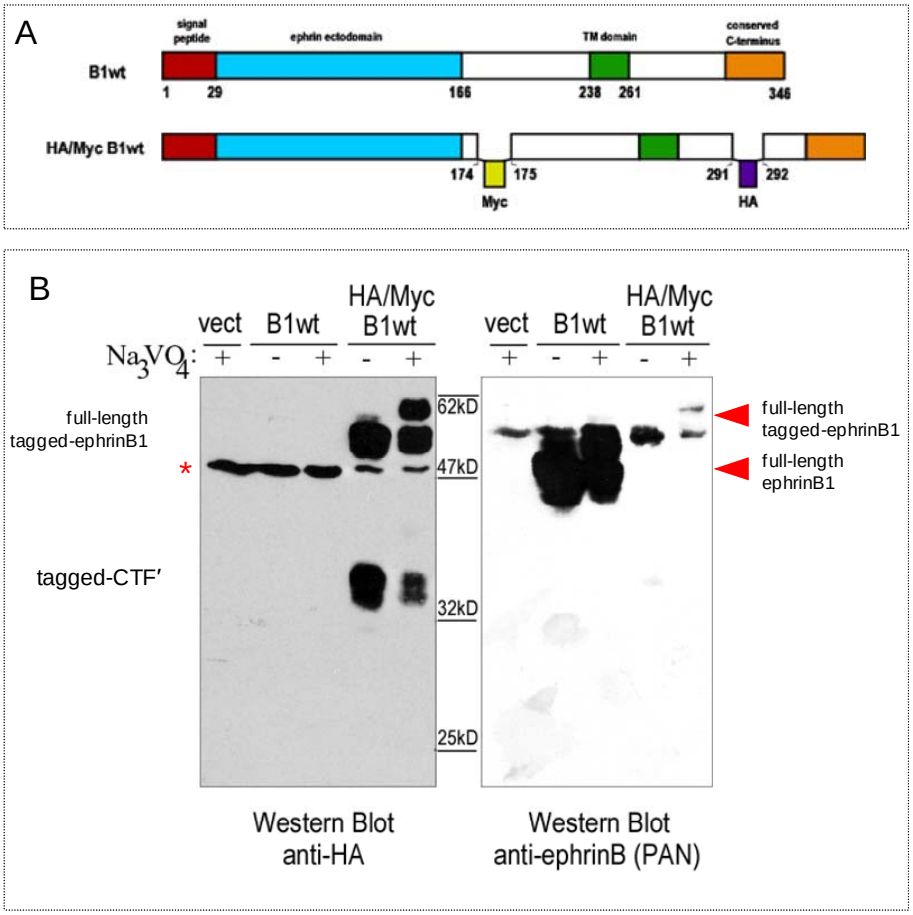

Figure 4.7: HA/Myc-tagged ephrinB1wt (HA/MycB1wt) was expressed in 3T3 cells.

(A) Schematic of Myc/HA tagged B1wt. (B) NIH3T3 cells expressing ephrinB1wt, HA/MycB1wt, or vector alone, were treated with 1 mM sodium orthovanadate for 1 hr, then lysed directly in sample buffer. The samples were blotted with anti-HA, then reprobed with anti-ephrinB1 (PAN). (n=1)

anti-ephrinB Western Blotting (**Figure 4.7B**). This observation was corroborated by the relatively lower number of cells found to have positive cell surface expression of ephrinB1 proteins in HA/MycB1wt (56% gated) relative to ephrinB1wt (81% gated) as assessed by flow cytometry of EphB2-Fc cellular staining (**Figure 4.8**).

The generation of pCTF by HA/MycB1wt in response to sodium orthovanadate was evident as assessed by anti-phospho-ephrinB Western blotting (**Figure 4.9**). Importantly, its pCTF also ran at a higher molecular weight in comparison to pCTF from ephrinB1wt, reflecting the size difference of their respective full-length proteins and indicating that pCTF were ephrinB1-specific. Very little or no detectable pCTF were generated in ephrinB1wt or HA/MycB1wt NIH3T3 cells in response to EphB2-Fc or PDGF. Interestingly, of the pCTF produced by HA/MycB1wt, a large proportion was ~40 kDa pCTF′ (**Figure 4.9**). Accompanying this observation, ~35 kDa CTF′ that was detected in unstimulated HA/MycB1wt cells exhibited reduced levels following addition of sodium orthovanadate (**Figure 4.7B**), suggesting some CTF′ was tyrosine phosphorylated to produce pCTF′ with the treatment. Tyrosine phosphorylated full-length HA/MycB1wt, and its pCTF and pCTF′, were immunoprecipitated with anti-HA antibodies and detected by anti-phospho-ephrinB antibody immunoblotting (**Figure 4.10**), further indicating that these fragments were ephrinB1-specific.

Taken together, the larger molecular weight of HA/MycB1wt pCTF relative to that of ephrinB1wt caused by the insertion of the antigenic tags, as well as the tag-specific immunoprecipitation of HA/MycB1wt pCTF, firmly demonstrated that pCTF are ephrinB1-specific. Insertion of the HA/MycB1wt led to an increased proportion of

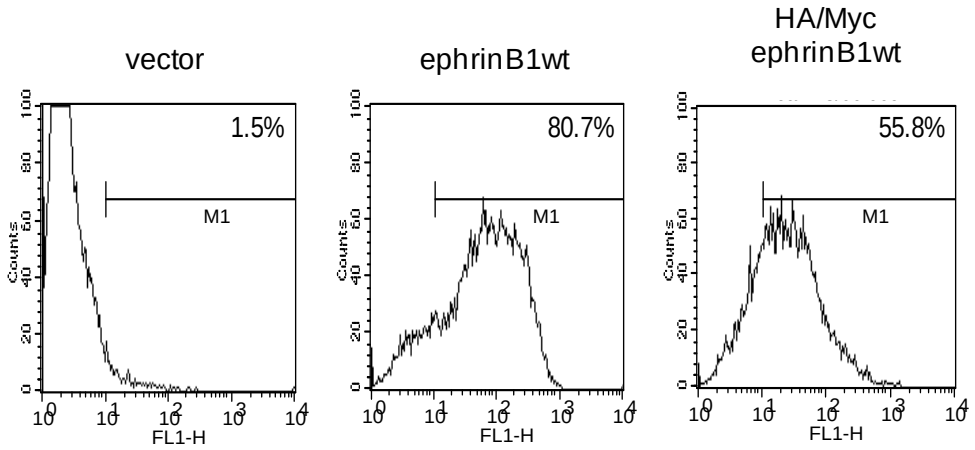

Figure 4.8: Positive cell surface expression of HA/Myc exphrin B1wt in NIH3T3 cells.

NIH3T3 cells expressing ephrinB1wt, HA/MycB1wt, or vector alone, were stained with EphB2-Fc receptor bodies detected by anti-human-Fc Alexa-488 fluorescently conjugated secondary antibody (fluorescence on x-axis). The percentage of gated cells were indicated in the top right hand corner for each sample. (n=1)

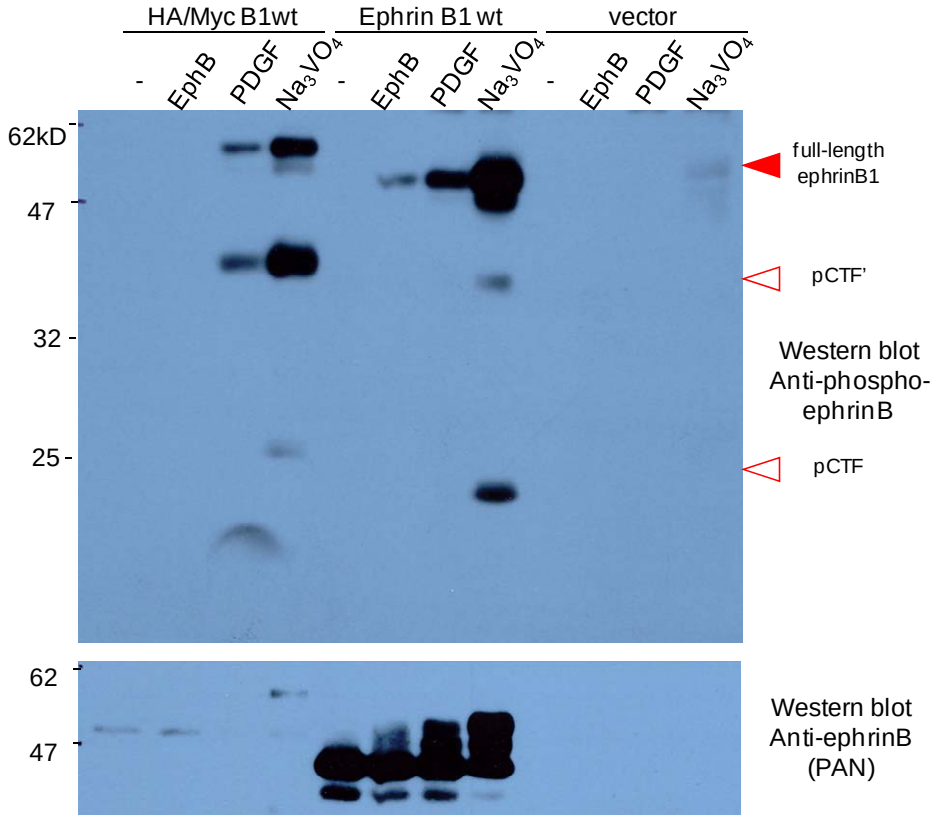

Figure 4.9: pCTFs were produced and HA/MycB1wt was tyrosine phosphorylated in response to EphB2-Fc, PDGF-BB, and sodium orthovanadate.

EphrinB1wt, HA/MycB1wt, or vector alone, expressing NIH3T3 cells were treated with 2 µg/ml EphB2-Fc for 30 min, 50 ng/ml PDGF-BB for 15 min, or 1 mM sodium orthovanadate for 1hr. The cells were then lysed directly in sample buffer. The samples were blotted with anti-phospho-ephrinB, then reprobed with anti-ephrinB1 (PAN). (n=2)

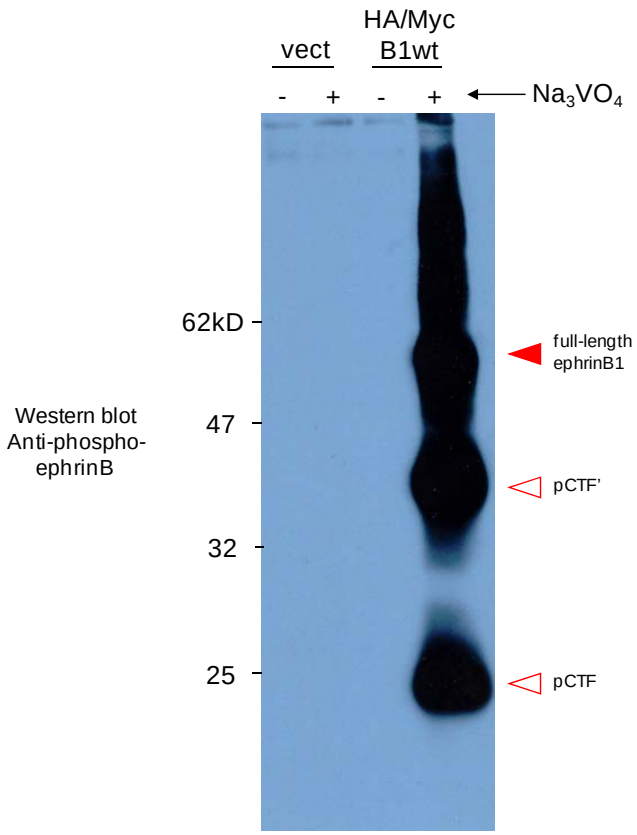

Figure 4.10: Immunoprecipitation of HA/MycB1wt with anti-HA antibody pulled-down HA/MycB1 pCTF.

HA/MycB1wt or vector alone expressing NIH3T3 cells were treated with 1 mM sodium orthovanadate for 1 hr, then lysed and immunoprecipitated with anti-HA antibody. (n=1)

pCTF′ relative to pCTF, suggesting that the tag insertion locations may have uncovered regions in ephrinB1wt involved in regulating these two species.

4.2.3 Phospho-Carboxy-Terminal-Fragments are Membrane-Associated

As it was likely that pCTF arose from ephrinB1 ectodomain shedding based on its molecular weight, the particulate and soluble fractions of sodium orthovanadate-treated ephrinB1wt 3T3 cells were isolated to evaluate the membrane-association of pCTF. A Western blot of these fractions by the anti-phospho-ephrinB and anti-ephrinB antibodies indicated that pCTF and CTF were found in the particulate fraction in which cellular membranes are pelleted (**Figure 4.11**). Full-length ephrinB1 and cyclinD1, a soluble protein functioning in cell cycle progression, served as particulate and soluble fraction markers, respectively. CyclinD1 appeared to be destabilized by treatment with sodium orthovanadate. Based on the membrane association of pCTF and CTF, and their approximate molecular weights, it was deduced they are products of an extracellular domain shedding event of ephrinB1. Our subsequent pursuit to describe the protease(s) class involved in the ectodomain shedding event was unsuccessful. Nonetheless, our discovery of this shedding event was the first demonstration of this process occurring for B-class ephrins.

4.2.4 PDZ Interactions are Involved in the Regulation of Phospho-Carboxy-Terminal Fragments

Cytoplasmic interactions of ephrinB1 that may regulate pCTF accumulation were assessed by analysis of sodium orthovanadate-treated ephrinB1 cytosolic mutant

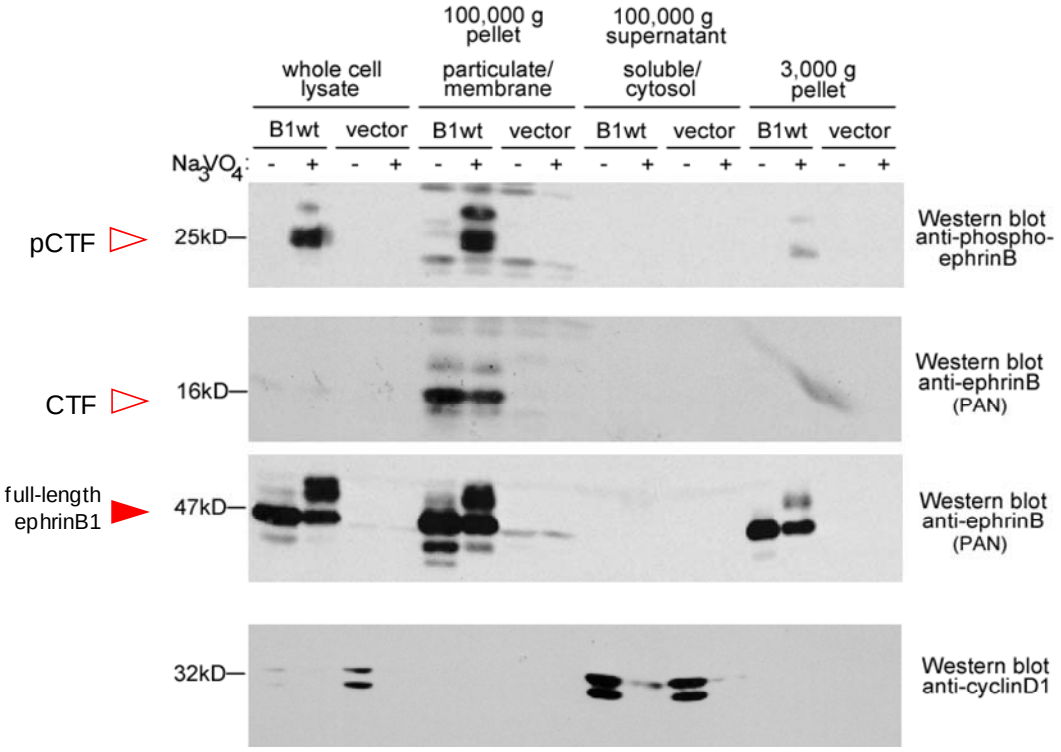

Figure 4.11: EphrinB1 pCTF was associated with the cellular membranes.

Particulate fractionation of EphrinB1wt NIH3T3 or vector control cells treated with 1 mM sodium orthovanadate for 1 hr. Equal amounts (100 µg) of particulate and soluble fractions were analyzed by anti-phospho-ephrinB immunoblotting, then reprobed with anti-ephrinB (PAN) first, and finally anti-cyclinD1 (used as soluble fraction marker). (n=2)

expressing NIH3T3 cells. The mutations of the ephrinB1Δ1, Δ4, Δ12, Δ33, ΔIV, and ΔKLR constructs used in this study were summarized in **Figure 3.1** and described in detail in section **3.2.1**. pCTF were produced by the ephrinB1 cytosolic mutants Δ1 and ΔIV when stimulated with sodium orthovanadate and analyzed by anti-phospho-ephrinB Western blotting (**Figure 4.12**). Importantly, the pCTF produced by ephrinB1Δ1 and ΔIV changed in molecular weight, in a similar manner to that of their phosphorylated full-length mutant proteins to ephrinB1wt, further confirming that pCTF are ephrinB1-specific. Howev er, pCTF was not produced in ephrinB1Δ4, Δ12, ΔKLR or Δ33 mutants, the latter having served as a negative control in this experiment since it is undetectable by the blotting antibody. EphrinB1Δ4 and Δ12 both possessed PDZ-motif ablations while the polybasic domain was largely deleted in ephrinB1ΔKLR. Thus, due to the inability of ephrinB1Δ4, Δ12, and ΔKLR to generate pCTF following sodium orthovanadate treatment, it is likely that the cytosolic PDZ-motif and polybasic domain of ephrinB1 regulate pCTF levels.

4.2.5 Characterization of the Proteolytic Processing of EphrinB1 Phospho-Carboxy-Terminal-Fragments: a Role for Gamma-Secretase

Due to the membrane-association and ectodomain-shedding origin of pCTF it was further hypothesized that it underwent regulated intramembrane proteolysis (RIP) mediated by gamma-secretase. EphrinB1wt 3T3 cells were pre-treated with the gamma-secretase inhibitor DAPT (**Figure 4.13**). Upon stimulation with sodium orthovanadate, the accumulation of pCTF was apparent suggesting pCTF was a substrate of gamma-secretase. Importantly, the pre-treatment with the gamma-secretase inhibitor also led to

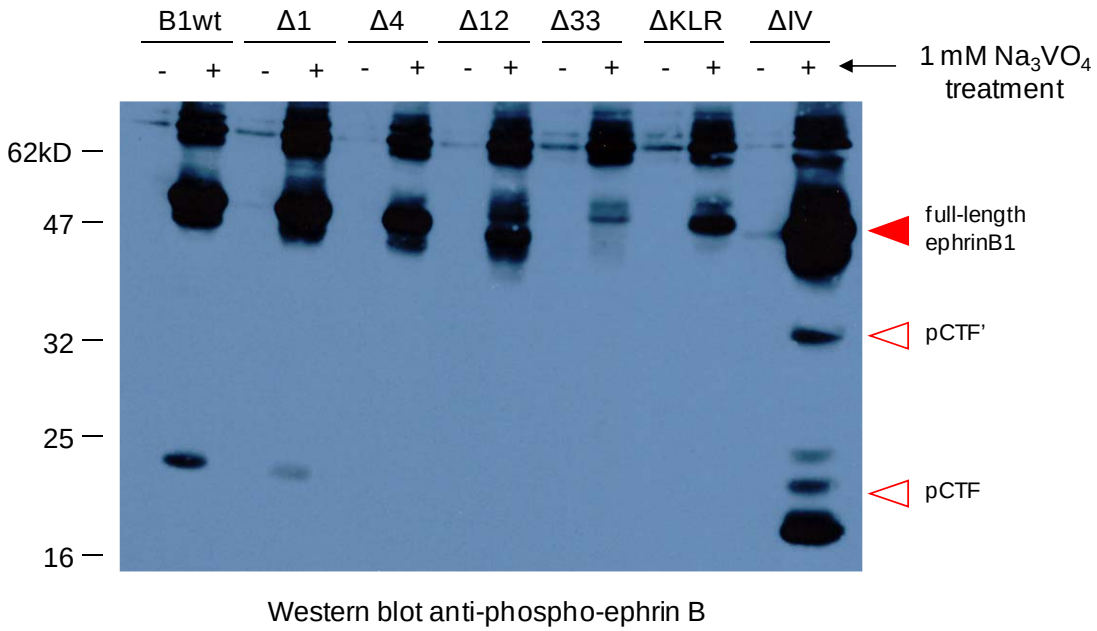

Figure 4.12: EphrinB1 cytosolic domain mutants Δ1 and ΔIV produce pCTFs when treated with sodium orthovanadate.

NIH3T3 cells expressing the ephrinB1 constructs (wt, Δ1, Δ4, Δ12, Δ33, ΔKLR and ΔIV; deletions affecting these mutants are detailed in Figure 3.1) or vector alone were treated with 1mM sodium orthovanadate for 1 hr and then lysed directly in sample buffer. (n=1)

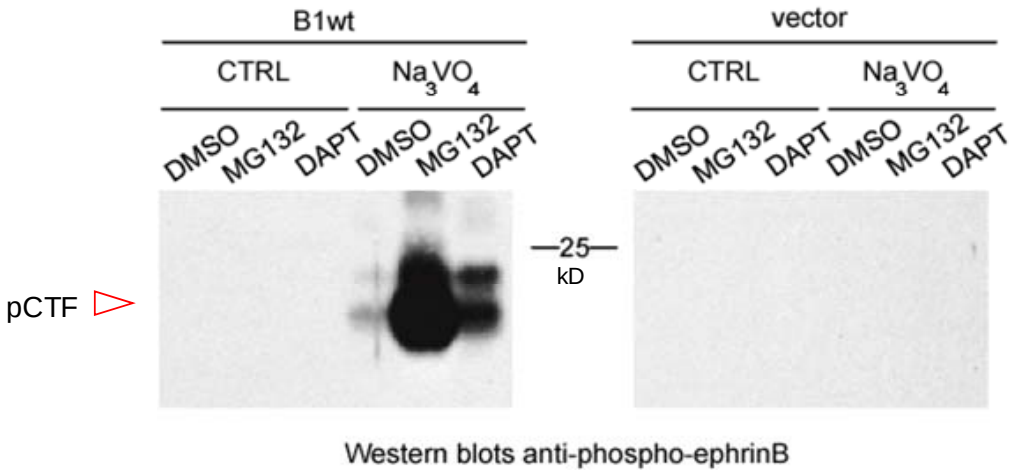

Figure 4.13: Gamma-secretase and the proteasome were involved in modulating levels of EphrinB1 pCTF following treatment with sodium orthovanadate.

NIH3T3 cells expressing ephrinB1wt or vector alone were pre-treated ~16 hrs with 10 µM DAPT, a gamma-secretase inhibitor, or 5 µM MG132, a proteasome inhibitor, prior to treatment with 1mM sodium orthovanadate for 1 hr. The cells were then lysed directly in sample buffer. (n=4)

the accumulation of pCTF when ephrinB1wt cells were stimulated with EphB2-Fc or PDGF (**Figure 4.14**), suggesting that gamma-secretase cleavage occurs in more classically described modes of ephrinB1 signaling. In addition, the accumulation of pCTF was observed by pre-treating cells with MG132, a proteasome inhibitor (**Figure 4.13**). These inhibitor studies suggested that RIP via gamma-secretase was modulating pCTF levels and thus suggested a further step of proteolytic processing occurs in ephrinB1 signaling that has not been previously described.

To further substantiate the involvement of gamma-secretase processing in ephrinB1 signaling, presenillin (PS) double knockout mouse embryonic fibroblasts (MEFs) were obtained (199). PS proteins act as the catalytic subunits of the gamma-secretase complex and in their absence the protease activity of the complex is inhibited. Thus, if gamma-secretase activity was involved in the processing of pCTF following ephrinB1 stimulation, pCTF should accumulate in *PS 1,2 -/-* cells since these cells would be unable to cleave pCTF. Stably expressing ephrinB1wt and vector control lines were established for the *PS 1,2 +/+* and *PS 1,2 -/-* MEFs. These cell lines were stimulated with sodium orthovanadate, EphB2-Fc, and PDGF and analyzed by anti-phospho-ephrinB immunoblotting (**Figure 4.15**) but pCTF accumulation was not detected in our experiments. However a discernable difference was apparent in ephrinB1wt phosphorylation between the cell lines in response to the different agonists. Stimulation of ephrinB1wt-expressing *PS 1,2-/-* cells with sodium orthovanadate or PDGF did not result in phosphorylation of ephrinB1wt. EphB2-Fc was the only agonist that led to ephrinB1 phosphorylation in these cells. Conversely, ephrinB1 was robustly

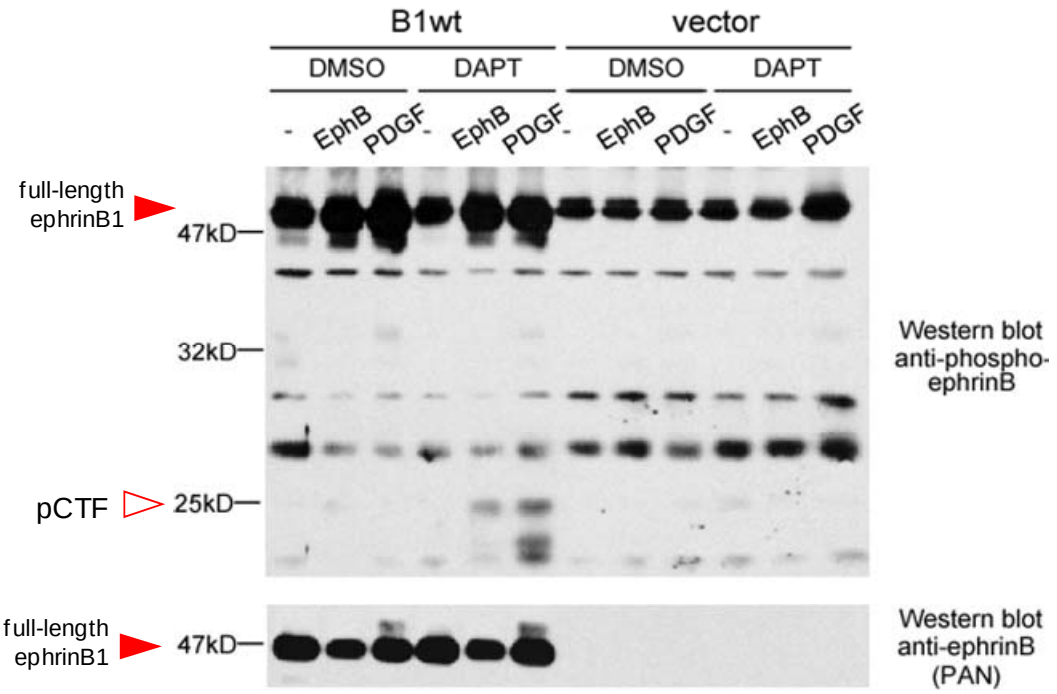

Figure 4.14: Gamma-secretase modulated levels of EphrinB1 pCTF produced following EphB2-Fc and PDGF stimulation.

NIH3T3 cells expressing ephrinB1wt or vector alone were pre-treated ~16 hrs with 10 µM DAPT, a gamma-secretase inhibitor, prior to treatment with either 4 µg/ml EphB2-Fc for 40 min, or with 50 ng/ml PDGF-BB for 15 min. The cells were then lysed directly in sample buffer, and analyzed by anti-phospho-ephrinB immunoblotting, then reprobed with anti-ephrinB (PAN). (n=1)

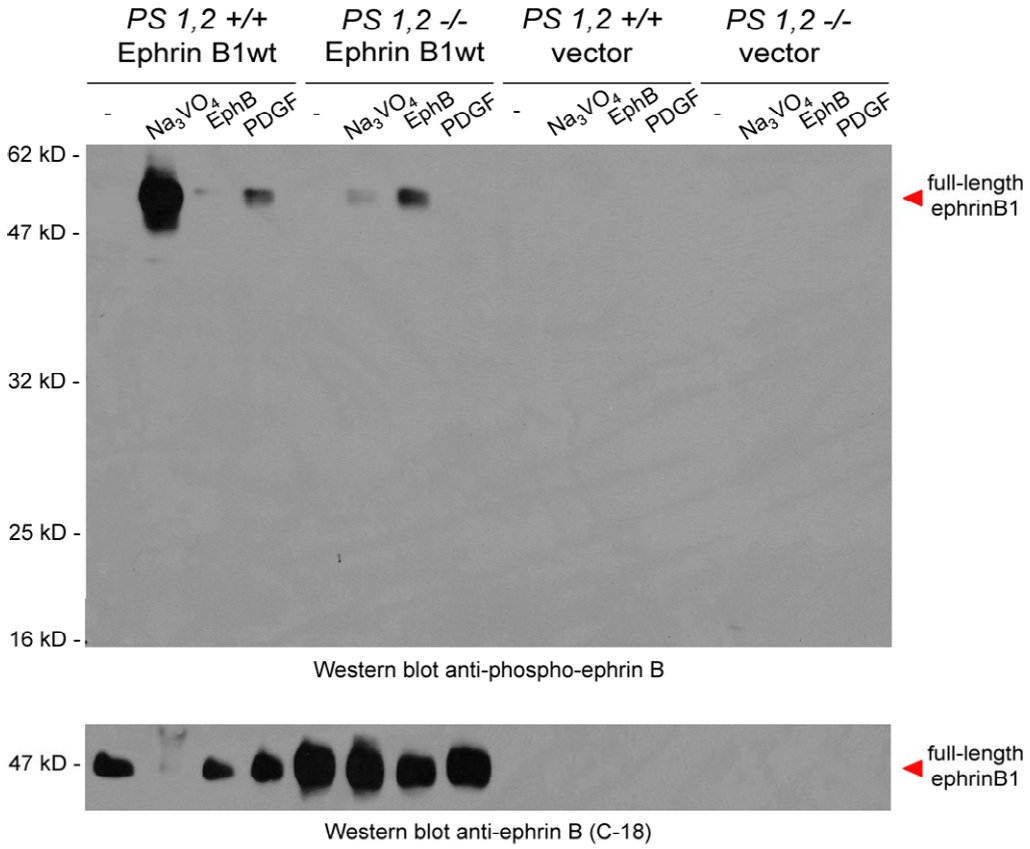

Figure 4.15: EphrinB1pCTF was not detected in EphrinB1wt expressing *PS 1,2+/+* or *PS 1,2-/-* mouse embryonic fibroblasts (MEFs).

EphrinB1wt expressing, or vector alone, *PS 1,2+/+* or *PS 1,2-/-* MEFs were treated with 1mM sodium orthovanadate for 1 hr, 4 µg/ml EphB2-Fc for 40 min, or with 30 ng/ml PDGF-BB for 15 min. The cells were then lysed directly in sample buffer. (n=2)

phosphorylated in response to sodium orthovanadate in ephrinB1wt *PS 1,2 +/+* cells, slightly with PDGF and not at all with EphB2-Fc.

It was not possible to conclude whether gamma-secretase activity is involved in pCTF regulation from the experiments with *PS -/-* MEFs since pCTF was not detect in wt MEFs either. The clearly divergent ephrinB1 signaling responses in the PS MEFs suggested that these cells may not be an appropriate model system to assess gamma-secretase involvement in ephrinB1 signaling.

4.2.6 Investigation of Phospho-Carboxy-Terminal-Fragments Regulation by Juxtamembrane Lysine Residues

Due to the molecular weight difference between CTF (16 kDa) and pCTF (25 kDa) of ~10 kDa, it was likely that this significant molecular weight difference was not due solely to tyrosine phosphorylation and instead due to post-translational modifications, such as a polypeptide modifier like ubiquitin (~7 kDa) which can attach at lysine residues (177). In Notch receptor signaling, a lysine residue lying in the juxtamembrane region is covalently-modified with a mono-ubiquitin and this modification is required for processing of Notch by gamma-secretase (200). Since it appears that pCTF possessed post-translational modification(s) of ~10 kDa relative to CTF, part of this size shift may have been due to ubiquitination of one of the three intracellular juxtamembrane lysines found in ephrinB1 and hence may be required for gamma-secretase processing of pCTF.

To investigate this possibility, site-directed-mutagenesis was employed to mutate the juxtamembrane lysine residues to arginine in ephrinB1wt, thus generating the ephrinB1Δ3K→R construct (**Figure 4.16A**) and NIH3T3 cells expressing the construct

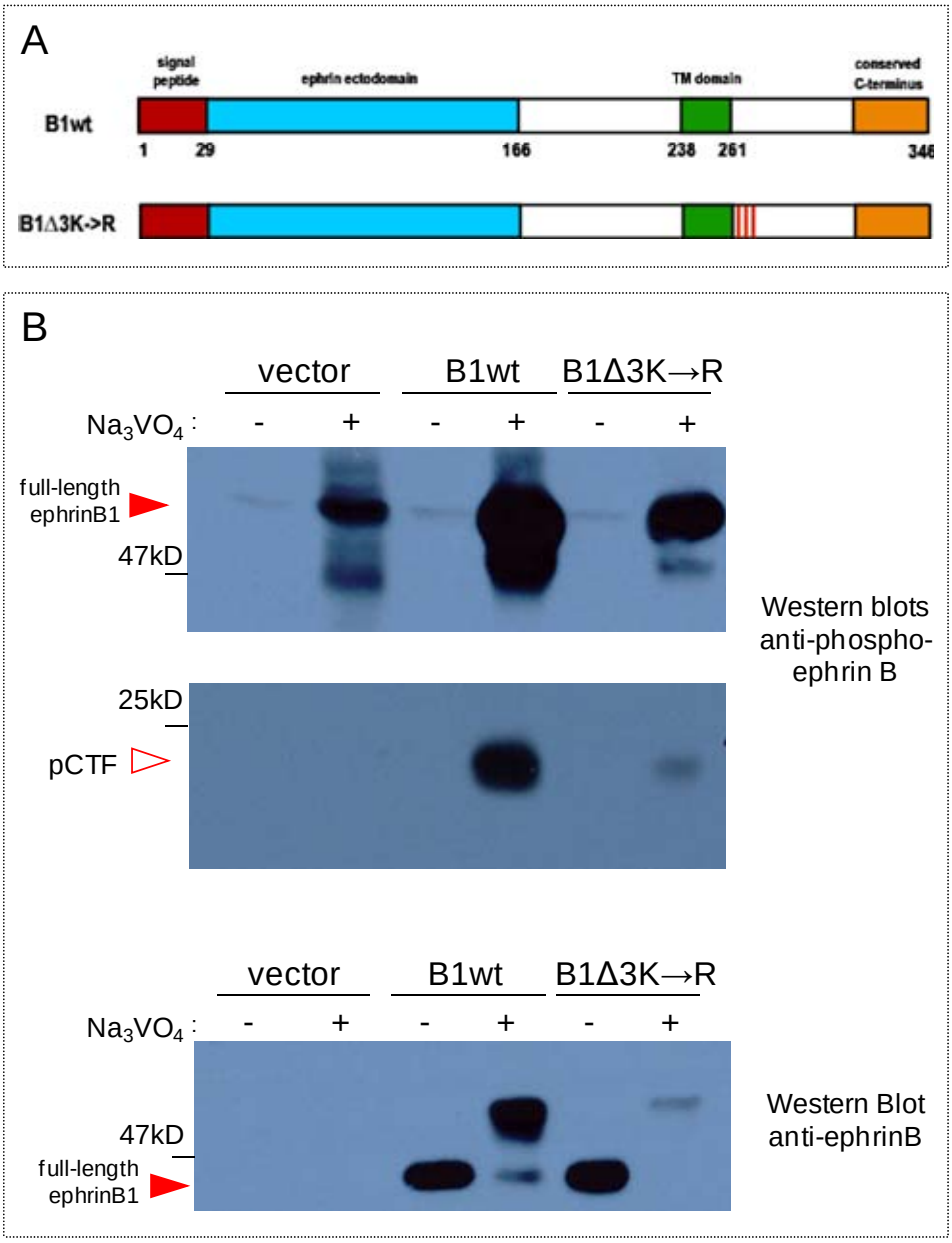

Figure 4.16: Post-translational modifications on three juxtamembrane lysines of ephrinB1 did not occur on ephrinB1 pCTF.

(A) Schematic of EphrinB1Δ3K→R mutant, the red lines indicate the sites of mutagenesis. (B) EphrinB1wt, EphrinB1Δ3K→R, or vector alone expressing NIH3T3 cells were treated with 1mM sodium orthovanadate for 1 hr, then lysed directly in sample buffer. (n=2)

were established. If ubiquitination at any of these lysines was required for gamma-secretase processing of pCTF, by mutating these residues, a robust accumulation of pCTF in sodium orthovanadate-treated ephrinB1Δ3K→R cells, when compared to ephrinB1wt, should occur since pCTF could not be processed by gamma-secretase. In addition, if ubiquitination at these residues was responsible for part of the size increase between CTF and pCTF accompanying phosphorylation of ephrinB1, pCTF ephrinB1Δ3K→R species should be relatively smaller in molecular weight than those of ephrinB1wt. When treated with sodium orthovanadate and immunoblotted for anti-phospho-ephrinB, no relative size change was discerned between ephrinB1Δ3K→R and ephrinB1wt in their respective pCTF (**Figure 4.16B**).

A decrease in pCTF production in sodium orthovanadate-treated ephrinB1Δ3K→R cells relative to the ephrinB1wt was observed. From this study, it was determined that post-translational modifications, such as ubiquitination, occurring at ephrinB1's three juxtamembrane lysine residues mutated were not responsible for part of the molecular weight difference between CTF and pCTF.

4.2.7 Investigations into the Intracellular Domain Fragment of EphrinB1

As it was suspected that pCTF was processed by gamma-secretase (**Figure 4.14**), the study of the proteolytic product of regulated intramembrane proteolysis (RIP), the intracellular domain (ICD), was undertaken for ephrinB1.

ICDs are generally unstable moieties (201) so a combination of proteasome and gamma-secretase inhibitors is commonly used to enhance the visualization of ICDs.

EphrinB1wt cells were pre-treated with epoxomicin, a proteasome inhibitor, and gamma-secretase inhibitor X (γ-sec X) together prior to addition of sodium orthovanadate to the cells, then analyzed by anti-phospho-ephrinB Western blotting (**Figure 4.17**). pCTF was found to accumulate by concurrent treatment with these inhibitors however the accumulation of an ICD was not detected.

A strategy where ICD production is enhanced was next employed in the study of ephrinB1 ICD. Previously, Notch ICD signaling has been studied with the use of an extracellular domain-deficient (ΔECD) mutant of Notch receptor. NotchΔECD is constitutively cleaved by gamma-secretase resulting in the continual production of ICD (196). Ergo, with the aim of studying ephrinB1 ICD function, an ephrinB1 construct lacking an extracellular domain, B1ΔECD, was designed and constructed. The B1ΔECD construct possessed the entire transmembrane and cytosolic domains of ephrinB1 along with the signal peptide and 43 aa of the extracellular linker region (**Figure 4.18A**). Cells stably transfected with B1ΔECD were pre-treated with MG132, proteasomal inhibitor, or with DAPT, a gamma-secretase inhibitor, prior to addition of sodium orthovanadate and then analyzed by anti-phospho-ephrinB immunoblotting (**Figure 4.18B**). Phosphorylated B1ΔECD was detectable in sodium orthovanadate-treated cells but not in untreated cells. In the presence of sodium orthovanadate, B1ΔECD was stabilized by pre-treatment with DAPT, suggesting phosphorylated B1ΔECD was a substrate of gamma-secretase, but not with the proteasome inhibitor MG132. However an ephrinB1 ICD fragment was not detected under these experimental conditions. B1ΔECD, when tyrosine-phosphorylated, ran higher than pCTF at ~30kDa. With the signal peptide cleaved, the predicted molecular weight of non-modified B1ΔECD is ~16 kDa. The observed ~30 kDa

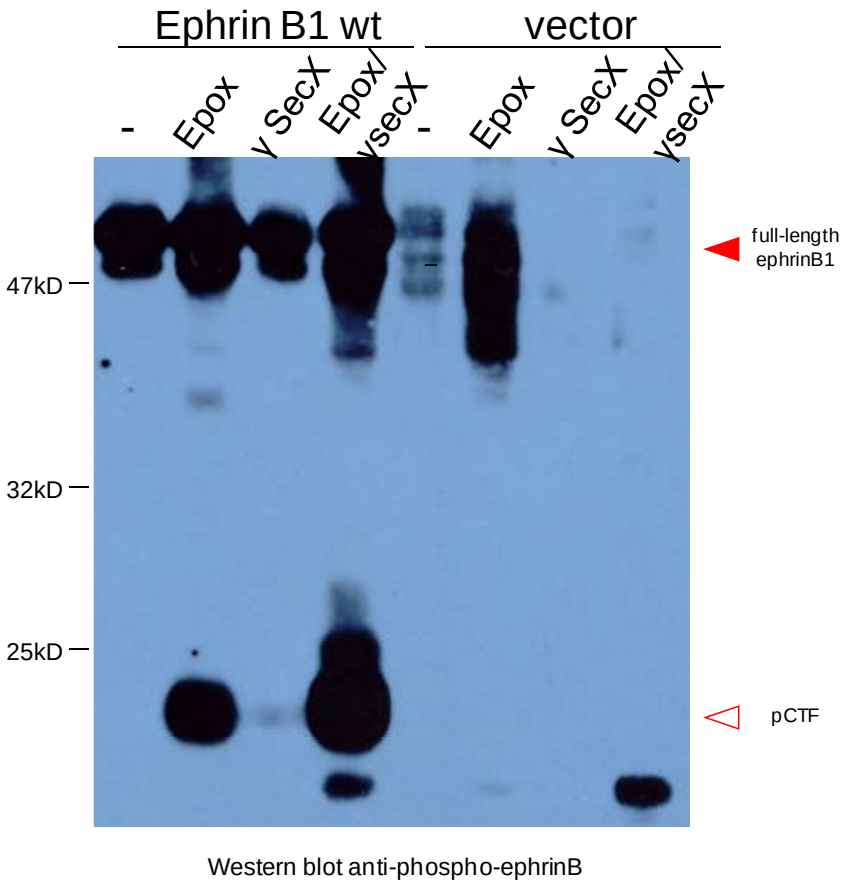

Figure 4.17: EphrinB1 pCTF sodium orthovanadate-induced accumulation was increased in cells when pre-treated with gamma-secretase and proteasome inhibitors in conjunction.

EphrinB1wt or vector alone expressing NIH3T3 cells were pre-treated for ~4 hrs with 1 µM epoxomicin, a proteasome inhibitor, and/or 50 µM gamma-secretase inhibitor-X, prior to addition of 1 mM sodium orthovanadate for 1 hr. (n=2)

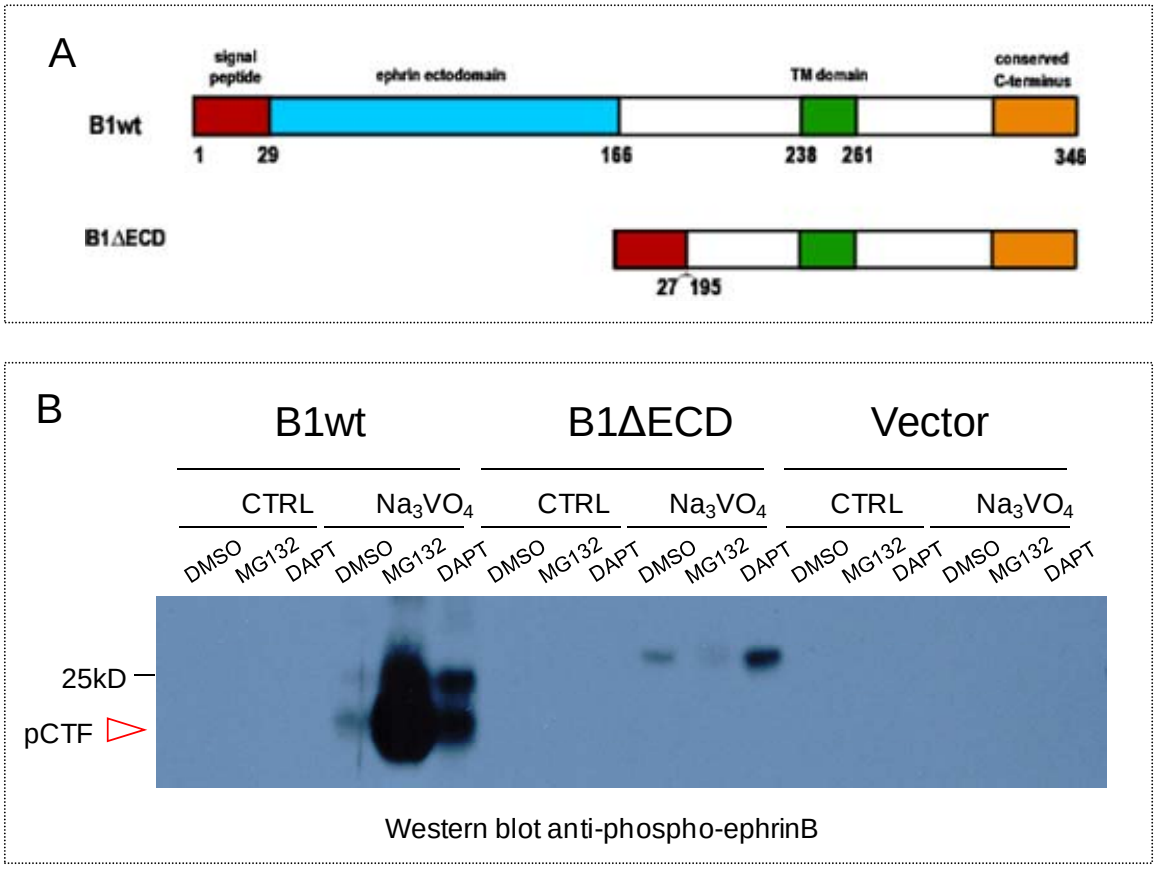

Figure 4.18: EphrinB1ΔECD was stabilized by treatment with sodium orthovanadate and gamma-secretase inhibitors.

(A) Schematic of EphrinB1ΔECD. (B) EphrinB1ΔECD, ephrinB1wt, or vector along expressing NIH3T3 cells were pre-treated ~16 hrs with 10 µM DAPT, a gamma-secretase inhibitor, or 5 µM MG132, a proteasome inhibitor, prior to treatment with 1mM sodium orthovanadate for 1 hr. The cells were then lysed directly in sample buffer. (n=3)

molecular weight of sodium orthovanadate-stabilized B1ΔECD suggests that it was likely post-translationally modified and/or underwent a conformational change. Changes in cellular morphology, or of gene transcription relative to vector control cells, were not detected in 3T3 cells following expression of B1ΔECD (data not shown). Thus, the B1ΔECD 3T3 expressing cells did not appear to produce ephrinB1 ICD, however B1ΔECD was found to be stabilized through tyrosine phosphorylation.

4.3 Discussion

Our novel observation that pCTF was a membrane-associated fragment derived from ephrinB1 ectodomain-shedding is the first report of a tyrosine phosphorylated ephrinB1-specific proteolytically generated fragment (see proposed model in **Figure 4.19**). Due to the tyrosine phosphorylation of pCTF it likely also retains signaling abilities. The temporal production of pCTF was also linked to the tyrosine phosphorylation of full-length ephrinB1 in response to EphB2-Fc and PDGF, suggesting a regulated accumulation of pCTF during ephrinB1 signaling. Importantly, pCTF were found in chick limbs (a tissue in which ephrinB1 functions) thus providing evidence for pCTF production *in vivo*. pCTF regulation was found to be associated with the PDZ-motif of ephrinB1, and mediated by the proteasome and regulated intramembrane proteolysis (RIP) by gamma-secretase. Thus, our study presented a novel avenue of signal refinement through proteolysis available to ephrinB proteins.

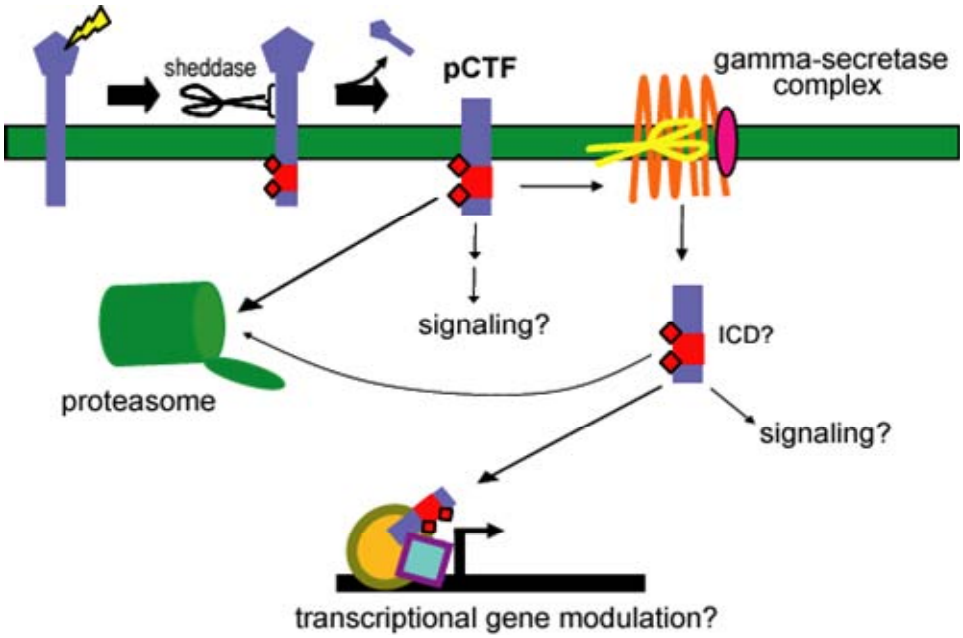

Figure 4.19: Model of ephrinB1 proteolytic processing.

pCTF production may arise from tyrosine phosphorylation of CTF and/or ectodomain shedding of tyrosine phosphorylated full-length ephrinB1, this remains to be determined. Red diamonds represent tyrosine phosphorylation.

4.3.1 Phospho-Carboxy-Terminal-Fragments are EphrinB1-Specific and Produced in Connection with EphrinB1 Phosphorylation

Initially, it was observed that pCTF was produced in response to stimulation by EphB2-Fc and PDGF and its overall temporal production mirrored those of full-length ephrinB1 activation. Sodium orthovanadate, a tyrosine phosphatase inhibitor, induced a large amount of pCTF production as well as phosphorylation of full-length ephrinB1. This response, and in particular pCTF generation, was also observed in MDCK cells, indicating that the proteolytic processing of this protein was not restricted to NIH3T3 cells. pCTF was proven to be ephrinB1-specific, rather than a signaling artifact detect by the anti-phospho-ephrinB antibody, by tag-specific immunoprecipitation of HA/Myc ephrinB1wt pCTF as well as the relative molecular weight increase of pCTF that was observed when the antigenic tags were inserted in ephrinB1.

Src-family kinases were implicated in mediating the tyrosine phosphorylation of ephrinB1 and pCTF production in cells following treatment with sodium orthovanadate. Pre-treatment of cells with the Src-family kinase inhibitor PP2 prior to cellular treatment with sodium orthovanadate significantly reduced the amount of pCTF and phosphorylated full-length ephrinB1. The cell adhesion molecule L1 shedding was also induced by sodium pervanadate (sodium orthovanadate mixed with peroxide) via a mechanism dependent on Src-family kinase activation (198). These kinases are implicated in EphB-mediated activation and downstream signaling of ephrinB1 (87, 89), thus sodium orthovanadate treatment likely resulted in hyper-inducing an endogenous mode of ephrinB1 activation through the Src-family kinases, leading to subsequent

shedding. In our hands, sodium orthovanadate induce similar amounts of shedding as sodium pervanadate. The amount of pCTF produced in cells following sodium orthovanadate treatment was more consistent in comparison to EphB2-Fc and PDGF hence it was adopted as the main stimulus in our studies.

4.3.2 Phospho-Carboxy-Terminal-Fragments are Produced in Chick Limb Tissue

pCTF was also observed in chick limbs, a tissue in which ephrinB1s have been shown to function (138, 139). Low levels of endogenous ephrinB pCTF were detected in ephrinB immunoprecipitations of crudely dissected chick limbs and these levels increased following treatment with sodium orthovanadate. There are two chick ephrinB genes, ephrinB1 and ephrinB2. Our ephrinB-antibody used for immunoprecipitations cannot discern between these two ephrinB proteins and it is likely that both proteins were pulled-down since two full-length protein bands were detected. The full-length chick ephrinBs and pCTFs exhibit slightly lower molecular weights relative to human ones. The endogenous presence and sodium-orthovanadate induction of chick pCTFs in limb tissue provided data to support that proteolytic processing of ephrinBs can occur *in vivo* and therefore may have physiological functions.

4.3.3 Phospho-Carboxy-Terminal-Fragments are the Product of Ectodomain Shedding of EphrinB1

The ~27 kDa molecular weight difference between phosphorylated full-length ephrinB1wt (~52 kDa) and pCTF (~25 kDa) was approximately the size of the extracellular domain of ephrinB1 (~23 kDa), suggesting that pCTF was derived from a

shedding event of ephrinB1. The loss of an extracellular domain (~23 kDa) in full-length ephrinB1 (~47 kDa) would also result in CTF (~16 kDa). To validate our hypothesis that CTF and pCTF were the remaining transmembrane-anchored portion follwing shedding of ephrinB1, the association of these fragments with the particulate fraction of cells, where membranes are pelleted, was confirmed. Our attempts to characterize the protease class involved in ephrinB1 shedding however were unsuccessful. Nonetheless, it was concluded, based on molecular weight, and their association with membranes in the particulate fraction of cells, that pCTF and CTF are products of ephrinB1 extracellular domain shedding and our novel discovery implied further refinement of ephrinB signaling could be achieved through proteolysis.

Ectodomain shedding of ephrinB1 and CTF/pCTF production may be involved in modulating ephrinB signaling in a number of ways. To begin, ectodomain shedding of ephrinBs could be used as a mechanism to facilitate the physical separation and subsequent signal downregulation of high affinity EphB/ephrinB interactions on juxtaposed cell surfaces as previously suggested in cell-contact mediated ephrinA2 shedding (**Figure 1.5**) (83).

Secondly, the shed ephrinB ectodomains may also modulate Eph forward signaling. Although monomeric ephrin ectodomains are unable to induce signaling in cells expressing their cognate Eph receptors (13), these unclustered ectodomains could antagonize signaling by binding to Eph receptors on cell surfaces, thereby blocking the ability of the receptor to form functional interactions. Indeed, there is growing precedent for this antagonistic theory for ephrin and Eph interactions since soluble monomeric EphB4 have been found to antagonize EphB4-ephrinB2 interactions in endothelial cells

(202) and soluble splice variants of ephrinA4 are secreted from B cells following B-cell antigen receptor stimulation (203). Soluble ephrinA1 and A5 have recently been described to be oligomerized *in vivo* via tissue transglutaminase (204). These multimerized ephrinA-ectodomains are able to induce EphA forward signaling and by doing so have succeeded in extending the influence of clustered ephrin ligands beyond cell-contact mediated signaling.

CTF/pCTF derived from cell surface shedding of ephrinB1 may themselves moderate signaling of full-length ephrinB1 via interactions *in cis*. Since CTF/pCTF still possess the full cytoplasmic tail they may be able to cluster with full-length ephrinB1wt via intracellular interactions with adaptor or scaffolding proteins. EphrinB1's ectodomain spatial configuration could also be altered by CTF/pCTF interactions *in cis* with the full-length proteins. Altered ectodomain arrangements would impact how signals are sent to EphB receptor bearing cells. Reciprocally, ephrinB1's ability to receive EphB-mediated signals may be moderated via interactions with CTF/pCTF since ephrinB1's ability to be clustered may be impaired.

Finally, CTF/pCTF proteins may independently signal on their own uncontrolled by ligand. For example, ErbB4 receptor is constitutively shed resulting in a phosphorylated membrane-bound fragment that has tyrosine kinase activity (192). Platelet-endothelial cell adhesion molecule (PECAM)-1 glycoprotein shedding results in a truncated membrane-associated molecule that possesses enhanced ability to interact with cell signaling proteins as compared to the full-length PECAM-1 to mediate apoptosis (205). It is possible the CTF′ and pCTF′ species (Table 6) detected in our

experiments are homodimers of CTF and pCTF, respectively. Thus, CTF/pCTF may also possess autonomous signaling ability relative to full-length ephrinB1 proteins.

It is clear that shedding of ephrinB1 described herein has the potential to broadly modulate several aspects of ephrinB signaling as well as Eph receptor signaling. Shedding of ephrinB1 ectodomains resulting in CTF/pCTF production may be particularly relevant in development and cancer where ectodomain proteolysis of proteins has been found to effectuate important functions (187, 188, 193). Src-family kinases, which likely function in mediating ephrinB shedding, are also dysregulated in cancer (206-209) and may modulate ephrinB ectodomain shedding when these two proteins are found together.

Interestingly, ephrinB3 was found to be cleaved *in vitro* by one of the mammalian rhomboids, RHBDL2, an intramembrane serine protease (210). Unlike gamma-secretase, rhomboid cleaves full-length Type I transmembrane proteins within their transmembrane domains near the extracellular surface, releasing their complete ectodomains. Thus, rhomboid cleavage of ephrinB3 provides another mode of ephrinB ectodomain shedding as well as serving in the production of membrane-associated CTF. Gamma-secretase requires a short extracellular stretch on the N-termini of its substrates in order to cleave them (211). The CTF products derived from rhomboid cleavage, would likely not possess luminal N-termini and therefore are likely be subjected to different down-regulatory dynamics on the cell surface when compared to conventional sheddase-produced CTF that serve as gamma-secretase substrates. For B-class ephrins, this may overlay additional complexity in both their shedding regulation, their CTF modulation and thus reverse signaling.

4.3.4 Phospho-Carboxy-Terminal-Fragments and Carboxy-Terminal-Fragments are Related Species Likely Differentiated by Phosphorylation

It is likely that the various CTF/pCTF species observed in our studies vary from each other in terms of post-translational modifications (e.g. phosphorylation, ubiquitination) or may be representative of homodimers (Table 6). Based on molecular weight, membrane-association, and inability to be detected by the phospho-ephrinB antibody, CTF likely represents the unmodified fragment and is postulated to be produced by low levels of constitutive shedding, as observed with ErbB4 (192). pCTF is tyrosine-phosphorylated and likely has other uncharacterized modification(s) and/or has undergone a conformational change, due to its ~10 kDa larger size than CTF. pCTF production may arise from tyrosine phosphorylation of CTF and/or ectodomain shedding of tyrosine phosphorylated full-length ephrinB1, this remains to be determined. pCTF′ is ~13 kDa larger than pCTF, it may possess a more substantial post-translational modification, such as ubiquitin, in addition to tyrosine phosphorylation relative to pCTF, or simply be a dimer of pCTF. Alternatively, pCTF′ may be very tightly associated with a small protein.

Smaller molecular weight differences are also distinguished within pCTF and CTF species themselves. In certain experiments, pCTF produced in response to stimuli resulted in two to three ~25kDa pCTF fragments (see Figures 4.1, 4.11, 4.13, 4.15, & 4.17) and CTF could also be distinguished in cells as a few 16 kDa bands (see Figure 4.11). The multiple fragments of ~25 kDa pCTF that are very similar in molecular weight may differ from each other in the number of phosphorylated residues.

Alternatively, these very similar-sized fragments, and those of the CTF, may arise from different ecto-sheddases which cleave at distinct sites deriving pCTF and CTF with differing N-termini of varying lengths. Overall, the existence of the various-sized pCTF and CTF species strongly suggests a dynamic regulation of these via proteolysis and/or post-translational modifications.

Interestingly, the insertion of HA and Myc tags into ephrinB1wt led to a predominant production of CTF′ in unstimulated cells, and of pCTF′ in cells treated with sodium orthovanadate. The internal insertions of these tags may have altered the processing or modulation of CTF/pCTF, by either increasing shedding or more likely resulting in increased stabilization of HA/MycB1wt CTF/pCTF dimers, suggesting the regions where the tags were inserted may be involved in regulation of pCTF.

4.3.5 PDZ-Based Interactions are Involved in Phospho-Carboxy-Terminal-Fragments Regulation

Δ1 and ΔIV mutant constructs of ephrinB1's cytoplasmic tail also produced pCTF in NIH3T3 cells when treated with sodium orthovanadate. Interestingly, the size of pCTF from ephrinB1Δ1 and ΔIV were relatively smaller than that of ephrinB1wt, paralleling the smaller sizes of their full-length phosphorylated proteins compared to ephrinB1wt. These relative size differences of the pCTF cytoplasmic mutants presented further evidence that pCTF are ephrinB1-specific. Since ephrinB1Δ4 or Δ12, which both possess ablations of ephrinB1's PDZ-motif, did not produce pCTF it suggests that PDZ interactions may be important for regulation of pCTF, possibly via shedding.

pCTF generated by ephrinB1ΔKLR was also not observed but this may be due to the relatively low expression levels of this construct (see **Figure 3.3**). However, it remains possible that the polybasic domain deleted in ephrinB1ΔKLR may itself be required for pCTF production.

4.3.6 Phospho-Carboxy-Terminal Fragments are Regulated by Gamma-Secretase and the Proteasome

It was postulated that pCTF was further processed by RIP via gamma-secretase, an intramembrane protease, since its preferred substrate are products of type I transmembrane protein shedding (193, 212). Pre-treatment of cells with gamma-secretase inhibitors led to enhanced accumulation of pCTF following stimulation of cells with either sodium orthovanadate, EphB2-Fc or PDGF, thus indicating pCTF is a substrate of gamma-secretase and implicating RIP in ephrinB1 signaling.

To further examine the potential role of gamma-secretase in the processing of pCTF, presinillin (PS) double knock-out (*PS 1,2 -/-*) and wt (*PS 1,2+/+)* MEFs were transfected with full-length ephrinB1wt. PS proteins are considered the catalytic subunit of gamma-secretase and in their absence gamma-secretase activity is severely inhibited. Unfortunately, pCTF was not generated in either cell line in response to treatment with sodium orthovanadate, EphB2-Fc or PDGF. Overall differences between the *PS 1,2 -/-* and *PS 1,2+/+* cells were observed. For example, there were apparent contrasts in the phosphorylation of full length ephrinB1wt in the transfected *PS 1,2 -/-* and *PS 1,2+/+* cells in response to sodium orthovanadate, EphB2-Fc and PDGF. These disparate responses could arise from the expression of different repertoires of signaling molecules

in these cell lines. In addition, the inherent morphology of these cells, in both untransfected or ephrinB1wt expressing cells, were in contradistinction to each other; the *PS+/+* cells were healthy and fibroblastic, whereas the *PS-/-* cells were more rounded, and unhealthy. From the experiments with the MEFs it was not possible to conclusively implicate gamma-secretase in pCTF regulation. However due to the intrinsic differences between *PS 1,2 -/-* and *PS 1,2+/+* cells it is possible that these were not the appropriate model system to evaluate pCTF regulation.

The proteasome was also implicated in the regulation of pCTF since pre-treatment with proteasomal inhibitors of ephrinB1wt expressing cells prior to sodium orthovanadate addition led to a large accumulation of pCTF. The ErbB4 receptor's analogous membrane-associated CTF is also regulated by the proteasome (192). Interestingly, EphB2-Fc mediated collapse of ventral retinal axon growth cones bearing B-class ephrins was found to be blocked by proteasome inhibitors (213). In contrast, ephrinB1-Fc mediated collapse of dorsal retinal axon growth cones bearing EphB receptors was not blocked when treated with these inhibitors. Hence, this study may represent a physiological system where ephrinB CTF/pCTF species are involved in moderating EphB2-mediated ephrinB reverse signaling via proteasomal regulation.

4.3.7 Phospho-Carboxy-Terminal-Fragments are not Post-Translationally Modified on Juxtamembrane Lysine Residues

Due to the significant molecular weight difference of ~10kDa between CTF and pCTF, it was hypothesized that a post-translational modification by a small polypeptide modifier such as ubiquitin was involved in this size change. During our work in this area,

a recent report indicated that Notch is ubiquitinated on a juxtamembrane lysine, a modification required for Notch to be proteolysed by gamma-secretase (200). Since ephrinB1 possesses a polybasic juxtamembrane region with three lysine residues, these lysines were mutated via site-directed mutagenesis to arginines in order to ascertain if ubiquitination at any of these residues was involved in (a) gamma-secretase processing of pCTF; and (b) part of the size difference observed between CTF and pCTF. If ubiquitination was required for gamma-secretase processing of pCTF at these lysine residues, a large accumulation of pCTF in ephrinB1Δ3K→R relative to the ephrinB1wt protein would be expected. In addition, if modifications at these lysine residues are responsible for part of the size increase observed following ephrinB1 phosphorylation, pCTF in ephrinB1Δ3K→R should be smaller in molecular weight than the pCTF of ephrinB1wt. Less pCTF was produced with the ephrinB1Δ3K→R mutant than B1wt relative to their full-length ephrinB1 protein amounts. The ephrinB1Δ3K→R mutations may have potentially altered the rate of pCTF production and/or processing. However, the principal finding remains that there is no difference in size between pCTF of ephrinB1Δ3K→R and ephrinB1wt implying that ubiquitination at these specific residues does not occur and is not required for gamma-secretase processing of ephrinB1.

4.3.8 Is There a Functional Intracellular Domain Fragment of EphrinB1?

As is known in the gamma-secretase field, substrates of this protease often have their ICD released into the cytosol to mediate unique actions and thus are important signaling mediators (214). Since pCTF may be regulated by this protease, studies to characterize the ICD of ephrinB1 were initiated.

A combinatorial pre-treatment with proteasome and gamma-secretase inhibitors, a common inhibitor mix used to enhanced visualization of ICDs, of our ephrinB1wt expressing cells followed by addition of sodium orthovanadate did not lead to the visible accumulation of ICD in ephrinB1wt cells. A strategy where ICD production is enhanced was next employed in the study of the ephrinB1 ICD. The Notch ICD is constitutively produced from a construct that lacks an extracellular domain (196). This mutant mimicks an ectodomain-shed version of the receptor and is therefore continually cleaved by gamma-secretase. This stratagem was adopted for our studies and B1ΔECD was designed, constructed and then expressed in 3T3 cells. B1ΔECD was detectable only when it was phosphorylated following treatment with sodium orthovanadate, suggesting that phosphorylation may stabilize the construct. B1ΔECD was further stabilized by pre-treatment with gamma-secretase inhibitor prior to stimulation with sodium orthovanadate, implying that gamma-secretase was processing phosphorylated B1ΔECD. Importantly, ephrinB1 ICD was not detected in these cells under any of the tested conditions, including treatment with proteasome inhibitors. Furthermore, 3T3 cells expressing B1ΔECD did not display any unique cellular phenotypes or any difference in gene transcription as assessed by preliminary microarray experiments (data not shown). Thus, the B1ΔECD 3T3 expressing cells did not appear to produce ephrinB1 ICD.

There are caveats associated with the study of gamma-secretase generated ICDs. Gamma-secretase has been considered as the “proteasome of the membrane” by some (215, 216) since it exhibits an apparent lack of cleavage site specificity and the ICDs it releases are notoriously unstable, even with the quintessential Notch receptor (217). For example, the ICD of amyloid precursor protein (APP) is rapidly degraded via a

proteasome-independent, lysosome-independent pathway (201). Thus gamma-secretase may function in terminally clearing ectodomain-shed substrates from cell membranes and, analogous to the proteasome, some of its substrates may yield biologically active fragments. Therefore our inability to observe the gamma-secretase generated ICD of ephrinB1 was not unprecedented and furthermore may not be biologically relevant. Nonetheless, gamma-secretase clearing of ephrinB1 CTF/pCTF from the membrane represents an important process that may impact ephrinB1 signaling as discussed earlier. Secondly, the stability of many ICDs is greatly increased in the presence of an appropriate protein binding partner, such as a CSL (for CBF1, Suppressor of Hairless, and Lag-1) transcription factor family member for Notch ICD (197), and Fe65 with APP (218). Hence, another caveat to our experiments is that ephrinB1 ICD may not have suitable stabilizing binding partners in NIH3T3 cells thus forestalling our ability to characterize the ICD's function. However, in an appropriate context, RIP of CTF/pCTF may yield a biological active ICD.

However, it is possible to conclude from our experiments that, similar to pCTF, B1ΔECD is stabilized when it is tyrosine phosphorylated in response to sodium orthovanadate and that gamma-secretase inhibitors led to its further accumulation. Due to stabilization of B1ΔECD induced by tyrosine phosphorylation, it can be extrapolated that the phosphorylation of pCTF may stabilize it as well. Therefore, in addition to characterizing pCTF as signaling competent, its tyrosine phosphorylation may function to temporally regulate it as well.

4.3.9 An Emerging Signaling Role for EphrinB Proteolytic Processing

During the course of this dissertation, a number of groups also reported that ephrinBs are proteolytically processed by MMPs and gamma-secretase to produce signaling proteolytic fragments. Their studies are briefly described below and contrasted with our findings.

Three groups reported that ephrinB1 and B2 were shed, or were induced to do so by the exogenous addition of EphB-Fc (219-221). The shedding event resulted in CTF production, defined as 14-17 kDa ephrinB bands, and was recorded in both cultured and primary cells, as well as mouse adult tissues. The published molecular weights of CTF are of the same size of the CTF discerned in our studies.

With the use of metalloproteinase inhibitors, such as GM6001, investigators implicated MMPs in the shedding of ephrinB1 and B2 (219-221). Tanaka *et al.* (220) more specifically determined that ephrinB1 was cleaved by MMP-8 and that the site of this cleavage occurred at 217 aa in the extracellular region. This latter group also reported that shedding occurs independently of tyrosine phosphorylation of ephrinB1's cytoplasmic tail but is dependent on its PDZ motif. Although our attempts of identifying the ephrinB1 sheddase and cleavage site were unsuccessful, PDZ-based interactions were similarly found to be important in pCTF production and ephrinB1 shedding.

Georgakopoulous *et al.* (219) and Tomita *et al.* (221) also described the involvement of gamma-secretase in further processing ephrinB CTF. These groups observed increased accumulation of CTF in ephrinB1 or B2 expressing *PS 1,2 -/-* MEFs when compared to *PS 1,2 +/+* cells thus firmly implicating gamma-secretase in ephrinB CTF cleavage. In contrast, our experiments with ephrinB1-expressing PS knock-out

MEFs did not yield CTF or pCTF accumulation. This discrepancy may be explained by our inability to detect them or perhaps protein level expression.

With the use of gamma-secretase and proteasome inhibitors, ICDs of ephrinB1 and B2, which were generally ~1-2 kDa smaller in molecular weight relative to their CTF, were distinguished Georgakopoulous *et al.* (219) and Tomita *et al.* (221). These two groups reported distinct regulatory and signaling characteristics for ephrinB ICD. Tomita *et al.* (221) showed that a tagged ephrinB1 ICD localized to the nucleus with the polybasic domain acting as a nuclear localization sequence. Furthermore, an ephrinB1ΔECD construct with an N-terminus mimicking MMP-8-mediated shedding was constitutively cleaved and produced ICD independently of the conserved 33 aa C-terminus, suggesting gamma-secretase was processing ephrinB1ΔECD independently of cytosolic interactions. Georgakopoulos *et al.* (219) detailed how gamma-secretase inhibitors prevented phosphorylation of Src kinase and of ephrinB2 in cells stimulated with EphB2-Fc. Remarkably, a tagged-version of ephrinB2's ICD was able to pull-down Src kinase. From their overall study, Georgakopoulos *et al.* (219) concluded that ephrinB2's ICD is required to modulate Src-dependent phosphorylation of ephrinB2. This latter study highlighted an important signaling function for ephrinB ICDs. Unfortunately, ephrinB1 ICD was not detected over the course of our studies forestalling our ability to characterize its function.

Tomita *et al.* (221) also discovered from their studies that CTF itself has signaling functions. When their ephrinB1ΔECD was overexpressed in cells, CTF induces actin-rich cellular processes in COS cells that were determined to be dependent upon the last 34 amino acids of the cytoplasmic tail of ephrinB1. Remarkably, the length of these

protrusions were dramatically increased by the addition of gamma-secretase inhibitors implying that CTF possesses independent signaling capabilities from full-length ephrinB1 and that gamma-secretase may act to downregulate these. With respect to our ΔECD results, a flaw in the design of this construct may explain the differences between our and Tomita *et al.*'s study (221), notwithstanding arguments regarding cell-specific effects or expression levels. Our B1ΔECD extracellular linker possessed 43 residues and started at aa 195. It has been subsequently described that Nicastrin, a subunit of the gamma-secretase complex, is the protein involved in substrate recognition. Nicastrin recognizes short N-termini of proteins and prefers substrates with ~15 aa stubs or less (211). Since our ΔECD linker is significantly larger than 15 aa, it may not have been detected by the complex, or had a reduced ability to be so, and therefore was not processed appropriately. In contrast, Tomita *et al.*'s ΔECD construct possessed only 20 aa of the extracellular linker (221) and also started at aa 218, matching the MMP-8 cleavage site described (220). So it is possible our ΔECD design curtailed our ICD study.

Taken together, these studies showed that B-class ephrins are shed by MMPs to produce CTF (14-17 kDa) in a PDZ-motif dependent manner. CTF independently exhibited cytoskeletal modulating abilities. CTF in turn was cleaved by gamma-secretase, independent of the conserved ephrinB C-terminus, producing ICD. EphrinB ICDs were found to interact with Src kinase and modulate signaling, and to localize to the nucleus.

Our results further add to the recent ephrinB1 proteolytic findings by providing the first description of an ephrinB CTF as being tyrosine-phosphorylated (ie. pCTF) both

in vitro in cultured cells as well as *in vivo* in embryonic chick tissues. Since pCTF are tyrosine-phosphorylated it suggests they retain signaling capability, and from our studies with ephrinB1ΔECD, the phosphorylation may help stabilize it allowing for temporal control. Our study also indicate the possibility that CTF/pCTF form dimers and it is possible that this configuration would result in their independent signalling.

EphrinB shedding and subsequent RIP by gamma-secretase may be particularly relevant in cancers where ephrinBs are overexpressed (e.g. glioma brain tumours (222)) and thus likely exposed to a proteolytic environment where increased shedding may occur leading to CTF/pCTF accumulation and associated signaling. Modulation of CTF/pCTF levels by gamma-secretase could yield higher levels of ephrinB ICD under these conditions possibly leading to aberrant ICD signalling, or if the intramembrane protease was overwhelmed by the increased amount of CTF/pCTF substrates, result in their sustained signalling.

4.4 Future Directions

Most of the studies have focused on *in vitro* systems to assess proteolytic processing of ephrinB1, thus a logical next step would be to establish knock-in mice strains with proteolytic processing mutations in ephrinB1, B2 or B3. This would permit the study of these processes at endogenous expression levels of ephrinBs, in biologically relevant ephrinB/EphB mediated functions, thereby distinguishing physiological activities dependent on ephrinB proteolytic processing. Taking into consideration the Tanaka *et al.* study (220), a mouse knock-in of ephrinB1 with the extracellular MMP-8 cleavage site mutated to alanines would be advisable. A mouse knock-in of an ephrinB3

that was uncleavable by the rhomboid RHBDL2 *in vitro* would also be relevant. Since RHBDL2 appears to recognize substrates based on the luminal end of their transmembranes domain, a 5-6 amino acid substitution of ephrinB3 at these positions would likely prevent rhomboid cleavage of ephrinB3. Due to the inconsequential size and location of these mutations, they would likely have negligible effects on ephrinB1 and B3 conventional signaling and function, therefore any phenotypes associated with the mouse knock-ins would be most likely directly related to those dependent on ephrinB1 or B3 shedding and may also be regions where CTF/pCTF signaling is involved.

The verification of the presence of CTF or pCTF in B-class ephrin bearing ventral retinal axon growth cones should be done to ascertain if these fragments accumulate in response to proteasome inhibitors following EphB2-Fc addition and thus if they modulate EphB2-Fc induced collapse in the growth cone. If CTF/pCTF were found to accumulate in this process, this would provide physiological evidence that the proteasome modulates CTF/pCTF levels.

To gain insight into the downstream signalling from pCTF, a B1ΔECD construct with the conserved tyrosine residues in ephrinB1's conserved 33aa C-terminus mutagenized to glutamic acid residues could be used to generate a phosphomimetic version of this construct. Thus, when expressed in various cell types, phosphomimetic B1ΔECD downstream signaling and function could be assessed.

Thus, our findings have provided a platform from which further mechanistic studies can be undertaken to characterize the function of phosphorylated proteolytic fragments generated by ephrinB1 signaling.

Chapter Five: Investigation of EphrinB1 Function in Neural Tube Development of the Chick

Chapter Five: Investigation of EphrinB1 Function in Neural Tube Development of the Chick

5.1 Introduction

B-class ephrins are expressed dorsally during the development of the spinal cord (223-225) however the functions that they mediate therein remain uncharacterized. In this chapter, the function of ephrinBs during development of the dorsal spinal cord was explored through *in vivo* studies in the chick model system.

The chick (*Gallus gallus*) is the longest used experimental model system in embryology, with documented studies conducted by ancient Greeks and Egyptians (226). The life cycle of the chicken is depicted in **Figure 5.1**. The genomic sequence of chick (227) showed that this haploid organism possesses approximately the same number of genes as humans, but its genome is extremely compact, being approximately 1 billion base pairs in size as compared to 3 billion base pairs in humans, with a remarkable level of conserved synteny with mammalian genomes (226). Study of the chick has contributed to the discovery of many key developmental concepts and processes, including competence, developmental plasticity, somitogenesis, hindbrain segmentation, limb and neural crest development (226, 228).

Relatively recently, *in ovo* electroporation of DNA for gene delivery was developed (144, 229) and this has once more accented chick as a powerful system for the analysis of gene function. *In ovo* electroporation allows for precise spatial and temporal introduction of constructs that can knockdown or direct expression of a gene at any

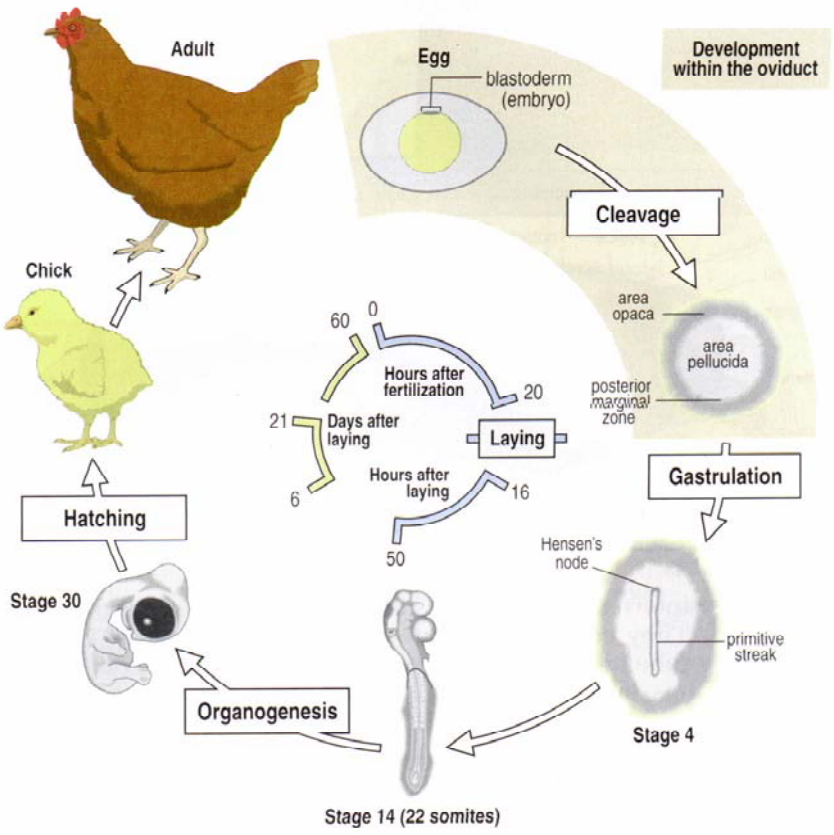

Figure 5.1: The life cycle of the chicken.

Adapted from Principles of Development (2nd Ed), Wolpert, 2002 (230).

stage of embryonic development. Thus, this technique provides a rapid and cost-efficient method for analysing gene function and is used in this chapter to study the role of ephrinB1 in early development of the spinal cord.

The brain and spinal cord are derived from the embryonic neural tube. The process of neural tube formation, termed neurulation, involves the neural plate, a flat sheet of ectoderm, elevating its bilateral neural borders that then fuse together at the midline forming a tube that is then covered by future epidermal ectoderm (231). The anterior portion of the neural tube becomes the brain while posterior portions form the spinal cord. Neural progenitors are found medially on the ventricular surface in the tube and give rise to neurons that migrate radially towards the lateral or pial surface. Dorso-ventral and medio-lateral patterning in the early neural tube is critical in providing correct differentiation and identity to neurons and hence proper functioning and maturation of the spinal cord (232).

The dorsal expression of ephrinB1 and ephrinB2 in the developing spinal cord was initially thought to restrict the longitudinal extension of commissural axons (223), however, recent studies have shown that the dorsal extension of these axons is not altered in mice lacking ephrinB1 and/or ephrinB2 (225). Thus, the function of B-class ephrins in the developing dorsal neural tube remains unclear (224). Here a gain-of-function approach was applied to **investigate the role ephrinB plays in the dorsal embryonic spinal cord using the chick as a model system**. Deletion constructs lacking the ectodomain or C-terminal conserved region were also used to examine the contribution of ephrinB signaling in this tissue.

5.2 Results

5.2.1 B-class Ephrins are Expressed in the Chick Developing Neural Tube

To date, only two B-class ephrins, ephrinB1 and B2, have been identified in chick. Wholemount immunohistochemistry of Hamburger-Hamilton (HH, a chronological staging method for chick (143)) stage 13 chick embryos using an antibody that detects B-class ephrins but cannot distinguish between these two gene products demonstrated that B-class ephrins are expressed early in the developing chick spinal cord (**Figures 5.2 A, B & B'**). Overall, expression appeared lower in anterior regions of the developing spinal cord where somites were segmented in comparison to the more elevated expression found posteriorly in regions where the neural tube was surrounded by presomitic mesoderm (**Figures 5.2 A, B & B'**). Little or no expression was observed in the dorsal most regions of the neural tube at this stage. At HH 20 (**Figure 5.2 C**), expression was primarily localized to the floor plate and dorsal neural tube (**Figure 5.2 D**). Both the floor plate, as well as roof plate and cells immediately adjacent to it, expressed noticeably higher levels of B-class ephrins. A stripe of slightly elevated ephrinB expression was also observed in the dorsal part of the spinal cord. Little or no expression was observed in other ventral regions of the neural tube.

5.2.2 Overexpression of EphrinB1 Constructs in the Chick Neural Tube

5.2.2.1 Experimental Design and Reporting of *in ovo* Electroporations

Electroporation of the neural tube results in the specific transfer of a DNA construct, which is negatively charged, to the half of the neural tube that is positioned next to the positive electrode (**Figure 2.4**). The contralateral side of the neural tube does

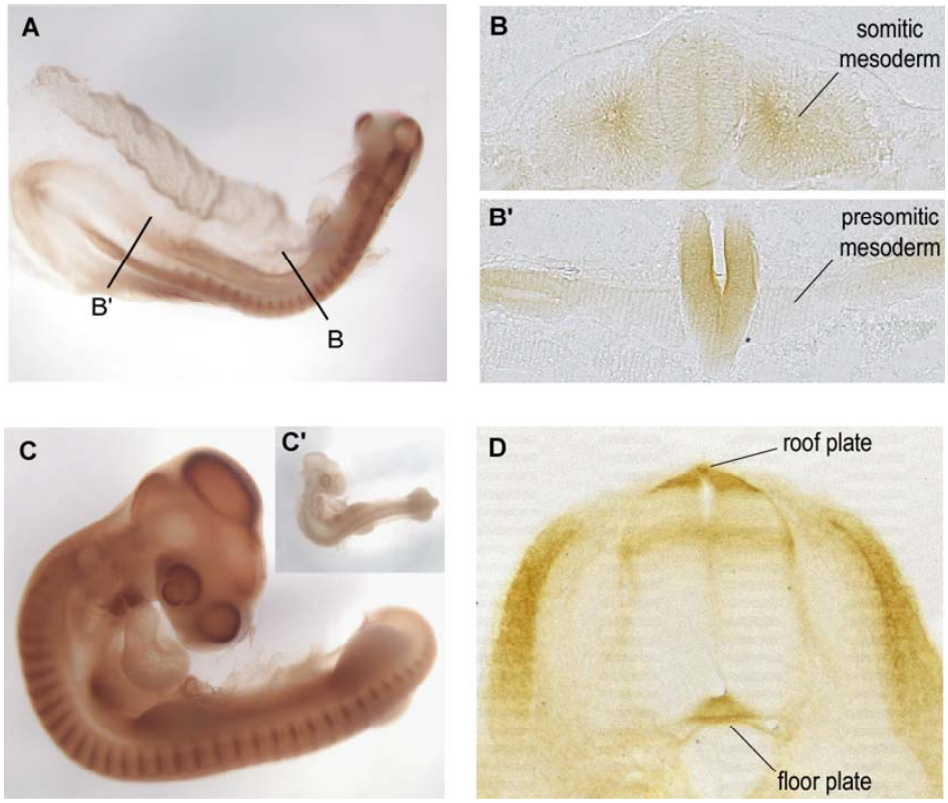

Figure 5.2: EphrinB Immunohistochemistry of HH13 and HH20 chick embryos.

(A) Wholemount HH13 embryo stained with anti-ephrinB antibody (PAN); transverse section through rostral (B) and caudal (B') spinal cord of HH12 embryo; (C) Wholemount HH20 embryo stained with anti-ephrinB antibody (PAN); (C') isotype control wholemount stained embryo; and cross-section through developing spinal cord of HH20 embryo stained with anti-ephrin B antibody (D). Pictures of sections captured with a 10x objective lens.

not receive electroporated DNA and serves as an internal, paired negative control. The expression vector used possesses an internal ribosome entry site (IRES)-GFP element, thus GFP is also expressed as a marker. All manipulations were performed between Hamburger-Hamilton stages (HH) (143) 9-12 (embryonic day (E) 1.75) and embryos harvested approximately 24-48 hours later at HH 18-21 as indicated below.

Downstream effects 24-48 hrs following electroporation were assessed morphologically as well as molecularly via immunohistochemistry or RNA *in situ* hybridization of the generic neuronal marker, Tuj1 (a Neuronal Class III β-Tubulin) together with markers of distinct populations of newly differentiated dorsal neurons. The early development of the spinal cord involves establishment of discrete domains along the dorsal-ventral (DV) axis of the neural tube (**Figure 5.3**) and is mediated by Bone-Morphogenetic-Proteins (BMPs) and Sonic Hedgehog (Shh) respectively secreted by the roof plate and floor plate cells (found at the apex of the dorsal and ventral regions of the neural tube, respectively) (233). Neurons found in each domain express unique transcription factor profiles and for our analysis, the transcription factors *Tlx-3* and LIM1/2 were used as markers (harvested at 48hr) (**Figure 5.3**). *Tlx-3*, a homeobox transcription factor, is expressed in dorsal interneurons dI3 & dI5 (234) while LIM1/2, a homeodomain transcription factor, is expressed by dI2, 4 & 6 neurons. Thus with these two markers, the fate of the bulk of the dorsally derived neurons was characterized.

All sections presented in the figures are at the level of the forelimb and were representative of dramatic phenotypic defects observed for each construct. The morphological phenotypes observed following electroporations with the various ephrinB1 constructs were discernable on whole embryos immunohistochemically stained for *Tlx-3*,

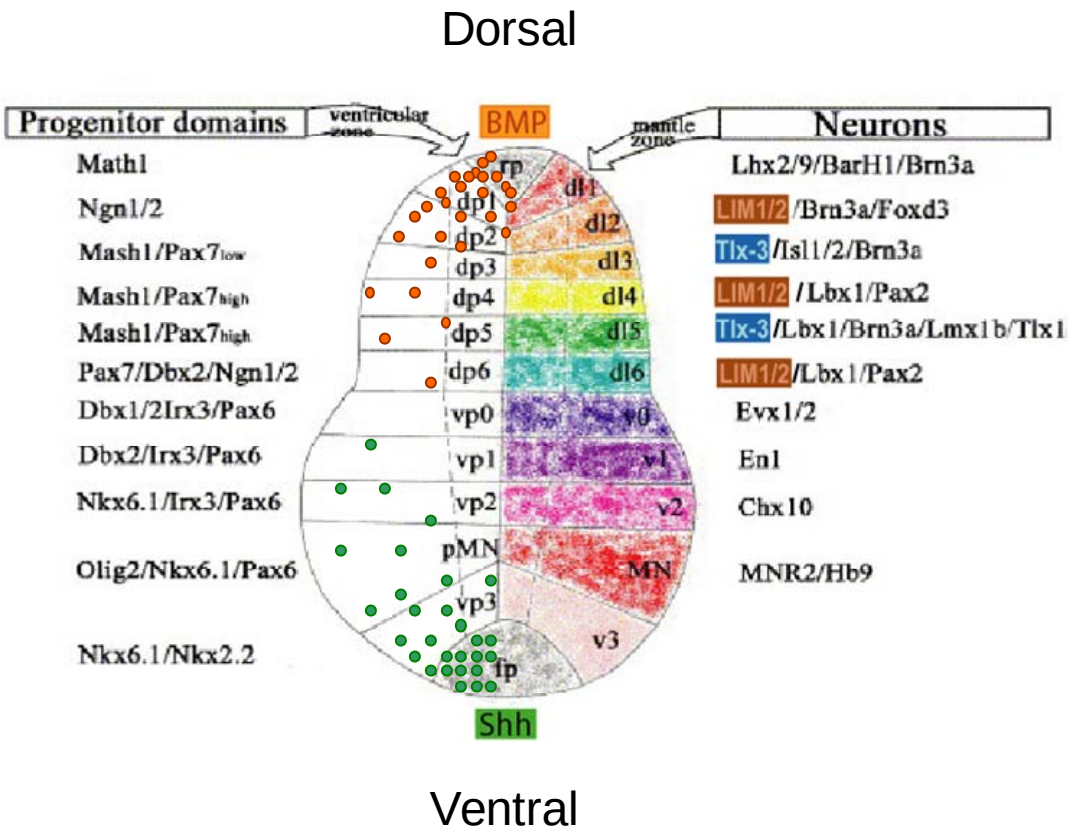

Figure 5.3: Dorso-ventral patterning of the developing spinal cord.

The left side of the figure lists the gene and protein markers for the progenitor domains, while the right side lists those for the neuronal types. LIM1/2 and *Tlx-3* neuronal markers used to assess the ephrinB1 construct electroporations are highlighted. dI: dorsal interneuron, dp: dorsal progenitor, v: ventral, vp: ventral progenitor, MN; motor neuron, pMN: progenitor motor neuron, rp: roof plate, fp: floor plate; orange circles: Bone-Morphogenetic-Protein; green circles: Sonic Hedgehog. Adapted from Wilson and Maden, *Dev Biol*, 2005.

LIM1/2, and GFP. Although electroporations resulted in a clearly discernable GFP expression region along the antero-posterior (AP) axis, phenotypic effects of the constructs occurred with highly variable penetrance such that some embryos displayed no phenotype while others had highly variable volumes of tissue affected. This variable penetrance and magnitude of phenotype appeared to be independent of electroporation method previously optimized for this model. An unbiased approach for selecting "successful" electroporation experiments was therefore difficult to establish. The high variability of affected tissue location and volume therefore rendered quantitation of cell number in a specific set of histological sections or measurements of tissue morphology to be simplistic and potentially misleading with a high probability of generating false positive or false negative results. For the sake of clarity, the incidence of observed phenotypes in the wholemount stained embryos were reported where the effects of the electroporations could be ascertained with confidence.

5.2.2.2 Overexpression of EphrinB1 wt Leads to Neural Tube Defects

A gain-of-function *in ovo* electroporation approach was used to overexpress ephrinB1wt in the developing neural tube to investigate a potential early role for this protein. The expression of ephrinB1wt and GFP following the electroporations were confirmed by immunohistochemical staining for the aforementioned proteins (**Figure 5.4**). As shown in **Figures 5.5 A & B**, electroporation of ephrinB1wt resulted in involution of the dorsal neural tube and/or protrusion of individual cells or small fragments into the ventricular lumen that was accompanied by an apparent loss and/or narrowing of the dorsal most portion of the neural tube. These defects were discernable

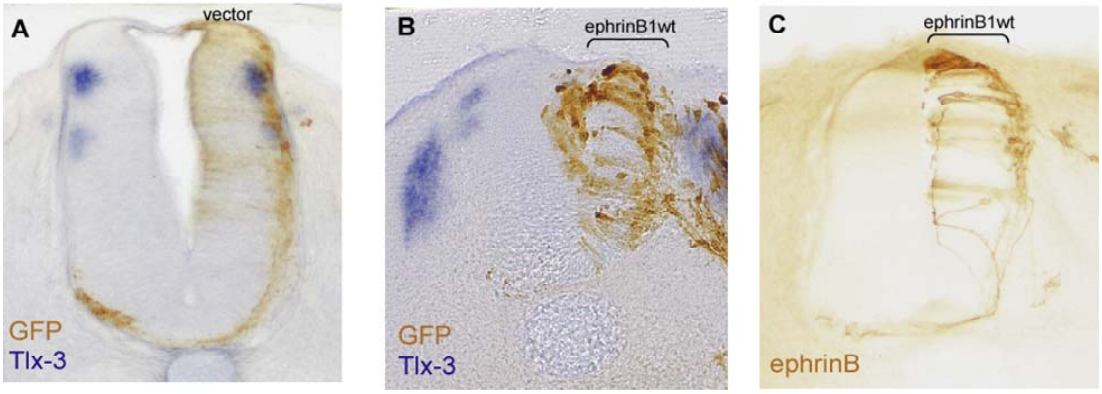

Figure 5.4: Positive expression of ephrinB1wt and GFP following *in ovo* electroporation of the developing spinal cord.

EphrinB1wt and GFP were expressed following i*n ovo* electroporation of pCIG2/EphrinB1wt/IRES-GFP expression construct at HH 11 and harvested 48 hrs later, as assessed by ephrinB (anti-ephrinB PAN) (C) and GFP immunohistochemistry (B). Neural tube defects were associated with electroporation of ephrinB1wt, as assessed by GFP staining and *Tlx-3 in situ* hybridization (B). These effects were not observed when the vector alone was electroporated (A). Pictures captured with a 10x objective lens.

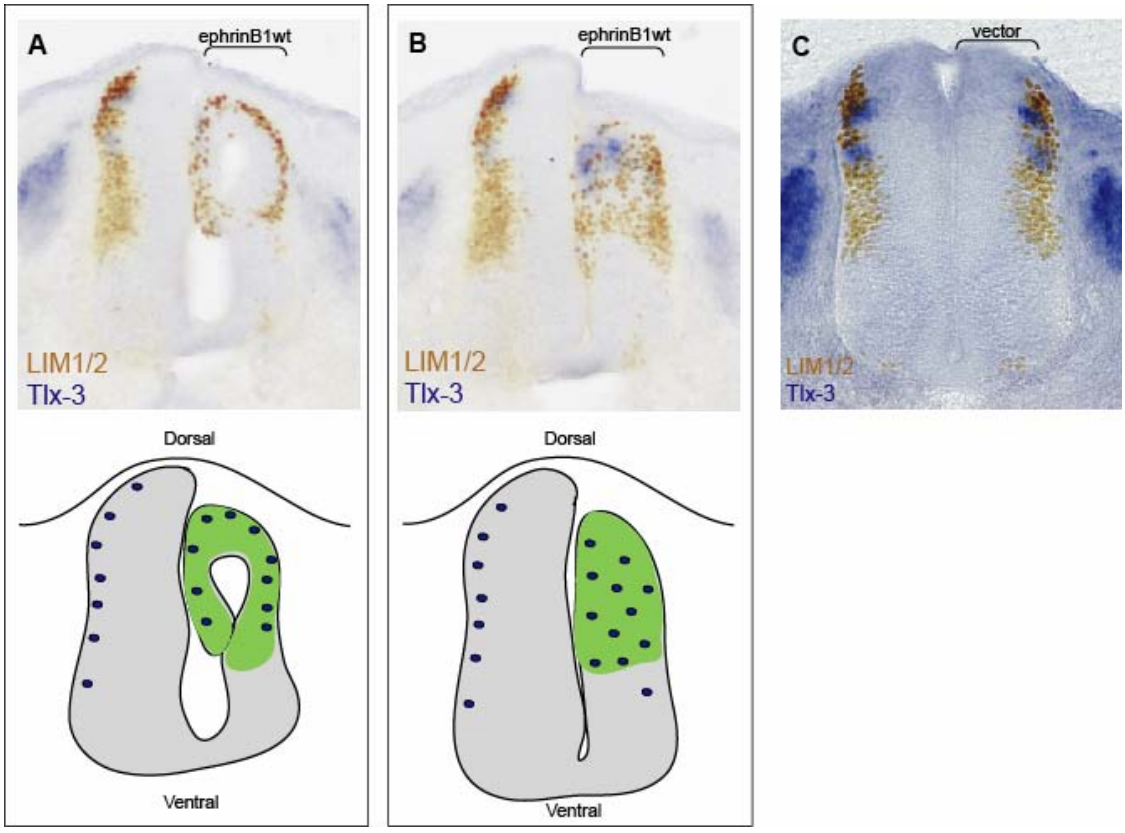

Figure 5.5: Overexpression of ephrinB1wt in the developing spinal cord results in defects in neural tube morphogenesis.

In ovo electroporation of EphrinB1 wt at HH11 and harvested 48 hours later lead to defects in neural tube morphology and disordered neurogenesis, as assessed by LIM1/2 immunohistochemistry and *Tlx-3 in situ* hybridization (A,B). Vector alone did not exhibit any phenotypes (C). Pictures captured with a 10x objective lens. Blue dots in schematic drawings represent neurons, green zone the electroporated region.

as bulges of tissue or cells with LIM1/2 staining invading the neural tube lumen of intact embryos (i.e. prior to sectioning) in 3/19 (16%) of specimens. The morphological defects observed directly correlated with expression of the electroporated construct as assessed by GFP staining (**Figure 5.4 B**). In addition, *Tlx-3* and LIM1/2 positive, differentiated neurons although appropriately positioned for the most part along the dorsoventral axis were often displaced mediolaterally. This phenotype was referred to as 'disordered neurogenesis' hereafter and was readily detectable in 9/19 (47.3%; 95% confidence interval was (22.6, 72.1), see **Figure 5.6**) intact embryos. Mediolaterally displaced neurons were also discerned using the general neuronal marker, Tuj1 (**Figure 5.7**). Furthermore, Tuj1 revealed potential defects in axon guidance. At this stage, neurons normally send their axons ventro-laterally toward the midline, as illustrated on the control non-electroporated side. However, following overexpression of ephrinB1wt, some axons appeared to extend medially and/or dorsally. No defects were observed following electroporation of vector alone (n=43) (**Figures 5.4 A and 5.5 C**).

5.2.2.3 Overexpression of EphrinB1Δ33 in the Neural Tube Results in Similar, Though Less Dramatic, Phenotypes Relative to EphrinB1wt

To assess whether the effects observed in the neural tube from the overexpression of ephrinB1wt were due to signaling from its cytoplasmic tail, an ephrinB1Δ33 construct, that lacks the last 33 amino acids of the cytoplasmic tail, was electroporated into the chick embryo. This deletion removes the most highly conserved region of B-class ephrins that is generally regarded to be required to mediate downstream signalling

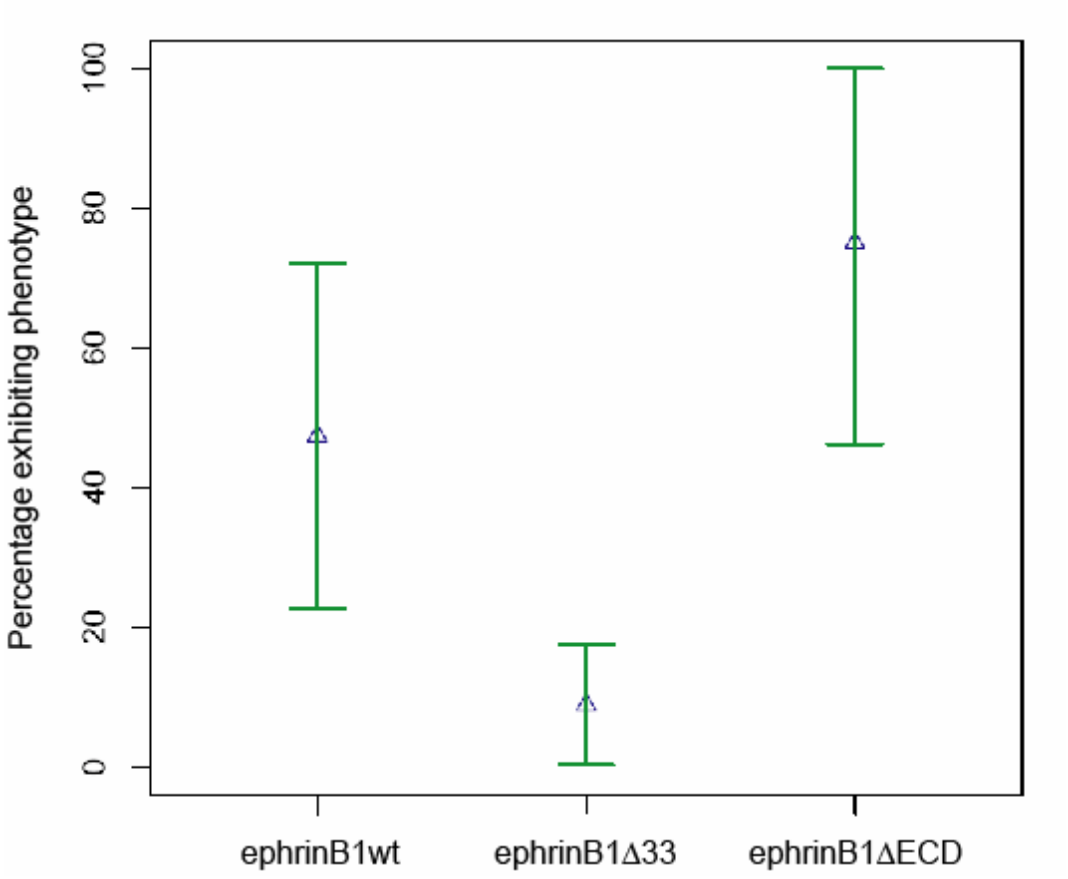

Figure 5.6: Percentage of chick neural tubes exhibiting a phenotype following overexpression of EphrinB1 constructs.

The percentage of chick neural tubes exhibiting a phenotype following overexpression of ephrinB1 constructs as well as their 95% confidence intervals.

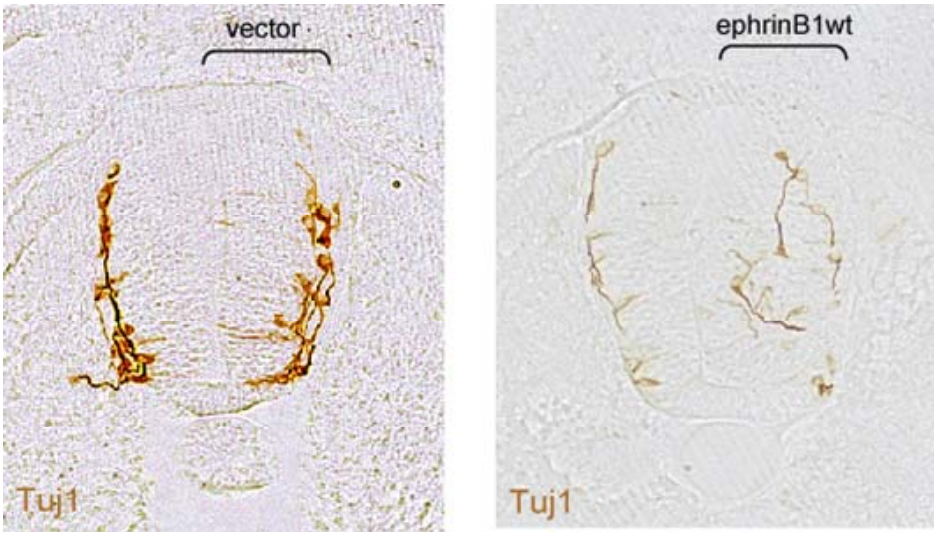

Figure 5.7: Overexpression of EphrinB1 wt results in disordered neurogenesis.

In ovo electroporation of EphrinB1 wt at HH 11 and harvested 24 hours later led to disordered neurogenesis and misguided axonal processes as assessed by Tuj1 immunohistochemistry (B). These effects were not observed when the vector alone was electroporated (A). Pictures captured with a 10x objective lens.

mediators (92). The effects of the ephrinB1Δ33 construct were similarly assessed with the differentiated neuronal markers, *Tlx-3* and LIM1/2.

Electroporation of a construct coding for ephrinB1Δ33 resulted in similar phenotypes as those of the wt protein however with much less severity (**Figure 5.8**). Although involution of the dorsal neural tube and/or protrusion of individual cells or small fragments into the ventricular lumen were observed following electroporation of ephrinB1Δ33 it was more moderate in comparison to that seen with ephrinB1wt (eg. **Figure 5.5 A vs 5.8 A**). Mediolaterally displaced LIM1/2 positive cells were readily apparent in only 4/45 (8.9%; 95% confidence interval was (0.2, 17.5), see **Figure 5.6**) of intact embryos where they seemed to be more restricted to the dorsal most portions of the neural tube (**Figures 5.8 A & B**). Taken together, the cell-autonomous nature of the observed defects with their decrease in severity and frequency following electroporation of a truncated version lacking the highly conserved cytoplasmic tail suggest that the morphological and molecular effects observed following electroporation of ephrinB1wt were mediated via ephrinB reverse signaling.

5.2.2.4 Overexpression of EphrinB1ΔECD Leads to a Loss of Dorsal Neural Tube

Ectodomain shedding and gamma-secretase processing of ephrinBs have recently been described to play an important role in ephrinB reverse signaling *in vitro* (219-221). Evidence of ephrinB shedding occurring in chick was presented earlier in Chapter 4 (**Figure 4.5**). To further elucidate the role of proteolytic processing of ephrinB shedding and/or gamma-secretase cleavage in its signaling *in ovo* during neural tube development,

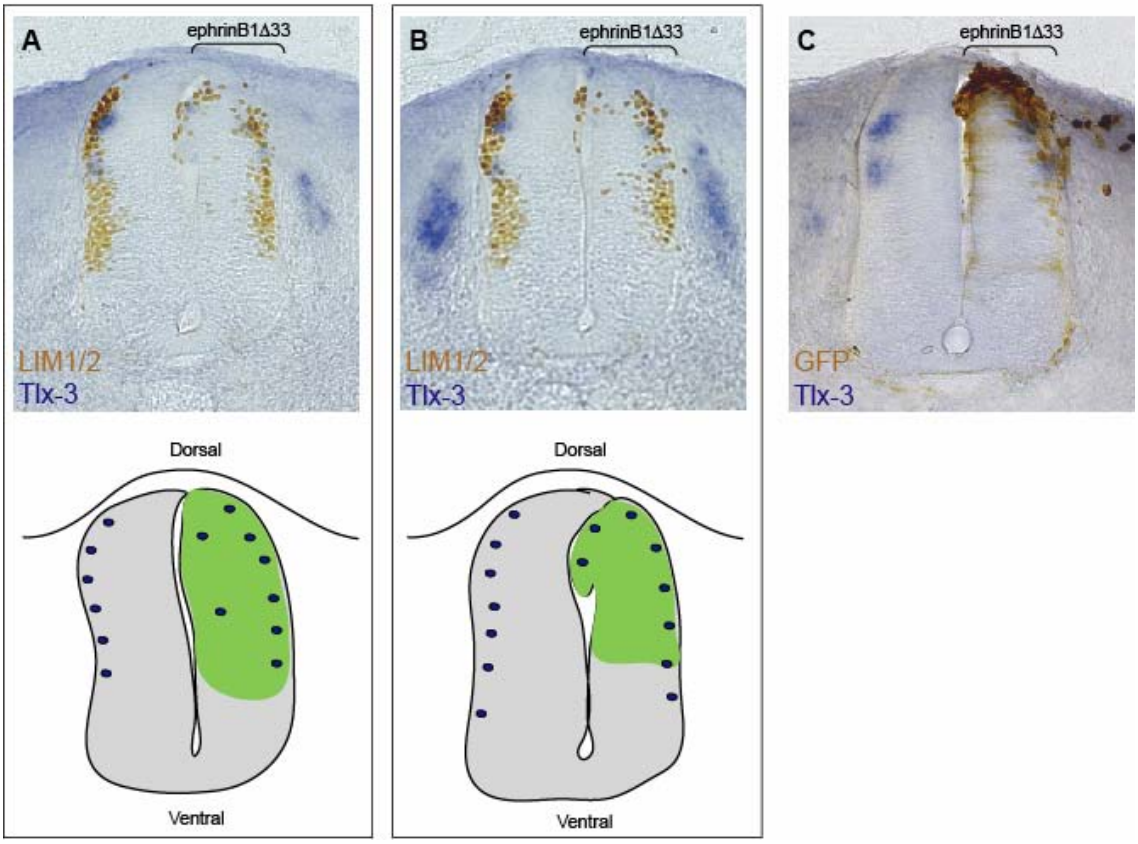

Figure 5.8: Overexpression of ephrinB1Δ33 results in defects in neural tube morphology which are less severe then those of ephrinB1wt.

In ovo electroporation of ephrinB1Δ33 at HH11 and harvested 48 hours later results in defects of neural tube morphology (A-C) and disordered neurogenesis (B). These phenotypes correlated with expression of the construct (C). Pictures captured with a 10x objective lens. Blue dots in schematic drawings represent neurons, green zone the electroporated region.

an ephrinB1ΔECD construct (**Figure 4.16**) that mimicks an ectodomain-shed version of ephrinB1 was electroporated. In comparison to ephrinB1wt and ephrinB1Δ33 manipulations, ephrinB1ΔECD overexpression yielded strongly penetrant phenotypes that occurred continuously along the electroporated field as discernable in intact embryos as well as in sectioned specimens. These observations also validated our electroporation approach used in these studies.

Electroporation of ephrinB1ΔECD into the developing neural tube led to a consistent notable loss of the dorsal neural tube tissue volume, as well as a narrowing of the remaining neural tube on the manipulated side (**Figures 5.9 A-B**) that directly correlated with expression of the electroporated construct (**Figure 5.9 C**). The ephrinB1ΔECD phenotypes were accompanied by a dramatic loss of differentiated *Tlx-3* and LIM1/2 positive cells in 9/12 (75.0%; 95% confidence interval was (46.2, 100.0), see **Figure 5.6**) embryos, that could be easily ascertained by examining wholemount embryos. Although no obvious invasion of cells into the ventricular lumen was observed on examination of wholemount embryos, more careful examination of sectioned embryos revealed that the few remaining LIM1/2 positive differentiated neurons were also occasionally displaced medio-laterally (**Figures 5.9 B**). The apparent loss of dorsal neurons in general was further demonstrated using Tuj1 (**Figure 5.9 D**). The remaining Tuj1 positive neurons however appeared to project normally.

5.3 Discussion

Overexpression of ephrinB1wt in the developing chick neural tube led to dramatic defects in neural tube morphogenesis characterized by involution and/or protrusion of the

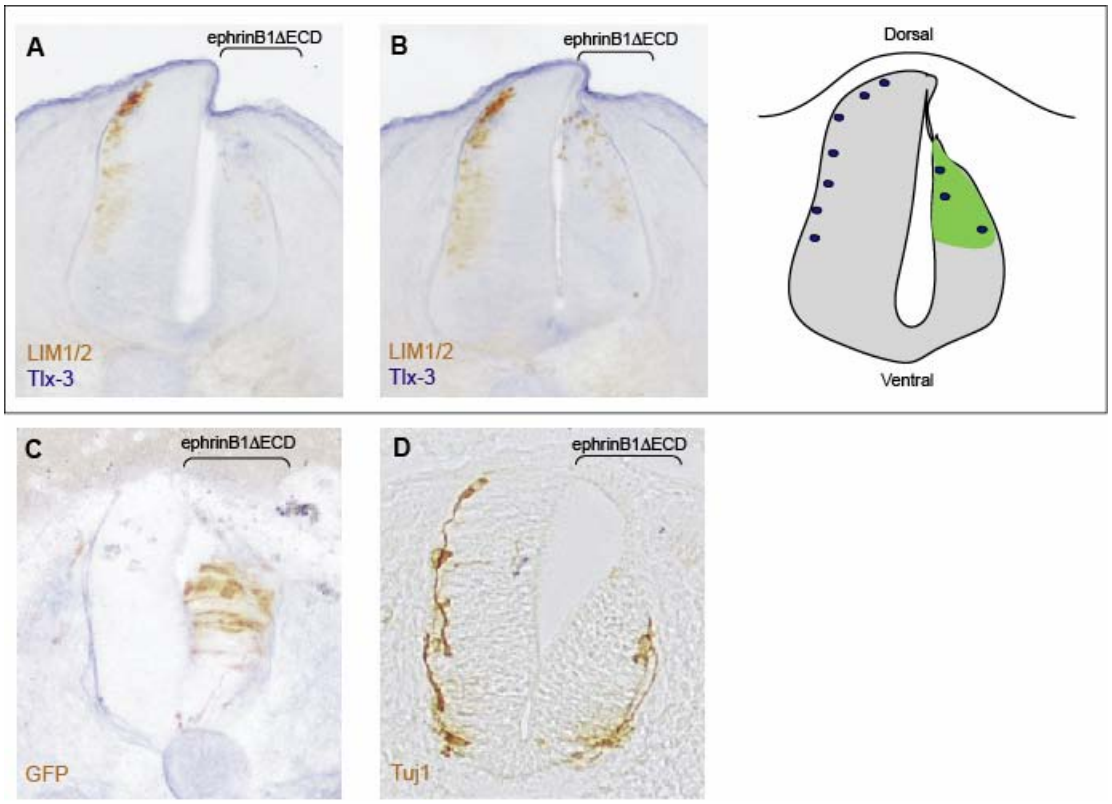

Figure 5.9: Overexpression of Ephrin B1ΔECD in the developing spinal cord results in a narrow neural tube morphology and decreased amounts of neuronal differentiation.

In ovo electroporation of ephrinB1ΔECD at HH11 and harvested 48 hours later results in disordered neurogenesis as assessed by LIM1/2 Immunohistochemistry and *Tlx-3 in situ* hybridization (A,B). These neural tube defects were associated with electroporation of ephrinB1ΔECD, as assessed by GFP staining (C). Tuj1 stain in (D) demonstrates decreased number of dorsally-derived neurons. Pictures captured with a 10x objective lens. Blue dots in schematic drawings represent neurons, green zone the electroporated region.

dorsal neural tube into the ventricular lumen and disordered neurogenesis. Deletion of the conserved region of the cytoplasmic tail resulted in a decrease in severity and frequency of the phenotypes observed. In Chapter 4, it was described that ephrinB1 is proteolytically cleaved *in vitro* by a sheddase and provided novel evidence for this process occurring *in ovo*. Consistent with this, electroporation of a construct mimicking the ectodomain-shed version of ephrinB1 led to a dramatic loss in dorsal neural tube cells. Taken together, our results indicate that ephrinB1 signaling functions early in development to maintain correct morphology of the developing neural tube.

5.3.1 Expression of EphrinBs in the Developing Neural Tube

Overall, the pattern observed at HH 20 in chick is similar to what has been reported previously for the mouse spinal cord at corresponding stages of development as assessed by both antibodies and EphB3-Fc receptor bodies (224, 225, 235, 236). Similar expression has been previously reported at slightly later stages of development in chick (i.e HH 26, E5) using EphB3-Fc receptor bodies (223). The pattern observed in chick likely results from the combined expression of ephrinB1 and/or ephrinB2, the only B-class ephrins identified to date in chick.

5.3.2 A Role for EphrinBs in Morphogenesis of the Neural Tube

Overexpression of ephrinB1wt led to dramatic defects in spinal cord morphogenesis, including involution of neural tubes and disordered neurogenesis. The altered phenotypes observed following overexpression of ephrinB1wt were far less dramatic when ephrinB1Δ33, whick lacks the conserved region of the cytoplasmic tail,

was electroporated *in ovo*. This suggests that signaling mediated from ephrinB1's conserved C-terminus led to the morphological effects observed following electroporation of ephrinB1wt. It was characterized that ephrinB1Δ33 is expressed on the cell surface in NIH3T3 cells (**Figure 3.2**) however the phenotypic differences between ephrinB1wt and Δ33 may result from expression level differences between them *in ovo*. Currently, comparing relative expression of these constructs in our electroporations is not possible as an antibody that recognizes ephrinB1Δ33 is not available. If expression level differences existed between ephrinB1wt and ephrinB1Δ33, for example if ephrinB1Δ33 was expressed at lower levels then ephrinB1wt during our manipulations, it is possible that the phenotypic defects observed in the neural tubes following electroporation with these constructs was mediated via aberrantly-induced Eph forward signalling. This potential caveat remains to be investigated.

During early stages of development, the stratification of neural progenitors and neurons in the neural tube is similar to that observed in other neuroepithelial tissues throughout the embryo. A similar disruption in both the morphology and organization of the chick neuroepithelium as distinguished from our ephrinB1wt *in ovo* manipulations was discerned by the overactivation of N-cadherin, a cell adhesion molecule (237). More specifically, small, spherical involuting fragments of neural tissue were observed in the tectum and dorsal thalamus 24-48 hours following injection of antibodies against N-cadherin into the midbrain of E4-E5 embryos. Organization of neurons within these regions was also disrupted. Similarly, when N-cadherin is conditionally deleted in the neuroepithelium of the developing cerebral cortex, mitotically active and post-mitotic cells were scattered randomly throughout the cortex (238). In both cases the effects

observed likely arise from loss of normal cell polarity and/or stratification of the developing neuroepithelium and suggest a possible mechanism for the similar disruption in morphology and organization observed herein.

Cell adhesion and/or other intercellular contact-instructive molecules, such as N-cadherin and ephrins, may also mediate appropriate sorting of differentiating neurons by supplying perimetric identification for their resident DV domain within the developing spinal cord (239) and there is growing evidence to support this hypothesis. For example, type II cadherins have been found to sort ventral motor neuron pools (239) while semaphorins and plexins have been implicated in sorting spinal cord motor pools (240). In addition, the morphogens involved in initiating dorsal-ventral patterning of the spinal cord have also been implicated in regulating cell-adhesion molecules. BMPs have been shown to modulate N-Cadherin signaling in the roof plate during neural crest delamination (241) and Shh to regulate adhesiveness of neuroepithelial cells via ß1-integrins (242). Finally, ephrinA5 and EphA5 have recently been suggested to function in mouse spinal cord development (243). The study of cell-adhesion and cell-cell instructive molecules in spinal cord development is a budding field with many challenges ahead including deciphering the multiple functions these molecules may play in the organization of this tissue.

In addition to mediating putative functions in neuroepithelial organization, our observation of involuting dorsal neural tubes following overexpression of ephrinB1wt, and to a lesser degree ephrinB1Δ33 expression, implicate that these neural tubes were not properly fused at the midline and that neural tube closure was impacted. Neural tube defects are the second most common congenital malformation occurring during human

pregnancies and the mechanism by which these arise is not well understood (244). The mechanisms involved in neural tube closure in the cranial and spinal regions are different and defects in these lead to lethal anencephaly or spina bifida in humans, respectively. Intererestingly, a subset of ephrinA5 knock-out mice exhibited defects in cranial neural folding resulting in anencephaly (78). It was therefore proposed that ephrinA5/EphA7 interactions were postulated to normally mediate adhesion during cranial neural tube fusion. Bi-directional signaling between ephrinB2 and EphB2 have been also been implicated in mediating adhesion of tissues at the midline in urorectal development, since in the absence of their signaling hypospadias occurs in mice (24). At the stage of development that ephrinB1 constructs were introduced *in ovo*, ephrinB immunohistochemistry indicated little or no expression of ephrinBs in the dorsal most region of the neural tube. Thus, it is possible by overexpressing ephrinB1 at early stages where neural tube adhesion, fusion, and remodeling occur, results in abrogation of unidentified ephrin/Eph interactions mediating these processes.

5.3.3 EphrinB1ΔECD Signaling Disrupts Neural Tube Morphogenesis

Overexpression of ephrinB1ΔECD resulted in narrowing and mild disorganization of the dorsal neural tube. This effect was observed as a strong and consistently penetrant phenotype that occurred continuously along the electroporated field indicating the importance of the signal modulation generated by ephrinB1ΔECD. This represents the first *in vivo* evidence that ephrinB membrane-associated CTF/pCTF generated by ectodomain shedding are able to modulate developmental processes. In Chapter 4, ephrinB1ΔECD construct was expressed in NIH3T3 cells and the protein was detected

only when tyrosine phosphorylated suggesting these modification(s) stabilized it (**Figure 4.16**). The spinal cord likely presents a permissive environment for ephrinB carboxy-terminal-fragment (CTF)/phospho-CTF (pCTF) signaling. This may be achieved by stabilization of ephrinB1ΔECD by tyrosine phosphorylation hence allowing it to modulate signaling while anchored to the cell surface independently or by via *in cis* cytosolic interactions with full-length ephrinB signaling. Alternatively, ephrinB1ΔECD may be cleaved by the regulated intramembrane proteolysis via gamma-secretase to release an intracellular domain (ICD) fragment that then binds to a stabilizing protein found in the neural tube cells. In any case, the results of electroporation with ephrinB1ΔECD demonstrate convincingly that ephrinB1 proteolytic fragments can modulate signaling.

A possible mechanism that could account for narrowing of the dorsal neural tube following electroporation with ephrinB1ΔECD is the premature differentiation and/or increased apoptosis of neural progenitors, either of which could result in an overall decrease in the number of differentiated neurons and size of the neural tube. Indeed, growing evidence indicates that Eph and ephrins are able to modulate proliferation and neurogenesis in the nervous system. For example, reverse signaling from ephrinA2 has previously been shown to act as a negative regulator of neural progenitor proliferation in the adult mouse brain (245), and disruption of Eph/ephrin signaling via infusion of ephrinB2-Fc and EphB2-Fc receptor bodies into the lateral ventricle of adult mice resulted in increased cell proliferation (246). EphrinB3 signaling can similarly negatively regulate cell proliferation and survival in the adult subventricular zone (247). In the developing rodent forebrain ephrinA/EphA signaling has also been shown to promote

apoptosis of neural progenitors and the final size of the forebrain (248). Most recently, EphB1 and ephrinB3 were found to co-regulate proliferation of neural progenitor cells in the hippocampus as well as their migration (249).

In summary, our results are the first to implicate B-class ephrin function during early development of the spinal cord to maintain the correct morphology and organization of the dorsal developing spinal cord. Furthermore, ephrinB1 interactions were found to have likely abrogated dorsal neural tube closure. Importantly, novel evidence was presented that demonstrates ephrinB1 proteolytic fragment(s) possess signaling functions *in vivo* as expression of an ephrinB1 construct lacking its extracellular domain, thus mimicking an ectodomain shed version of the protein, strongly impacted development of the dorsal neural tube.

5.4 Future Directions

The overexpression studies reported herein demonstrate that the morphogenesis of the neural tube was dramatically altered by ephrinB1 signaling. However, it is unclear mechanistically how these effects manifested and further experiments to characterize it are needed.

Characterization of EphB receptors in the neural tube at these stages would be a logical next step to more firmly determine which of these receptors may work in concert with the B-class ephrins. Also, infusion of soluble ephrinB-Fc or EphB-Fc proteins into the neural tube lumen to induce EphB receptor or ephrinB signaling, respectively, could indicate whether signaling from just the ephrinB ligands is required for this process.

Further gain-of-function studies in the chick where other domain markers, including those of neural progenitors, are surveyed at different time points following electroporations would aid in more specifically characterizing the neural populations affected as well as more immediate effects occurring following the manipulations.

Loss-of-function genetic approaches would provide further insight by highlighting which processes are aberrant in the absence of ephrinBs. As such, surveillance of early spinal cord markers in ephrinB knock-out mice at analogous stages of development studied herein would be advisable. Alternatively, knocking down endogenous ephrinB expression by RNA interference in the developing chick spinal cord by *in ovo* electroporation offers a spatial and temporal loss-of-function approach. The ephrinB genes expressed in this tissue would first need to be characterized via *in situ* hybridization of ephrinB1 or B2. Following confirmed knock-down of the ephrinB gene(s) of interest, the embryonic spinal cords could be stained for neural markers.

The loss of dorsal cells from overexpression of ephrinB1ΔECD in the neural tube suggests that the resulting signaling may be modulating cell proliferation or apoptosis of neural progenitor and/or neuronal cells. Staining manipulated embryos for actived Caspase-3 and phosphorylated histone H3 at different time points following electroporation would demonstrate any increases or decreases in apoptosis or cell proliferation, respectively, and likely localize which neural populations are most affected by ΔECD expression.

The dramatic phenotype observed in the neural tube following overexpression of ephrinB1ΔECD indicates that this tissue is quite amenable to the study of ephrinB CTF/pCTF signal modulation. Dissection and isolation of unmanipulated early spinal

cord tissue could be evaluated for endogenous ephrinB-CTF/pCTF to characterize if these species are normally produced in this tissue or possibly enriched. A tagged version of ephrinB1ΔECD could be overexpressed in the neural tube and then pulled-down from the dissected tissue in order to identify cytoplasmic binding partners likely involved in CTF signal modulation.

Our studies in the chick have highlighted the neural tube as an important tissue that can be used for future studies of the importance of *in vivo* ephrinB proteolytic processing.

Chapter Six: Thesis Perspective

Chapter Six: Thesis Perspective

Our studies have uncovered important regulatory mechanisms in ephrinB1 signaling, involving the cytosolic tail as well as the proteolytic processing of the entire molecule. We were also the first to demonstrate the utility and versatility of the chick as a model for pursuing ephrinB function studies *in vivo*.

Recently, the *in vivo* significance of ephrinB1 PDZ interactions was demonstrated by the phenotypes observed in mouse strains with PDZ-motif truncations of ephrinB1 and ephrinB2. Chimeric mouse embryos with an ephrinB1Δ1 mutation exhibited cleft palate, a phenotype observed in ephrinB1 knock-out mice (138, 139) , while ephrinB2Δ1 knock-in mice die shortly after birth due to chylothorax, that is effusion of chyle from the thoracic duct into the pleural space, a defect related to aberrant lymphatic vasculature remodeling (184). Interestingly, transgenic mice with phenylalanine substitutions at the five conserved tyrosine residues in ephrinB2 presented normally and survived to adulthood, with only a mild defect in lymphatic vasculature detected in one strain (127, 184, 250). Taken together, these studies indicate heavier significance of PDZ-motif interactions in mediating the physiological functions of B-class ephrins, and our study has aided in the characterization of the associated molecular mechanisms by which these may be transduced. The experiments herein have revealed that within the ephrinB1 cytosolic tail, the PDZ-binding motif was required for the tyrosine phosphorylation of ephrinB1 in response to soluble EphB2 ectodomains or PDGF. We proposed a mechanism whereby cytosolic ephrinB1 tails are clustered after treatment with soluble EphB2 ectodomains, then via the PDZ binding motif, is detected and bound by a PDZ-

domain containing protein, such as syntenin (implicated in our study; see model in **Figure 6.1**) EphrinB1 clustering may also be required for the observed tyrosine phosphorylation that occurred via PDGF cross-activation, since the PDZ binding motif was also required in this scenario.

Our studies also narrowed down the region in the cytoplasmic domain that may be responsible for the lipid raft association of ephrinB1 following soluble EphB2 ectodomain treatment to a 21 aa stretch. The 21 aa's precisely corresponded to the region that (i) could undergo a conformational change after a PDZ domain-mediated interaction with syntenin, and (ii) is where three conserved tyrosines are found. These tyrosine residues could be newly exposed post conformational change, and phosphorylated by a recruited kinase, such as a Src-family kinase. In our study, we extrapolated from our results that phosphorylation at conserved tyrosine 317 may be required to mediate lipid raft translocation, possibly by an SH2-based interaction with the adaptor Grb4. This proposed model of a PDZ-based interaction detecting and initiating ephrinB1 intracellular signaling may be important to understanding overall ephrinB signaling.

Ectodomain shedding of ephrinB1 was discerned in our cells as evidenced by the presence of the transmembrane/cytosolic portion of ephrinB1 that was membrane bound in both phosphorylated (pCTF) and unphosphorylated versions (CTF). Shedding may be regulated by ligand binding however it is postulated to involve Src-family kinase activation, that is likely to occur following treatment with soluble EphB2 ectodomains, PDGF, or sodium orthovanadate. pCTF may be generated by either shedding of full-

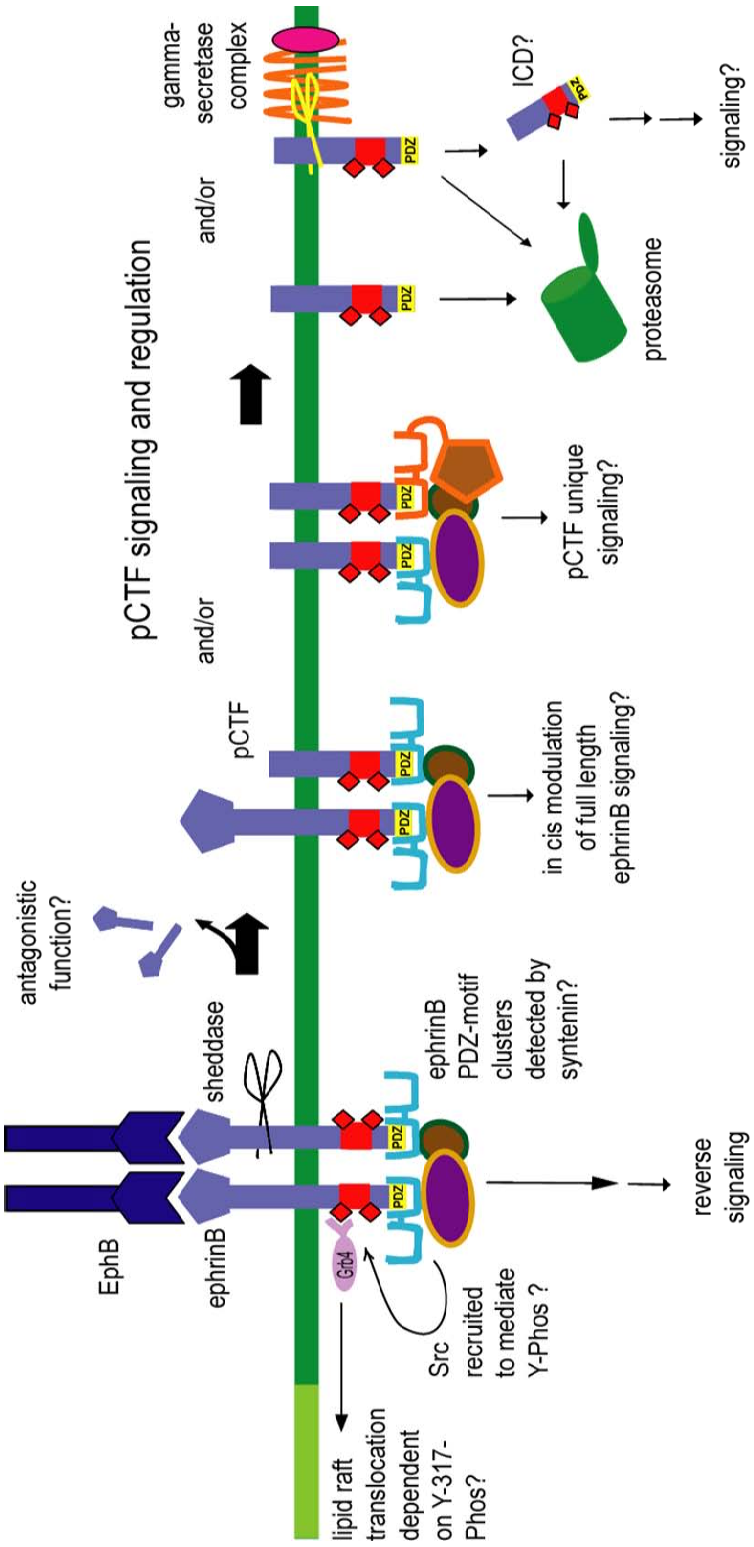

Figure 6.1: Model of proposed ephrinB signalling mechanisms described in this thesis.

length phosphorylated ephrinB1 or by tyrosine phosphorylation of the analogous CTF fragment. CTF/pCTF were found to be further regulated by the proteasome and by the intramembrane protease gamma-secretase. The latter protease may generate an ICD. Our studies add to the concurrently published reports of proteolytic processing of ephrinBs in cultured cells, and we further provided evidence in our studies that this process occurs in chick limbs *in ovo,* and that CTF/pCTF signaling from B1ΔECD can signal in a physiological setting.

Growing evidence indicates that Eph and ephrins are able to modulate proliferation and neurogenesis in the nervous system (245-248). Due to these recent studies, it seems that Ephs and ephrins have joined the ranks of other signaling molecules originally identified during development to regulate these processes.

Our studies of ephrinB function in chick neural development via *in ovo* electroporations indicated an early embryonic role for these proteins in maintaining correct morphology and organization of the developing dorsal spinal cord. Furthermore, ephrinB1 interactions were likely to have abrogated dorsal neural tube closure. Novel evidence was presented that demonstrated that ephrinB1 proteolytic fragment(s) possess signaling function(s) *in vivo,* as expression of an ephrinB1 construct lacking its extracellular domain, and thus mimicking a shed version of the ectodomain protein, strongly impacted development of the dorsal neural tube. A possible mechanism that could account for narrowing of the dorsal neural tube following electroporation with ephrinB1ΔECD is the premature differentiation and/or increased apoptosis of neural progenitors, either of which could result in an overall decrease in the number of differentiated neurons and size of the neural tube.

It would seem that roles for Ephs and ephrins are being described that expand their influence on cellular activities, including functions in which they were previously not implicated, that is, to effectuate changes in cellular proliferation or apoptosis. The dramatic phenotype observed in the chick neural tube following overexpression of ephrinB1ΔECD indicates that this tissue is strongly amenable for the study of ephrinB CTF/pCTF signal modulation and could be used as a model system to assess CTF, pCTF, versus gamma-secretase generated ICD signaling functions. As such, it represents the first model system that could be used for the study of these molecules.

The overall goal of this thesis was to further investigate ephrinB signaling from its cytoplasmic tail. We identified the PDZ-motif as an important regulator of ephrinB activation, and proteolytic processing of ephrinB producing transmembrane/cytosolic fragments that possess signaling activities. Finally, our studies in chick demonstrated that ephrinB signaling impacts neural tube morphogenesis and established an *in vivo* system with which to study ephrinB proteolytic fragment signaling.

References

References

1. Edwards, P.A. 1999. The impact of developmental biology on cancer research: an overview. *Cancer Metastasis Rev* 18:175-180.
2. Dodelet, V.C., and E.B. Pasquale. 2000. Eph receptors and ephrin ligands: embryogenesis to tumorigenesis. *Oncogene* 19:5614-5619.
3. Pasquale, E.B. 2005. Eph receptor signalling casts a wide net on cell behaviour. *Nat Rev Mol Cell Biol* 6:462-475.
4. Holder, N., and R. Klein. 1999. Eph receptors and ephrins: effectors of morphogenesis. *Development* 126:2033-2044.
5. Kullander, K., and R. Klein. 2002. Mechanisms and functions of Eph and ephrin signalling. *Nat Rev Mol Cell Biol* 3:475-486.
6. Wang, X., P.J. Roy, S.J. Holland, L.W. Zhang, J.G. Culotti, and T. Pawson. 1999. Multiple ephrins control cell organization in C. elegans using kinase-dependent and -independent functions of the VAB-1 Eph receptor. *Mol Cell* 4:903-913.
7. Bossing, T., and A.H. Brand. 2002. Dephrin, a transmembrane ephrin with a unique structure, prevents interneuronal axons from exiting the Drosophila embryonic CNS. *Development* 129:4205-4218.
8. Hirai, H., Y. Maru, K. Hagiwara, J. Nishida, and F. Takaku. 1987. A novel putative tyrosine kinase receptor encoded by the eph gene. *Science* 238:1717-1720.
9. Pandey, A., R.A. Lindberg, and V.M. Dixit. 1995. Cell signalling. Receptor orphans find a family. *Curr Biol* 5:986-989.
10. Bartley, T.D., R.W. Hunt, A.A. Welcher, W.J. Boyle, V.P. Parker, R.A. Lindberg, H.S. Lu, A.M. Colombero, R.L. Elliott, B.A. Guthrie, and et al. 1994. B61 is a ligand for the ECK receptor protein-tyrosine kinase. *Nature* 368:558-560.
11. 1997. Unified nomenclature for Eph family receptors and their ligands, the ephrins. Eph Nomenclature Committee. *Cell* 90:403-404.
12. Gale, N.W., S.J. Holland, D.M. Valenzuela, A. Flenniken, L. Pan, T.E. Ryan, M. Henkemeyer, K. Strebhardt, H. Hirai, D.G. Wilkinson, T. Pawson, S. Davis, and G.D. Yancopoulos. 1996. Eph receptors and ligands comprise two major specificity subclasses and are reciprocally compartmentalized during embryogenesis. *Neuron* 17:9-19.
13. Davis, S., N.W. Gale, T.H. Aldrich, P.C. Maisonpierre, V. Lhotak, T. Pawson, M. Goldfarb, and G.D. Yancopoulos. 1994. Ligands for EPH-related receptor tyrosine kinases that require membrane attachment or clustering for activity. *Science* 266:816-819.
14. Himanen, J.P., K.R. Rajashankar, M. Lackmann, C.A. Cowan, M. Henkemeyer, and D.B. Nikolov. 2001. Crystal structure of an Eph receptor-ephrin complex. *Nature* 414:933-938.
15. Adams, R.H., and R. Klein. 2000. Eph receptors and ephrin ligands. essential mediators of vascular development. *Trends Cardiovasc Med* 10:183-188.

16. Cheng, N., D.M. Brantley, and J. Chen. 2002. The ephrins and Eph receptors in angiogenesis. *Cytokine Growth Factor Rev* 13:75-85.
17. Holmberg, J., M. Genander, M.M. Halford, C. Anneren, M. Sondell, M.J. Chumley, R.E. Silvany, M. Henkemeyer, and J. Frisen. 2006. EphB receptors coordinate migration and proliferation in the intestinal stem cell niche. *Cell* 125:1151-1163.
18. Moore, K.B., K. Mood, I.O. Daar, and S.A. Moody. 2004. Morphogenetic movements underlying eye field formation require interactions between the FGF and ephrinB1 signaling pathways. *Dev Cell* 6:55-67.
19. Barrios, A., R.J. Poole, L. Durbin, C. Brennan, N. Holder, and S.W. Wilson. 2003. Eph/Ephrin signaling regulates the mesenchymal-to-epithelial transition of the paraxial mesoderm during somite morphogenesis. *Curr Biol* 13:1571-1582.
20. Durbin, L., C. Brennan, K. Shiomi, J. Cooke, A. Barrios, S. Shanmugalingam, B. Guthrie, R. Lindberg, and N. Holder. 1998. Eph signaling is required for segmentation and differentiation of the somites. *Genes Dev* 12:3096-3109.
21. Robinson, V., A. Smith, A.M. Flenniken, and D.G. Wilkinson. 1997. Roles of Eph receptors and ephrins in neural crest pathfinding. *Cell Tissue Res* 290:265-274.
22. Santiago, A., and C.A. Erickson. 2002. Ephrin-B ligands play a dual role in the control of neural crest cell migration. *Development* 129:3621-3632.
23. Egea, J., and R. Klein. 2007. Bidirectional Eph-ephrin signaling during axon guidance. *Trends Cell Biol* 17:230-238.
24. Dravis, C., N. Yokoyama, M.J. Chumley, C.A. Cowan, R.E. Silvany, J. Shay, L.A. Baker, and M. Henkemeyer. 2004. Bidirectional signaling mediated by ephrin-B2 and EphB2 controls urorectal development. *Dev Biol* 271:272-290.
25. Yu, G., H. Luo, Y. Wu, and J. Wu. 2003. Mouse ephrinB3 augments T-cell signaling and responses to T-cell receptor ligation. *J Biol Chem* 278:47209-47216.
26. Yu, G., H. Luo, Y. Wu, and J. Wu. 2004. EphrinB1 is essential in T-cell-T-cell co-operation during T-cell activation. *J Biol Chem* 279:55531-55539.
27. Murai, K.K., and E.B. Pasquale. 2004. Eph receptors, ephrins, and synaptic function. *Neuroscientist* 10:304-314.
28. Cooke, J.E., and C.B. Moens. 2002. Boundary formation in the hindbrain: Eph only it were simple. *Trends Neurosci* 25:260-267.
29. Lackmann, M., R.J. Mann, L. Kravets, F.M. Smith, T.A. Bucci, K.F. Maxwell, G.J. Howlett, J.E. Olsson, T. Vanden Bos, D.P. Cerretti, and A.W. Boyd. 1997. Ligand for EPH-related kinase (LERK) 7 is the preferred high affinity ligand for the HEK receptor. *J Biol Chem* 272:16521-16530.
30. Himanen, J.P., M. Henkemeyer, and D.B. Nikolov. 1998. Crystal structure of the ligand-binding domain of the receptor tyrosine kinase EphB2. *Nature* 396:486-491.
31. Himanen, J.P., and D.B. Nikolov. 2003. Eph signaling: a structural view. *Trends Neurosci* 26:46-51.
32. Chrencik, J.E., A. Brooun, M.I. Recht, M.L. Kraus, M. Koolpe, A.R. Kolatkar, R.H. Bruce, G. Martiny-Baron, H. Widmer, E.B. Pasquale, and P. Kuhn. 2006.

Structure and thermodynamic characterization of the EphB4/Ephrin-B2 antagonist peptide complex reveals the determinants for receptor specificity. *Structure* 14:321-330.

33. Pasquale, E.B. 2004. Eph-ephrin promiscuity is now crystal clear. *Nat Neurosci* 7:417-418.
34. van der Geer, P., T. Hunter, and R.A. Lindberg. 1994. Receptor protein-tyrosine kinases and their signal transduction pathways. *Annu Rev Cell Biol* 10:251-337.
35. Toth, J., T. Cutforth, A.D. Gelinas, K.A. Bethoney, J. Bard, and C.J. Harrison. 2001. Crystal structure of an ephrin ectodomain. *Dev Cell* 1:83-92.
36. Nikolov, D.B., C. Li, W.A. Barton, and J.P. Himanen. 2005. Crystal structure of the ephrin-B1 ectodomain: implications for receptor recognition and signaling. *Biochemistry* 44:10947-10953.
37. Nikolov, D., C. Li, M. Lackmann, P. Jeffrey, and J. Himanen. 2007. Crystal structure of the human ephrin-A5 ectodomain. *Protein Sci* 16:996-1000.
38. Song, J. 2003. Tyrosine phosphorylation of the well packed ephrinB cytoplasmic beta-hairpin for reverse signaling. Structural consequences and binding properties. *J Biol Chem* 278:24714-24720.
39. Song, J., W. Vranken, P. Xu, R. Gingras, R.S. Noyce, Z. Yu, S.H. Shen, and F. Ni. 2002. Solution structure and backbone dynamics of the functional cytoplasmic subdomain of human ephrin b2, a cell-surface ligand with bidirectional signaling properties. *Biochemistry* 41:10942-10949.
40. Bong, Y.S., Y.H. Park, H.S. Lee, K. Mood, A. Ishimura, and I.O. Daar. 2004. Tyr-298 in ephrinB1 is critical for an interaction with the Grb4 adaptor protein. *Biochem J* 377:499-507.
41. Cowan, C.A., and M. Henkemeyer. 2001. The SH2/SH3 adaptor Grb4 transduces B-ephrin reverse signals. *Nature* 413:174-179.
42. Su, Z., P. Xu, and F. Ni. 2004. Single phosphorylation of Tyr304 in the cytoplasmic tail of ephrin B2 confers high-affinity and bifunctional binding to both the SH2 domain of Grb4 and the PDZ domain of the PDZ-RGS3 protein. *Eur J Biochem* 271:1725-1736.
43. Himanen, J.P., M.J. Chumley, M. Lackmann, C. Li, W.A. Barton, P.D. Jeffrey, C. Vearing, D. Geleick, D.A. Feldheim, A.W. Boyd, M. Henkemeyer, and D.B. Nikolov. 2004. Repelling class discrimination: ephrin-A5 binds to and activates EphB2 receptor signaling. *Nat Neurosci* 7:501-509.
44. Chrencik, J.E., A. Brooun, M.L. Kraus, M.I. Recht, A.R. Kolatkar, G.W. Han, J.M. Seifert, H. Widmer, M. Auer, and P. Kuhn. 2006. Structural and biophysical characterization of the EphB4*ephrinB2 protein-protein interaction and receptor specificity. *J Biol Chem* 281:28185-28192.
45. Cutforth, T., and C.J. Harrison. 2002. Ephs and ephrins close ranks. *Trends Neurosci* 25:332-334.
46. Bergemann, A.D., L. Zhang, M.K. Chiang, R. Brambilla, R. Klein, and J.G. Flanagan. 1998. Ephrin-B3, a ligand for the receptor EphB3, expressed at the midline of the developing neural tube. *Oncogene* 16:471-480.

47. Kullander, K., S.J. Butt, J.M. Lebret, L. Lundfald, C.E. Restrepo, A. Rydstrom, R. Klein, and O. Kiehn. 2003. Role of EphA4 and EphrinB3 in local neuronal circuits that control walking. *Science* 299:1889-1892.
48. Poliakov, A., M. Cotrina, and D.G. Wilkinson. 2004. Diverse roles of eph receptors and ephrins in the regulation of cell migration and tissue assembly. *Dev Cell* 7:465-480.
49. Wang, H.U., and D.J. Anderson. 1997. Eph family transmembrane ligands can mediate repulsive guidance of trunk neural crest migration and motor axon outgrowth. *Neuron* 18:383-396.
50. Stein, E., A.A. Lane, D.P. Cerretti, H.O. Schoecklmann, A.D. Schroff, R.L. Van Etten, and T.O. Daniel. 1998. Eph receptors discriminate specific ligand oligomers to determine alternative signaling complexes, attachment, and assembly responses. *Genes Dev* 12:667-678.
51. Huynh-Do, U., E. Stein, A.A. Lane, H. Liu, D.P. Cerretti, and T.O. Daniel. 1999. Surface densities of ephrin-B1 determine EphB1-coupled activation of cell attachment through alphavbeta3 and alpha5beta1 integrins. *Embo J* 18:2165-2173.
52. Flanagan, J.G., and P. Vanderhaeghen. 1998. The ephrins and Eph receptors in neural development. *Annu Rev Neurosci* 21:309-345.
53. Garner, C.C., J. Nash, and R.L. Huganir. 2000. PDZ domains in synapse assembly and signalling. *Trends Cell Biol* 10:274-280.
54. Torres, R., B.L. Firestein, H. Dong, J. Staudinger, E.N. Olson, R.L. Huganir, D.S. Bredt, N.W. Gale, and G.D. Yancopoulos. 1998. PDZ proteins bind, cluster, and synaptically colocalize with Eph receptors and their ephrin ligands. *Neuron* 21:1453-1463.
55. Harris, B.Z., and W.A. Lim. 2001. Mechanism and role of PDZ domains in signaling complex assembly. *J Cell Sci* 114:3219-3231.
56. Hung, A.Y., and M. Sheng. 2002. PDZ domains: structural modules for protein complex assembly. *J Biol Chem* 277:5699-5702.
57. Lackmann, M., A.C. Oates, M. Dottori, F.M. Smith, C. Do, M. Power, L. Kravets, and A.W. Boyd. 1998. Distinct subdomains of the EphA3 receptor mediate ligand binding and receptor dimerization. *J Biol Chem* 273:20228-20237.
58. Thanos, C.D., S. Faham, K.E. Goodwill, D. Cascio, M. Phillips, and J.U. Bowie. 1999. Monomeric structure of the human EphB2 sterile alpha motif domain. *J Biol Chem* 274:37301-37306.
59. Binns, K.L., P.P. Taylor, F. Sicheri, T. Pawson, and S.J. Holland. 2000. Phosphorylation of tyrosine residues in the kinase domain and juxtamembrane region regulates the biological and catalytic activities of Eph receptors. *Mol Cell Biol* 20:4791-4805.
60. Wybenga-Groot, L.E., B. Baskin, S.H. Ong, J. Tong, T. Pawson, and F. Sicheri. 2001. Structural basis for autoinhibition of the Ephb2 receptor tyrosine kinase by the unphosphorylated juxtamembrane region. *Cell* 106:745-757.
61. Zisch, A.H., C. Pazzagli, A.L. Freeman, M. Schneller, M. Hadman, J.W. Smith, E. Ruoslahti, and E.B. Pasquale. 2000. Replacing two conserved tyrosines of the EphB2 receptor with glutamic acid prevents binding of SH2 domains without abrogating kinase activity and biological responses. *Oncogene* 19:177-187.

62. Zisch, A.H., M.S. Kalo, L.D. Chong, and E.B. Pasquale. 1998. Complex formation between EphB2 and Src requires phosphorylation of tyrosine 611 in the EphB2 juxtamembrane region. *Oncogene* 16:2657-2670.
63. Knoll, B., and U. Drescher. 2004. Src family kinases are involved in EphA receptor-mediated retinal axon guidance. *J Neurosci* 24:6248-6257.
64. Holland, S.J., N.W. Gale, G.D. Gish, R.A. Roth, Z. Songyang, L.C. Cantley, M. Henkemeyer, G.D. Yancopoulos, and T. Pawson. 1997. Juxtamembrane tyrosine residues couple the Eph family receptor EphB2/Nuk to specific SH2 domain proteins in neuronal cells. *Embo J* 16:3877-3888.
65. Becker, E., U. Huynh-Do, S. Holland, T. Pawson, T.O. Daniel, and E.Y. Skolnik. 2000. Nck-interacting Ste20 kinase couples Eph receptors to c-Jun N-terminal kinase and integrin activation. *Mol Cell Biol* 20:1537-1545.
66. Elowe, S., S.J. Holland, S. Kulkarni, and T. Pawson. 2001. Downregulation of the Ras-mitogen-activated protein kinase pathway by the EphB2 receptor tyrosine kinase is required for ephrin-induced neurite retraction. *Mol Cell Biol* 21:7429-7441.
67. Lai, K.O., Y. Chen, H.M. Po, K.C. Lok, K. Gong, and N.Y. Ip. 2004. Identification of the Jak/Stat proteins as novel downstream targets of EphA4 signaling in muscle: implications in the regulation of acetylcholinesterase expression. *J Biol Chem* 279:13383-13392.
68. Sahin, M., P.L. Greer, M.Z. Lin, H. Poucher, J. Eberhart, S. Schmidt, T.M. Wright, S.M. Shamah, S. O'Connell, C.W. Cowan, L. Hu, J.L. Goldberg, A. Debant, G. Corfas, C.E. Krull, and M.E. Greenberg. 2005. Eph-dependent tyrosine phosphorylation of ephexin1 modulates growth cone collapse. *Neuron* 46:191-204.
69. Shamah, S.M., M.Z. Lin, J.L. Goldberg, S. Estrach, M. Sahin, L. Hu, M. Bazalakova, R.L. Neve, G. Corfas, A. Debant, and M.E. Greenberg. 2001. EphA receptors regulate growth cone dynamics through the novel guanine nucleotide exchange factor ephexin. *Cell* 105:233-244.
70. Iwasato, T., H. Katoh, H. Nishimaru, Y. Ishikawa, H. Inoue, Y.M. Saito, R. Ando, M. Iwama, R. Takahashi, M. Negishi, and S. Itohara. 2007. Rac-GAP alpha-chimerin regulates motor-circuit formation as a key mediator of EphrinB3/EphA4 forward signaling. *Cell* 130:742-753.
71. Wegmeyer, H., J. Egea, N. Rabe, H. Gezelius, A. Filosa, A. Enjin, F. Varoqueaux, K. Deininger, F. Schnutgen, N. Brose, R. Klein, K. Kullander, and A. Betz. 2007. EphA4-dependent axon guidance is mediated by the RacGAP alpha2-chimaerin. *Neuron* 55:756-767.
72. Richter, M., K.K. Murai, C. Bourgin, D.T. Pak, and E.B. Pasquale. 2007. The EphA4 receptor regulates neuronal morphology through SPAR-mediated inactivation of Rap GTPases. *J Neurosci* 27:14205-14215.
73. Marston, D.J., S. Dickinson, and C.D. Nobes. 2003. Rac-dependent trans-endocytosis of ephrinBs regulates Eph-ephrin contact repulsion. *Nat Cell Biol* 5:879-888.

74. Zimmer, M., A. Palmer, J. Kohler, and R. Klein. 2003. EphB-ephrinB bi-directional endocytosis terminates adhesion allowing contact mediated repulsion. *Nat Cell Biol* 5:869-878.
75. Lauterbach, J., and R. Klein. 2006. Release of full-length EphB2 receptors from hippocampal neurons to cocultured glial cells. *J Neurosci* 26:11575-11581.
76. Cowan, C.W., Y.R. Shao, M. Sahin, S.M. Shamah, M.Z. Lin, P.L. Greer, S. Gao, E.C. Griffith, J.S. Brugge, and M.E. Greenberg. 2005. Vav family GEFs link activated Ephs to endocytosis and axon guidance. *Neuron* 46:205-217.
77. Shintani, T., M. Ihara, H. Sakuta, H. Takahashi, I. Watakabe, and M. Noda. 2006. Eph receptors are negatively controlled by protein tyrosine phosphatase receptor type O. *Nat Neurosci* 9:761-769.
78. Holmberg, J., D.L. Clarke, and J. Frisen. 2000. Regulation of repulsion versus adhesion by different splice forms of an Eph receptor. *Nature* 408:203-206.
79. Chin-Sang, I.D., S.E. George, M. Ding, S.L. Moseley, A.S. Lynch, and A.D. Chisholm. 1999. The ephrin VAB-2/EFN-1 functions in neuronal signaling to regulate epidermal morphogenesis in C. elegans. *Cell* 99:781-790.
80. Davy, A., N.W. Gale, E.W. Murray, R.A. Klinghoffer, P. Soriano, C. Feuerstein, and S.M. Robbins. 1999. Compartmentalized signaling by GPI-anchored ephrin-A5 requires the Fyn tyrosine kinase to regulate cellular adhesion. *Genes Dev* 13:3125-3135.
81. Davy, A., and S.M. Robbins. 2000. Ephrin-A5 modulates cell adhesion and morphology in an integrin-dependent manner. *Embo J* 19:5396-5405.
82. Huai, J., and U. Drescher. 2001. An ephrin-A-dependent signaling pathway controls integrin function and is linked to the tyrosine phosphorylation of a 120-kDa protein. *J Biol Chem* 276:6689-6694.
83. Hattori, M., M. Osterfield, and J.G. Flanagan. 2000. Regulated cleavage of a contact-mediated axon repellent. *Science* 289:1360-1365.
84. Cowan, C.A., N. Yokoyama, A. Saxena, M.J. Chumley, R.E. Silvany, L.A. Baker, D. Srivastava, and M. Henkemeyer. 2004. Ephrin-B2 reverse signaling is required for axon pathfinding and cardiac valve formation but not early vascular development. *Dev Biol* 271:263-271.
85. Mellitzer, G., Q. Xu, and D.G. Wilkinson. 1999. Eph receptors and ephrins restrict cell intermingling and communication. *Nature* 400:77-81.
86. Holland, S.J., N.W. Gale, G. Mbamalu, G.D. Yancopoulos, M. Henkemeyer, and T. Pawson. 1996. Bidirectional signalling through the EPH-family receptor Nuk and its transmembrane ligands. *Nature* 383:722-725.
87. Bruckner, K., E.B. Pasquale, and R. Klein. 1997. Tyrosine phosphorylation of transmembrane ligands for Eph receptors. *Science* 275:1640-1643.
88. Chong, L.D., E.K. Park, E. Latimer, R. Friesel, and I.O. Daar. 2000. Fibroblast growth factor receptor-mediated rescue of x-ephrin B1-induced cell dissociation in Xenopus embryos. *Mol Cell Biol* 20:724-734.
89. Palmer, A., M. Zimmer, K.S. Erdmann, V. Eulenburg, A. Porthin, R. Heumann, U. Deutsch, and R. Klein. 2002. EphrinB phosphorylation and reverse signaling: regulation by Src kinases and PTP-BL phosphatase. *Mol Cell* 9:725-737.

90. Kalo, M.S., H.H. Yu, and E.B. Pasquale. 2001. In vivo tyrosine phosphorylation sites of activated ephrin-B1 and ephB2 from neural tissue. *J Biol Chem* 276:38940-38948.
91. Segura, I., C.L. Essmann, S. Weinges, and A. Acker-Palmer. 2007. Grb4 and GIT1 transduce ephrinB reverse signals modulating spine morphogenesis and synapse formation. *Nat Neurosci* 10:301-310.
92. Bruckner, K., J. Pablo Labrador, P. Scheiffele, A. Herb, P.H. Seeburg, and R. Klein. 1999. EphrinB ligands recruit GRIP family PDZ adaptor proteins into raft membrane microdomains. *Neuron* 22:511-524.
93. Lu, Q., E.E. Sun, R.S. Klein, and J.G. Flanagan. 2001. Ephrin-B reverse signaling is mediated by a novel PDZ-RGS protein and selectively inhibits G protein-coupled chemoattraction. *Cell* 105:69-79.
94. Huynh-Do, U., C. Vindis, H. Liu, D.P. Cerretti, J.T. McGrew, M. Enriquez, J. Chen, and T.O. Daniel. 2002. Ephrin-B1 transduces signals to activate integrin-mediated migration, attachment and angiogenesis. *J Cell Sci* 115:3073-3081.
95. Simons, K., and E. Ikonen. 1997. Functional rafts in cell membranes. *Nature* 387:569-572.
96. Simionescu, N. 1983. Cellular aspects of transcapillary exchange. *Physiol Rev* 63:1536-1579.
97. Parton, R.G., B. Joggerst, and K. Simons. 1994. Regulated internalization of caveolae. *J Cell Biol* 127:1199-1215.
98. Fivaz, M., L. Abrami, and F.G. van der Goot. 1999. Landing on lipid rafts. *Trends Cell Biol* 9:212-213.
99. Shin, J.S., and S.N. Abraham. 2001. Cell biology. Caveolae--not just craters in the cellular landscape. *Science* 293:1447-1448.
100. Shin, J.S., Z. Gao, and S.N. Abraham. 2000. Involvement of cellular caveolae in bacterial entry into mast cells. *Science* 289:785-788.
101. Smart, E.J., Y. Ying, W.C. Donzell, and R.G. Anderson. 1996. A role for caveolin in transport of cholesterol from endoplasmic reticulum to plasma membrane. *J Biol Chem* 271:29427-29435.
102. Isshiki, M., and R.G. Anderson. 1999. Calcium signal transduction from caveolae. *Cell Calcium* 26:201-208.
103. Anderson, R.G. 1998. The caveolae membrane system. *Annu Rev Biochem* 67:199-225.
104. Simons, K., and D. Toomre. 2000. Lipid rafts and signal transduction. *Nat Rev Mol Cell Biol* 1:31-39.
105. Zajchowski, L.D., and S.M. Robbins. 2002. Lipid rafts and little caves. Compartmentalized signalling in membrane microdomains. *Eur J Biochem* 269:737-752.
106. Robbins, S.M., N.A. Quintrell, and J.M. Bishop. 1995. Myristoylation and differential palmitoylation of the HCK protein-tyrosine kinases govern their attachment to membranes and association with caveolae. *Mol Cell Biol* 15:3507-3515.

107. Shenoy-Scaria, A.M., D.J. Dietzen, J. Kwong, D.C. Link, and D.M. Lublin. 1994. Cysteine3 of Src family protein tyrosine kinase determines palmitoylation and localization in caveolae. *J Cell Biol* 126:353-363.
108. Varma, R., and S. Mayor. 1998. GPI-anchored proteins are organized in submicron domains at the cell surface. *Nature* 394:798-801.
109. Gauthier, L.R., and S.M. Robbins. 2003. Ephrin signaling: One raft to rule them all? One raft to sort them? One raft to spread their call and in signaling bind them? *Life Sci* 74:207-216.
110. Wu, C., S. Butz, Y. Ying, and R.G. Anderson. 1997. Tyrosine kinase receptors concentrated in caveolae-like domains from neuronal plasma membrane. *J Biol Chem* 272:3554-3559.
111. Vihanto, M.M., C. Vindis, V. Djonov, D.P. Cerretti, and U. Huynh-Do. 2006. Caveolin-1 is required for signaling and membrane targeting of EphB1 receptor tyrosine kinase. *J Cell Sci* 119:2299-2309.
112. Marquardt, T., R. Shirasaki, S. Ghosh, S.E. Andrews, N. Carter, T. Hunter, and S.L. Pfaff. 2005. Coexpressed EphA receptors and ephrin-A ligands mediate opposing actions on growth cone navigation from distinct membrane domains. *Cell* 121:127-139.
113. Dickson, B.J. 2002. Molecular mechanisms of axon guidance. *Science* 298:1959-1964.
114. Graham, A. 2003. The neural crest. *Curr Biol* 13:R381-384.
115. Cheng, H.J., M. Nakamoto, A.D. Bergemann, and J.G. Flanagan. 1995. Complementary gradients in expression and binding of ELF-1 and Mek4 in development of the topographic retinotectal projection map. *Cell* 82:371-381.
116. Drescher, U., C. Kremoser, C. Handwerker, J. Loschinger, M. Noda, and F. Bonhoeffer. 1995. In vitro guidance of retinal ganglion cell axons by RAGS, a 25 kDa tectal protein related to ligands for Eph receptor tyrosine kinases. *Cell* 82:359-370.
117. Feldheim, D.A., Y.I. Kim, A.D. Bergemann, J. Frisen, M. Barbacid, and J.G. Flanagan. 2000. Genetic analysis of ephrin-A2 and ephrin-A5 shows their requirement in multiple aspects of retinocollicular mapping. *Neuron* 25:563-574.
118. Monschau, B., C. Kremoser, K. Ohta, H. Tanaka, T. Kaneko, T. Yamada, C. Handwerker, M.R. Hornberger, J. Loschinger, E.B. Pasquale, D.A. Siever, M.F. Verderame, B.K. Muller, F. Bonhoeffer, and U. Drescher. 1997. Shared and distinct functions of RAGS and ELF-1 in guiding retinal axons. *Embo J* 16:1258-1267.
119. Nakamoto, M., H.J. Cheng, G.C. Friedman, T. McLaughlin, M.J. Hansen, C.H. Yoon, D.D. O'Leary, and J.G. Flanagan. 1996. Topographically specific effects of ELF-1 on retinal axon guidance in vitro and retinal axon mapping in vivo. *Cell* 86:755-766.
120. Kiecker, C., and A. Lumsden. 2005. Compartments and their boundaries in vertebrate brain development. *Nat Rev Neurosci* 6:553-564.
121. Fraser, S., R. Keynes, and A. Lumsden. 1990. Segmentation in the chick embryo hindbrain is defined by cell lineage restrictions. *Nature* 344:431-435.

122. Wizenmann, A., and A. Lumsden. 1997. Segregation of rhombomeres by differential chemoaffinity. *Mol Cell Neurosci* 9:448-459.
123. Xu, Q., G. Mellitzer, V. Robinson, and D.G. Wilkinson. 1999. In vivo cell sorting in complementary segmental domains mediated by Eph receptors and ephrins. *Nature* 399:267-271.
124. Cooke, J.E., H.A. Kemp, and C.B. Moens. 2005. EphA4 is required for cell adhesion and rhombomere-boundary formation in the zebrafish. *Curr Biol* 15:536-542.
125. Surawska, H., P.C. Ma, and R. Salgia. 2004. The role of ephrins and Eph receptors in cancer. *Cytokine Growth Factor Rev* 15:419-433.
126. Heroult, M., F. Schaffner, and H.G. Augustin. 2006. Eph receptor and ephrin ligand-mediated interactions during angiogenesis and tumor progression. *Exp Cell Res* 312:642-650.
127. Cortina, C., S. Palomo-Ponce, M. Iglesias, J.L. Fernandez-Masip, A. Vivancos, G. Whissell, M. Huma, N. Peiro, L. Gallego, S. Jonkheer, A. Davy, J. Lloreta, E. Sancho, and E. Batlle. 2007. EphB-ephrin-B interactions suppress colorectal cancer progression by compartmentalizing tumor cells. *Nat Genet* 39:1376-1383.
128. Koolpe, M., R. Burgess, M. Dail, and E.B. Pasquale. 2005. EphB receptor-binding peptides identified by phage display enable design of an antagonist with ephrin-like affinity. *J Biol Chem* 280:17301-17311.
129. Koolpe, M., M. Dail, and E.B. Pasquale. 2002. An ephrin mimetic peptide that selectively targets the EphA2 receptor. *J Biol Chem* 277:46974-46979.
130. Murai, K.K., L.N. Nguyen, M. Koolpe, R. McLennan, C.E. Krull, and E.B. Pasquale. 2003. Targeting the EphA4 receptor in the nervous system with biologically active peptides. *Mol Cell Neurosci* 24:1000-1011.
131. Chaudhari, A., M. Mahfouz, A.M. Fialho, T. Yamada, A.T. Granja, Y. Zhu, W. Hashimoto, B. Schlarb-Ridley, W. Cho, T.K. Das Gupta, and A.M. Chakrabarty. 2007. Cupredoxin-cancer interrelationship: azurin binding with EphB2, interference in EphB2 tyrosine phosphorylation, and inhibition of cancer growth. *Biochemistry* 46:1799-1810.
132. Punj, V., S. Bhattacharyya, D. Saint-Dic, C. Vasu, E.A. Cunningham, J. Graves, T. Yamada, A.I. Constantinou, K. Christov, B. White, G. Li, D. Majumdar, A.M. Chakrabarty, and T.K. Das Gupta. 2004. Bacterial cupredoxin azurin as an inducer of apoptosis and regression in human breast cancer. *Oncogene* 23:2367-2378.
133. Twigg, S.R., R. Kan, C. Babbs, E.G. Bochukova, S.P. Robertson, S.A. Wall, G.M. Morriss-Kay, and A.O. Wilkie. 2004. Mutations of ephrin-B1 (EFNB1), a marker of tissue boundary formation, cause craniofrontonasal syndrome. *Proc Natl Acad Sci U S A* 101:8652-8657.
134. Wieland, I., S. Jakubiczka, P. Muschke, M. Cohen, H. Thiele, K.L. Gerlach, R.H. Adams, and P. Wieacker. 2004. Mutations of the ephrin-B1 gene cause craniofrontonasal syndrome. *Am J Hum Genet* 74:1209-1215.
135. Wieacker, P., and I. Wieland. 2005. Clinical and genetic aspects of craniofrontonasal syndrome: towards resolving a genetic paradox. *Mol Genet Metab* 86:110-116.

136. Torii, C., K. Izumi, H. Nakajima, T. Takahashi, and K. Kosaki. 2007. EFNB1 mutation at the ephrin ligand-receptor dimerization interface in a patient with craniofrontonasal syndrome. *Congenit Anom (Kyoto)* 47:49-52.
137. Wieland, I., W. Reardon, S. Jakubiczka, B. Franco, W. Kress, C. Vincent-Delorme, P. Thierry, M. Edwards, R. Konig, C. Rusu, S. Schweiger, E. Thompson, S. Tinschert, F. Stewart, and P. Wieacker. 2005. Twenty-six novel EFNB1 mutations in familial and sporadic craniofrontonasal syndrome (CFNS). *Hum Mutat* 26:113-118.
138. Compagni, A., M. Logan, R. Klein, and R.H. Adams. 2003. Control of skeletal patterning by ephrinB1-EphB interactions. *Dev Cell* 5:217-230.
139. Davy, A., J. Aubin, and P. Soriano. 2004. Ephrin-B1 forward and reverse signaling are required during mouse development. *Genes Dev* 18:572-583.
140. Megason, S.G., and A.P. McMahon. 2002. A mitogen gradient of dorsal midline Wnts organizes growth in the CNS. *Development* 129:2087-2098.
141. Rabilloud, T., G. Carpentier, and P. Tarroux. 1988. Improvement and simplification of low-background silver staining of proteins by using sodium dithionite. *Electrophoresis* 9:288-291.
142. Blum, H., H. Beier, and H.J. Gross. 1987. Improved silver staining of plant proteins, RNA and DNA in polyacrylamide gels. *Electrophoresis* 8:93-99.
143. Hamburger, V., and H.L. Hamilton. 1951. A series of normal stages in the development of the chick embryo. *J Morph* 88:49-92.
144. Nakamura, H., and J. Funahashi. 2001. Introduction of DNA into chick embryos by in ovo electroporation. *Methods* 24:43-48.
145. Hornbruch, A. 1999. New Culture. In Molecular Embryology: Methods and Protocols. P. Sharpe, and I. Mason, editors. Humana Press, 539-551.
146. Logan, C., C. Millar, V. Bharadia, and K. Rouleau. 2002. Onset of Tlx-3 expression in the chick cerebellar cortex correlates with the morphological development of fissures and delineates a posterior transverse boundary. *J Comp Neurol* 448:138-149.
147. Wilkinson, D.G. 1992. Whole-mount *in situ* hybridization of vertebrate embryos. In *In situ* hybridization. Oxford, 75-83.
148. Davis, C.A., D.P. Holmyard, K.J. Millen, and A.L. Joyner. 1991. Examining pattern formation in mouse, chicken and frog embryos with an En-specific antiserum. *Development* 111:287-298.
149. Thompson, S.K. 2002. Estimating Proportion, Ratios, and Subpopulation Means. In Sampling. Wiley-Interscience, New York, New York.
150. Team, R.D.C. 2007. R: A Language and Environment for Statistical Computing, Version 2.6.1. In R Foundation for Statistical Computing, Vienna.
151. Davy, A., and S. Robbins. unpublished results.
152. Meyer, S., E. Orso, G. Schmitz, M. Landthaler, and T. Vogt. 2007. Lubrol-RAFTs in melanoma cells: a molecular platform for tumor-promoting ephrin-B2-integrin-beta1 interaction. *J Invest Dermatol* 127:1615-1621.
153. Palmer, A., and R. Klein. 2003. Multiple roles of ephrins in morphogenesis, neuronal networking, and brain function. *Genes Dev* 17:1429-1450.

154. Lin, D., G.D. Gish, Z. Songyang, and T. Pawson. 1999. The carboxyl terminus of B class ephrins constitutes a PDZ domain binding motif. *J Biol Chem* 274:3726-3733.
155. Songyang, Z., A.S. Fanning, C. Fu, J. Xu, S.M. Marfatia, A.H. Chishti, A. Crompton, A.C. Chan, J.M. Anderson, and L.C. Cantley. 1997. Recognition of unique carboxyl-terminal motifs by distinct PDZ domains. *Science* 275:73-77.
156. Jones, D.T., W.R. Taylor, and J.M. Thornton. 1994. A model recognition approach to the prediction of all-helical membrane protein structure and topology. *Biochemistry* 33:3038-3049.
157. Tusnady, G.E., and I. Simon. 1998. Principles governing amino acid composition of integral membrane proteins: application to topology prediction. *J Mol Biol* 283:489-506.
158. von Heijne, G. 1992. Membrane protein structure prediction. Hydrophobicity analysis and the positive-inside rule. *J Mol Biol* 225:487-494.
159. Krogh, A., B. Larsson, G. von Heijne, and E.L. Sonnhammer. 2001. Predicting transmembrane protein topology with a hidden Markov model: application to complete genomes. *J Mol Biol* 305:567-580.
160. Hofmann, K., and W. Stoffel. 1993. TMbase - A database of membrane spanning proteins segments. *Biol. Chem. Hoppe-Seyler* 374:166.
161. Wang, J., A. Arbuzova, G. Hangyas-Mihalyne, and S. McLaughlin. 2001. The effector domain of myristoylated alanine-rich C kinase substrate binds strongly to phosphatidylinositol 4,5-bisphosphate. *J Biol Chem* 276:5012-5019.
162. Horowitz, A., M. Murakami, Y. Gao, and M. Simons. 1999. Phosphatidylinositol-4,5-bisphosphate mediates the interaction of syndecan-4 with protein kinase C. *Biochemistry* 38:15871-15877.
163. Oh, E.S., A. Woods, and J.R. Couchman. 1997. Multimerization of the cytoplasmic domain of syndecan-4 is required for its ability to activate protein kinase C. *J Biol Chem* 272:11805-11811.
164. Santagata, S., T.J. Boggon, C.L. Baird, C.A. Gomez, J. Zhao, W.S. Shan, D.G. Myszka, and L. Shapiro. 2001. G-protein signaling through tubby proteins. *Science* 292:2041-2050.
165. Murray, D., A. Arbuzova, B. Honig, and S. McLaughlin. 2002. The Role of Electrostatic and Nonpolar Interactions in the Assocation of Peripheral Proteins with Membranes. *Current Topics in Membranes* 52:277-307.
166. Zhang, B., and Y. Zheng. 1998. Negative regulation of Rho family GTPases Cdc42 and Rac2 by homodimer formation. *J Biol Chem* 273:25728-25733.
167. Hope, H.R., and L.J. Pike. 1996. Phosphoinositides and phosphoinositide-utilizing enzymes in detergent-insoluble lipid domains. *Mol Biol Cell* 7:843-851.
168. Henkemeyer, M., L.E. Marengere, J. McGlade, J.P. Olivier, R.A. Conlon, D.P. Holmyard, K. Letwin, and T. Pawson. 1994. Immunolocalization of the Nuk receptor tyrosine kinase suggests roles in segmental patterning of the brain and axonogenesis. *Oncogene* 9:1001-1014.
169. Brone, B., and J. Eggermont. 2005. PDZ proteins retain and regulate membrane transporters in polarized epithelial cell membranes. *Am J Physiol Cell Physiol* 288:C20-29.

170. Fialka, I., P. Steinlein, H. Ahorn, G. Bock, P.D. Burbelo, M. Haberfellner, F. Lottspeich, K. Paiha, C. Pasquali, and L.A. Huber. 1999. Identification of syntenin as a protein of the apical early endocytic compartment in Madin-Darby canine kidney cells. *J Biol Chem* 274:26233-26239.
171. Grootjans, J.J., P. Zimmermann, G. Reekmans, A. Smets, G. Degeest, J. Durr, and G. David. 1997. Syntenin, a PDZ protein that binds syndecan cytoplasmic domains. *Proc Natl Acad Sci U S A* 94:13683-13688.
172. Kalo, M.S., and E.B. Pasquale. 1999. Signal transfer by Eph receptors. *Cell Tissue Res* 298:1-9.
173. Alvarez, R.H., H.M. Kantarjian, and J.E. Cortes. 2006. Biology of platelet-derived growth factor and its involvement in disease. *Mayo Clin Proc* 81:1241-1257.
174. Hoch, R.V., and P. Soriano. 2003. Roles of PDGF in animal development. *Development* 130:4769-4784.
175. Leger, J., M. Kempf, G. Lee, and R. Brandt. 1997. Conversion of serine to aspartate imitates phosphorylation-induced changes in the structure and function of microtubule-associated protein tau. *J Biol Chem* 272:8441-8446.
176. Bong, Y.S., H.S. Lee, L. Carim-Todd, K. Mood, T.G. Nishanian, L. Tessarollo, and I.O. Daar. 2007. ephrinB1 signals from the cell surface to the nucleus by recruitment of STAT3. *Proc Natl Acad Sci U S A* 104:17305-17310.
177. Schwartz, D.C., and M. Hochstrasser. 2003. A superfamily of protein tags: ubiquitin, SUMO and related modifiers. *Trends Biochem Sci* 28:321-328.
178. Jiang, H., and P.B. Fisher. 1993. Use of a sensitive and efficient subtraction hybridization protocol for the identification of genes differentially regulated during the induction of differentiated in human melanoma cells. *Mol. Cell. Different. 1 3, pp. 285–299* Mol. Cell. Different.:285–299.
179. Boukerche, H., Z.Z. Su, L. Emdad, P. Baril, B. Balme, L. Thomas, A. Randolph, K. Valerie, D. Sarkar, and P.B. Fisher. 2005. mda-9/Syntenin: a positive regulator of melanoma metastasis. *Cancer Res* 65:10901-10911.
180. Koo, T.H., J.J. Lee, E.M. Kim, K.W. Kim, H.D. Kim, and J.H. Lee. 2002. Syntenin is overexpressed and promotes cell migration in metastatic human breast and gastric cancer cell lines. *Oncogene* 21:4080-4088.
181. Hirbec, H., S. Martin, and J.M. Henley. 2005. Syntenin is involved in the developmental regulation of neuronal membrane architecture. *Mol Cell Neurosci* 28:737-746.
182. Tomoda, T., J.H. Kim, C. Zhan, and M.E. Hatten. 2004. Role of Unc51.1 and its binding partners in CNS axon outgrowth. *Genes Dev* 18:541-558.
183. Grootjans, J.J., G. Reekmans, H. Ceulemans, and G. David. 2000. Syntenin-syndecan binding requires syndecan-synteny and the co-operation of both PDZ domains of syntenin. *J Biol Chem* 275:19933-19941.
184. Makinen, T., R.H. Adams, J. Bailey, Q. Lu, A. Ziemiecki, K. Alitalo, R. Klein, and G.A. Wilkinson. 2005. PDZ interaction site in ephrinB2 is required for the remodeling of lymphatic vasculature. *Genes Dev* 19:397-410.

185. Garton, K.J., P.J. Gough, and E.W. Raines. 2006. Emerging roles for ectodomain shedding in the regulation of inflammatory responses. *J Leukoc Biol* 79:1105-1116.
186. Huovila, A.P., E.A. Almeida, and J.M. White. 1996. ADAMs and cell fusion. *Curr Opin Cell Biol* 8:692-699.
187. Rocks, N., G. Paulissen, M. El Hour, F. Quesada, C. Crahay, M. Gueders, J.M. Foidart, A. Noel, and D. Cataldo. 2007. Emerging roles of ADAM and ADAMTS metalloproteinases in cancer. *Biochimie*
188. Zhou, B.B., J.S. Fridman, X. Liu, S.M. Friedman, R.C. Newton, and P.A. Scherle. 2005. ADAM proteases, ErbB pathways and cancer. *Expert Opin Investig Drugs* 14:591-606.
189. Arribas, J., and A. Borroto. 2002. Protein ectodomain shedding. *Chem Rev* 102:4627-4638.
190. Huovila, A.P., A.J. Turner, M. Pelto-Huikko, I. Karkkainen, and R.M. Ortiz. 2005. Shedding light on ADAM metalloproteinases. *Trends Biochem Sci* 30:413-422.
191. Rose-John, S., and P.C. Heinrich. 1994. Soluble receptors for cytokines and growth factors: generation and biological function. *Biochem J* 300 (Pt 2):281-290.
192. Vecchi, M., and G. Carpenter. 1997. Constitutive proteolysis of the ErbB-4 receptor tyrosine kinase by a unique, sequential mechanism. *J Cell Biol* 139:995-1003.
193. Artavanis-Tsakonas, S., M.D. Rand, and R.J. Lake. 1999. Notch signaling: cell fate control and signal integration in development. *Science* 284:770-776.
194. Schulz, J.G., W. Annaert, J. Vandekerckhove, P. Zimmermann, B. De Strooper, and G. David. 2003. Syndecan 3 intramembrane proteolysis is presenilin/gamma-secretase-dependent and modulates cytosolic signaling. *J Biol Chem* 278:48651-48657.
195. Domeniconi, M., N. Zampieri, T. Spencer, M. Hilaire, W. Mellado, M.V. Chao, and M.T. Filbin. 2005. MAG induces regulated intramembrane proteolysis of the p75 neurotrophin receptor to inhibit neurite outgrowth. *Neuron* 46:849-855.
196. Kopan, R., E.H. Schroeter, H. Weintraub, and J.S. Nye. 1996. Signal transduction by activated mNotch: importance of proteolytic processing and its regulation by the extracellular domain. *Proc Natl Acad Sci U S A* 93:1683-1688.
197. Schroeter, E.H., J.A. Kisslinger, and R. Kopan. 1998. Notch-1 signalling requires ligand-induced proteolytic release of intracellular domain. *Nature* 393:382-386.
198. Gutwein, P., M. Oleszewski, S. Mechtersheimer, N. Agmon-Levin, K. Krauss, and P. Altevogt. 2000. Role of Src kinases in the ADAM-mediated release of L1 adhesion molecule from human tumor cells. *J Biol Chem* 275:15490-15497.
199. Herreman, A., L. Serneels, W. Annaert, D. Collen, L. Schoonjans, and B. De Strooper. 2000. Total inactivation of gamma-secretase activity in presenilin-deficient embryonic stem cells. *Nat Cell Biol* 2:461-462.
200. Gupta-Rossi, N., E. Six, O. LeBail, F. Logeat, P. Chastagner, A. Olry, A. Israel, and C. Brou. 2004. Monoubiquitination and endocytosis direct gamma-secretase cleavage of activated Notch receptor. *J Cell Biol* 166:73-83.

201. Cupers, P., I. Orlans, K. Craessaerts, W. Annaert, and B. De Strooper. 2001. The amyloid precursor protein (APP)-cytoplasmic fragment generated by gamma-secretase is rapidly degraded but distributes partially in a nuclear fraction of neurones in culture. *J Neurochem* 78:1168-1178.
202. Kertesz, N., V. Krasnoperov, R. Reddy, L. Leshanski, S.R. Kumar, S. Zozulya, and P.S. Gill. 2006. The soluble extracellular domain of EphB4 (sEphB4) antagonizes EphB4-EphrinB2 interaction, modulates angiogenesis, and inhibits tumor growth. *Blood* 107:2330-2338.
203. Aasheim, H.C., E. Munthe, S. Funderud, E.B. Smeland, K. Beiske, and T. Logtenberg. 2000. A splice variant of human ephrin-A4 encodes a soluble molecule that is secreted by activated human B lymphocytes. *Blood* 95:221-230.
204. Alford, S.C., J. Bazowski, H. Lorimer, S. Elowe, and P.L. Howard. 2007. Tissue transglutaminase clusters soluble A-type ephrins into functionally active high molecular weight oligomers. *Exp Cell Res* 313:4170-4179.
205. Ilan, N., A. Mohsenin, L. Cheung, and J.A. Madri. 2001. PECAM-1 shedding during apoptosis generates a membrane-anchored truncated molecule with unique signaling characteristics. *Faseb J* 15:362-372.
206. Lee, D., and O. Gautschi. 2006. Clinical development of SRC tyrosine kinase inhibitors in lung cancer. *Clin Lung Cancer* 7:381-384.
207. Li, S. 2007. Src kinase signaling in leukaemia. *Int J Biochem Cell Biol* 39:1483-1488.
208. Parsons, J.T., and S.J. Parsons. 1997. Src family protein tyrosine kinases: cooperating with growth factor and adhesion signaling pathways. *Curr Opin Cell Biol* 9:187-192.
209. Wang, L.H. 1987. The mechanism of transduction of proto-oncogene c-src by avian retroviruses. *Mutat Res* 186:135-147.
210. Pascall, J.C., and K.D. Brown. 2004. Intramembrane cleavage of ephrinB3 by the human rhomboid family protease, RHBDL2. *Biochem Biophys Res Commun* 317:244-252.
211. Shah, S., S.F. Lee, K. Tabuchi, Y.H. Hao, C. Yu, Q. LaPlant, H. Ball, C.E. Dann, 3rd, T. Sudhof, and G. Yu. 2005. Nicastrin functions as a gamma-secretase-substrate receptor. *Cell* 122:435-447.
212. Struhl, G., and A. Adachi. 2000. Requirements for presenilin-dependent cleavage of notch and other transmembrane proteins. *Mol Cell* 6:625-636.
213. Mann, F., E. Miranda, C. Weinl, E. Harmer, and C.E. Holt. 2003. B-type Eph receptors and ephrins induce growth cone collapse through distinct intracellular pathways. *J Neurobiol* 57:323-336.
214. Medina, M., and C.G. Dotti. 2003. RIPped out by presenilin-dependent gamma-secretase. *Cell Signal* 15:829-841.
215. Kopan, R., and M.X. Ilagan. 2004. Gamma-secretase: proteasome of the membrane? *Nat Rev Mol Cell Biol* 5:499-504.
216. Small, D.H. 2002. Is gamma-secretase a multienzyme complex for membrane protein degradation? Models and speculations. *Peptides* 23:1317-1321.

217. Huppert, S.S., A. Le, E.H. Schroeter, J.S. Mumm, M.T. Saxena, L.A. Milner, and R. Kopan. 2000. Embryonic lethality in mice homozygous for a processing-deficient allele of Notch1. *Nature* 405:966-970.
218. Kimberly, W.T., J.B. Zheng, S.Y. Guenette, and D.J. Selkoe. 2001. The intracellular domain of the beta-amyloid precursor protein is stabilized by Fe65 and translocates to the nucleus in a notch-like manner. *J Biol Chem* 276:40288-40292.
219. Georgakopoulos, A., C. Litterst, E. Ghersi, L. Baki, C. Xu, G. Serban, and N.K. Robakis. 2006. Metalloproteinase/Presenilin1 processing of ephrinB regulates EphB-induced Src phosphorylation and signaling. *Embo J* 25:1242-1252.
220. Tanaka, M., K. Sasaki, R. Kamata, and R. Sakai. 2007. The C-terminus of ephrin-B1 regulates metalloproteinase secretion and invasion of cancer cells. *J Cell Sci* 120:2179-2189.
221. Tomita, T., S. Tanaka, Y. Morohashi, and T. Iwatsubo. 2006. Presenilin-dependent intramembrane cleavage of ephrin-B1. *Mol Neurodegener* 1:2.
222. Nakada, M., K.L. Drake, S. Nakada, J.A. Niska, and M.E. Berens. 2006. Ephrin-B3 ligand promotes glioma invasion through activation of Rac1. *Cancer Res* 66:8492-8500.
223. Imondi, R., and Z. Kaprielian. 2001. Commissural axon pathfinding on the contralateral side of the floor plate: a role for B-class ephrins in specifying the dorsoventral position of longitudinally projecting commissural axons. *Development* 128:4859-4871.
224. Jevince, A.R., S.R. Kadison, A.J. Pittman, C.B. Chien, and Z. Kaprielian. 2006. Distribution of EphB receptors and ephrin-B1 in the developing vertebrate spinal cord. *J Comp Neurol* 497:734-750.
225. Kadison, S.R., T. Makinen, R. Klein, M. Henkemeyer, and Z. Kaprielian. 2006. EphB receptors and ephrin-B3 regulate axon guidance at the ventral midline of the embryonic mouse spinal cord. *J Neurosci* 26:8909-8914.
226. Stern, C.D. 2005. The chick; a great model system becomes even greater. *Dev Cell* 8:9-17.
227. 2004. Sequence and comparative analysis of the chicken genome provide unique perspectives on vertebrate evolution. *Nature* 432:695-716.
228. Wolpert, L. 2004. Much more from the chicken's egg than breakfast--a wonderful model system. *Mech Dev* 121:1015-1017.
229. Nakamura, H., T. Katahira, T. Sato, Y. Watanabe, and J. Funahashi. 2004. Gain- and loss-of-function in chick embryos by electroporation. *Mech Dev* 121:1137-1143.
230. Wolpert, L. 2002. Principles of Development. Oxford University Press, New York. 542 pp.
231. Sadler, T.W. 2005. Embryology of neural tube development. *Am J Med Genet C Semin Med Genet* 135:2-8.
232. Matise, M. 2002. A dorsal elaboration in the spinal cord. *Neuron* 34:491-493.
233. Wilson, L., and M. Maden. 2005. The mechanisms of dorsoventral patterning in the vertebrate neural tube. *Dev Biol* 282:1-13.

234. Logan, C., R.J. Wingate, I.J. McKay, and A. Lumsden. 1998. Tlx-1 and Tlx-3 homeobox gene expression in cranial sensory ganglia and hindbrain of the chick embryo: markers of patterned connectivity. *J Neurosci* 18:5389-5402.
235. Imondi, R., C. Wideman, and Z. Kaprielian. 2000. Complementary expression of transmembrane ephrins and their receptors in the mouse spinal cord: a possible role in constraining the orientation of longitudinally projecting axons. *Development* 127:1397-1410.
236. Kullander, K., S.D. Croll, M. Zimmer, L. Pan, J. McClain, V. Hughes, S. Zabski, T.M. DeChiara, R. Klein, G.D. Yancopoulos, and N.W. Gale. 2001. Ephrin-B3 is the midline barrier that prevents corticospinal tract axons from recrossing, allowing for unilateral motor control. *Genes Dev* 15:877-888.
237. Ganzler-Odenthal, S.I., and C. Redies. 1998. Blocking N-cadherin function disrupts the epithelial structure of differentiating neural tissue in the embryonic chicken brain. *J Neurosci* 18:5415-5425.
238. Kadowaki, M., S. Nakamura, O. Machon, S. Krauss, G.L. Radice, and M. Takeichi. 2007. N-cadherin mediates cortical organization in the mouse brain. *Dev Biol* 304:22-33.
239. Price, S.R., N.V. De Marco Garcia, B. Ranscht, and T.M. Jessell. 2002. Regulation of motor neuron pool sorting by differential expression of type II cadherins. *Cell* 109:205-216.
240. Cohen, S., L. Funkelstein, J. Livet, G. Rougon, C.E. Henderson, V. Castellani, and F. Mann. 2005. A semaphorin code defines subpopulations of spinal motor neurons during mouse development. *Eur J Neurosci* 21:1767-1776.
241. Shoval, I., A. Ludwig, and C. Kalcheim. 2007. Antagonistic roles of full-length N-cadherin and its soluble BMP cleavage product in neural crest delamination. *Development* 134:491-501.
242. Jarov, A., K.P. Williams, L.E. Ling, V.E. Koteliansky, J.L. Duband, and C. Fournier-Thibault. 2003. A dual role for Sonic hedgehog in regulating adhesion and differentiation of neuroepithelial cells. *Dev Biol* 261:520-536.
243. Washburn, C.P., M.A. Cooper, and R. Zhou. 2007. Expression of the tyrosine kinase receptor EphA5 and its ligand ephrin-A5 during mouse spinal cord development. *Neurosci Bull* 23:249-255.
244. Copp, A.J., N.D. Greene, and J.N. Murdoch. 2003. The genetic basis of mammalian neurulation. *Nat Rev Genet* 4:784-793.
245. Holmberg, J., A. Armulik, K.A. Senti, K. Edoff, K. Spalding, S. Momma, R. Cassidy, J.G. Flanagan, and J. Frisen. 2005. Ephrin-A2 reverse signaling negatively regulates neural progenitor proliferation and neurogenesis. *Genes Dev* 19:462-471.
246. Conover, J.C., F. Doetsch, J.M. Garcia-Verdugo, N.W. Gale, G.D. Yancopoulos, and A. Alvarez-Buylla. 2000. Disruption of Eph/ephrin signaling affects migration and proliferation in the adult subventricular zone. *Nat Neurosci* 3:1091-1097.
247. Ricard, J., J. Salinas, L. Garcia, and D.J. Liebl. 2006. EphrinB3 regulates cell proliferation and survival in adult neurogenesis. *Mol Cell Neurosci* 31:713-722.

248. Depaepe, V., N. Suarez-Gonzalez, A. Dufour, L. Passante, J.A. Gorski, K.R. Jones, C. Ledent, and P. Vanderhaeghen. 2005. Ephrin signalling controls brain size by regulating apoptosis of neural progenitors. *Nature* 435:1244-1250.
249. Chumley, M.J., T. Catchpole, R.E. Silvany, S.G. Kernie, and M. Henkemeyer. 2007. EphB receptors regulate stem/progenitor cell proliferation, migration, and polarity during hippocampal neurogenesis. *J Neurosci* 27:13481-13490.
250. Davy, A., and P. Soriano. 2007. Ephrin-B2 forward signaling regulates somite patterning and neural crest cell development. *Dev Biol* 304:182-193.